2012

THE EVOLUTION OF GRENVILLE BASEMENT IN THE EASTERN GREAT SMOKY MOUNTAINS; CONSTRAINTS FROM U-PB ZIRCON GEOCHRONOLOGY, WHOLE ROCK SM-ND, AND FELDSPAR PB GEOCHEMISTRY

Ryan Joel Quinn
University of Kentucky, rquinn2@wisc.edu

STUDENT AGREEMENT:

I represent that my thesis or dissertation and abstract are my original work. Proper attribution has been given to all outside sources. I understand that I am solely responsible for obtaining any needed copyright permissions. I have obtained and attached hereto needed written permission statements(s) from the owner(s) of each third-party copyrighted matter to be included in my work, allowing electronic distribution (if such use is not permitted by the fair use doctrine).

I hereby grant to The University of Kentucky and its agents the non-exclusive license to archive and make accessible my work in whole or in part in all forms of media, now or hereafter known. I agree that the document mentioned above may be made available immediately for worldwide access unless a preapproved embargo applies.

I retain all other ownership rights to the copyright of my work. I also retain the right to use in future works (such as articles or books) all or part of my work. I understand that I am free to register the copyright to my work.

REVIEW, APPROVAL AND ACCEPTANCE

The document mentioned above has been reviewed and accepted by the student's advisor, on behalf of the advisory committee, and by the Director of Graduate Studies (DGS), on behalf of the program; we verify that this is the final, approved version of the student's dissertation including all changes required by the advisory committee. The undersigned agree to abide by the statements above.

Ryan Joel Quinn, Student

Dr. David P. Moecher, Major Professor

Dr. Alan E. Fryar, Director of Graduate Studies

THE EVOLUTION OF GRENVILLE BASEMENT IN THE EASTERN GREAT SMOKY MOUNTAINS; CONSTRAINTS FROM U-PB ZIRCON GEOCHRONOLOGY, WHOLE ROCK SM-ND, AND FELDSPAR PB GEOCHEMISTRY

THESIS

A thesis submitted in partial fulfillment of the requirements for the degree of Master of Science in the College of Arts and Sciences at the University of Kentucky

By

Ryan Joel Quinn

Lexington, Kentucky

Director: Dr. David P. Moecher, Professor of Geology

Lexington, Kentucky

2012

ABSTRACT OF THESIS

THE EVOLUTION OF GRENVILLE BASEMENT IN THE EASTERN GREAT SMOKY MOUNTAINS; CONSTRAINTS FROM U-PB ZIRCON GEOCHRONOLOGY, WHOLE ROCK SM-ND, AND FELDSPAR PB GEOCHEMISTRY

Identifying the crustal affinity of Grenville basement rocks in the Dellwood quadrangle, western NC, provides insight into the tectonic evolution of eastern Laurentia during Grenville orogenesis. U-Pb zircon geochronology of orthogneiss, augen gneiss, and mafic xenoliths in orthogneiss reveal magmatic pulses at 1130, 1180, and 1330 Ma and metamorphic episodes at 450 and 1040 Ma. Xenoliths in 1330 Ma orthogneiss are as old as 1382 Ma and represent the oldest component of Blue Ridge basement identified to-date. Feldspar Pb isotope values span a range between juvenile-Laurentian and southern-central Appalachian basement/Amazonia. Most Pb isotope data define an array consistent with crustal mixing between Laurentia and Amazonia, however, one xenolith has a unique Pb isotopic composition interpreted as Laurentian crust. Sm-Nd isotope data yield depleted mantle model ages ranging from 1.52 to 1.79 Ga (200 to 650 Ma older than their crystallization ages) indicating a broadly non-juvenile heritage for Dellwood basement. Three biotite gneiss samples contain detrital zircon grains derived from 1060, 1160, 1330, and 1750 Ma sources. Multiple magmatic zircon age populations, variable depleted mantle model ages, and regionally unique isotopic Pb signatures are evidence of protracted Grenville magmatism in the southern Appalachians involving both Laurentian and Amazonian crustal components.

KEYWORDS: Blue Ridge, Grenville, Zircon geochronology, Sm-Nd, Pb geochemistry

Ryan Joel Quinn

August 19, 2012

THE EVOLUTION OF GRENVILLE BASEMENT IN THE EASTERN GREAT SMOKY MOUNTAINS; CONSTRAINTS FROM U-PB ZIRCON GEOCHRONOLOGY, WHOLE ROCK SM-ND, AND FELDSPAR PB GEOCHEMISTRY

By

Ryan Joel Quinn

David P. Moecher
Director of Thesis

Alan E. Fryar
Director of Graduate Studies

August 19, 2012
Date

ACKNOWLEDGMENTS

I thank my advisor Dr. David P. Moecher from whom I have learned so much. He provided great assistance through the entire scientific process and outside the academic realm as well. I am truly a better person having completed this MS program under his tutelage. I thank Dr. Scott D. Samson, Aaron Satkoski, and Jack Hietpas at the Syracuse University for the laboratory assistance provided for sample preparation and TIMS analysis. Mark Pecha, Clayton Loehn, Chen Li, and Nicky Giesler at the Arizona LaserChron Center provided excellent help with zircon imaging and LA-ICP-MS analysis. Committee members Dr. Kent Ratejeski and Dr. Chris Romanek provided very helpful comments regarding aspects of the thesis. I thank the Department of Earth and Environmental Sciences at the University of Kentucky for providing the opportunity and resources to pursue an advanced degree in geology. Everybody within the entire EES department contributed to a quality scientific environment, particularly, my office mates Gabriel RiCharde and Susan Leib.

I was greatly benefited by my parents Bill and Carolyn Quinn who provided the developmental resources that equipped me to pursue advanced scientific study and the personal support through all of my life. Tom Quinn, Kat Oot-Quinn, and family who I stayed with during lab work in Syracuse the summer of 2011 contributed tremendous support and hospitality. I could not have completed this work without everybody mentioned, thanks.

TABLE OF CONTENTS

LIST OF FIGURES

CHAPTER I. INTRODUCTION

The Superior Province in Canada (> 2.6 Ga) comprises the core of the Laurentian craton. A geochronological traverse of Laurentian continental basement from Canada toward the Appalachians shows a gradual decrease in crustal age (Hoffman, 1988), which can be explained by the sequential addition of juvenile magma and reworking of existing crust during successively younger orogenic events. However, the eastwardly younging trend terminates at the NY-AL lineament (Fig. 1.1) where anonymously old ages (1.8 Ga; Carrigan *et al.*, 2003) and non-juvenile isotopic signatures appear (Tohver *et al.*, 2004; Fisher *et al.*, 2010). The Grenville orogeny (*ca.* 1.0-1.4 Ga) may have contributed additional crustal material to Laurentia via terrane transfer (*e.g.,* Amazonia; Loewy *et al.,* 2003; Tohver *et al.,* 2004) and/or by further addition of juvenile crust (Whitmeyer and Karlstrom, 2007). Complex lithological, geochronological, and geochemical patterns among terranes in the southern Appalachian basement are thus expected. Paleozoic crustal reworking further contributed to the complexity of the Appalachian Grenville basement (Hatcher *et al.,* 2004).

Investigation of these complexities yields useful data for paleogeographic reconstructions and provides insight for relative timing and location of orogenesis. Although some evidence supports the hypothesis of Grenvillian crustal exchange from Amazonia to Laurentia in the southern Appalachians (Carrigan *et al.*, 2003; Loewy *et al.*, 2003, 2004; Ownby *et al.*, 2004; Tohver *et al.*, 2004; Berquist *et al.*, 2005; Fisher *et al.*, 2010), detailed timing and paleogeography are not well understood. Most areas of the southern and central Appalachians have not been examined in sufficient detail to confirm

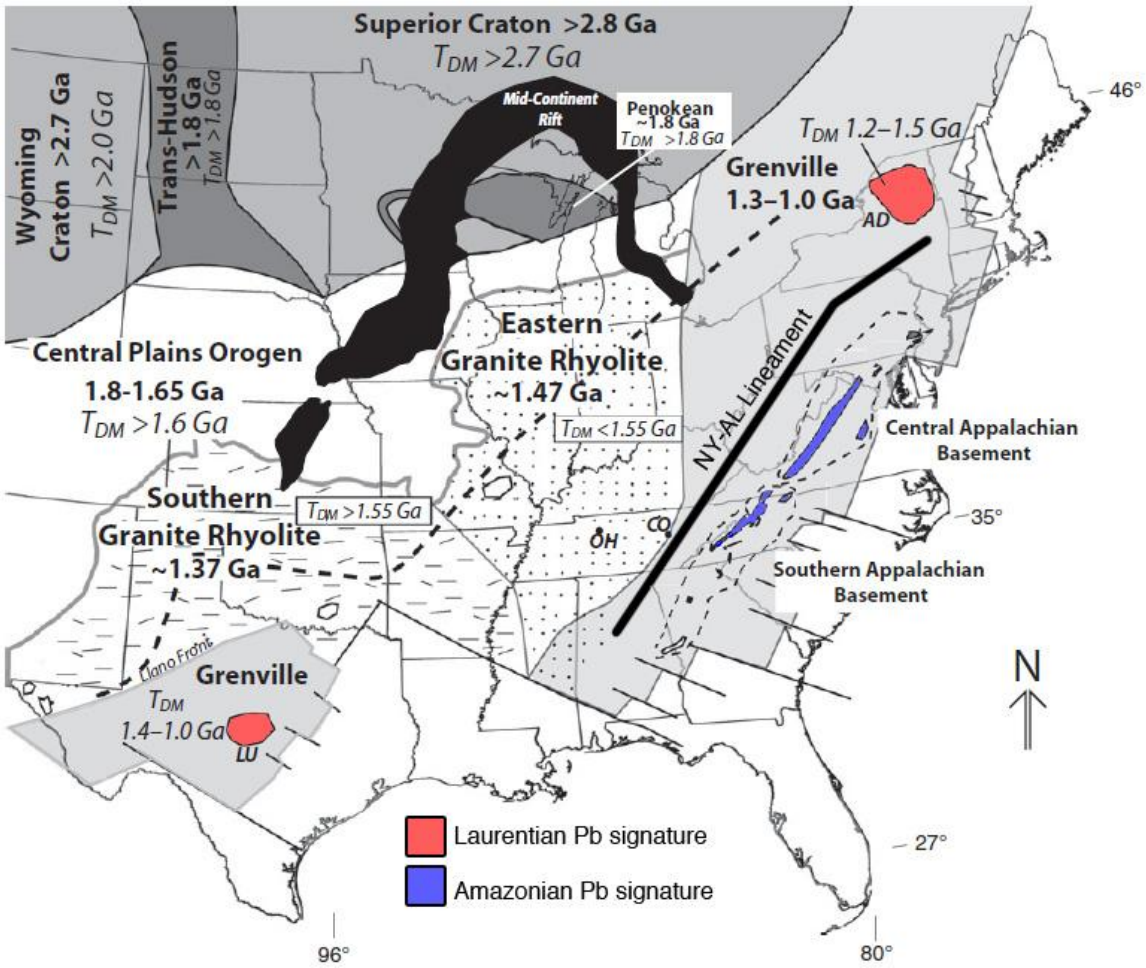

Figure 1.1: Generalized map of U-Pb zircon and T_{DM} age distributions for Proterozoic basement of various crustal age provinces in southeastern North America. Major locations of exposed basement with juvenile Laurentian Pb signatures (red) and exotic Amazonian Pb signatures (blue) are highlighted. The dashed line represents the interpreted border between T_{DM} ages greater and younger than 1.55 Ga. SCAB- southern and central Appalachian basement. Figure modified slightly from Fisher *et al.* (2010).

ubiquitous Amazonian affinity (Sinha et al., 1996; Sinha and McLelland, 1999). Multiple and intense Paleozoic metamorphism that overprints Mesoproterozoic basement and Neoproterozoic cover, lack of map coverage, and poor exposure also inhibit elucidation of the original geological relationship among basement units in the southern Appalachians. Additional field studies and geochemical and geochronological data are required to test the Amazonian crustal affinity hypothesis and to bring a deeper understanding to the complex developmental history of terranes in the eastern Great Smoky Mountains. The Dellwood quadrangle has been mapped at 1:24000 scale, and numerous investigations have identified critical exposures for evaluating the complex history of orogenesis, making it a benchmark for comparison with other areas of exposed Grenville basement in the southern Blue Ridge.

The Cartoogechaye Terrane in the southern and central Appalachians has Pb and Nd isotopic compositions that are distinct from surrounding juvenile Laurentian material and U-Pb zircon crystallization ages (1.27-1.02 Ga; Aleinikoff *et al.*, 2000; 2004) that are younger than their depleted mantle model derivation ages (1.75-1.25 Ga; Fullagar *et al.*, 1997; Ownby *et al.*, 2004; Berquist *et al.*, 2005; Fisher *et al.*, 2010). These differences introduce the possibility that the Cartoogechaye terrane was emplaced via terrane transfer from Amazonia. The main focus of this study is to test the hypothesis that basement rocks within the Dellwood area of western North Carolina (Figs. 1.2 and 1.3) are of Amazonian affinity. For a positive outcome, the EGSM basement should possess Pb isotopic compositions that are similar to Amazonian Pb isotope compositions and have depleted mantle ages greater than 1.5 Ga, consistent with non-juvenile source(s).

Geologic Setting

The Blue Ridge province in the eastern Great Smoky Mountains (ESGM) area of North Carolina (Fig. 1.2) exhibits complex polycyclic structural and lithologic relations resulting from orogenic activity from the Mesoproterozoic to the late Paleozoic. Mesoproterozoic basement rocks in the region are largely granitic orthogneisses. U-Pb zircon geochronology from these rocks reveal numerous magmatic and metamorphic events including several Grenvillian pulses (*ca*. 1330 Ma, 1180 Ma, and 1050 Ma: Aleinikoff et al., 2006; Anderson and Moecher, 2008; Southworth *et al.*, 2010; Tollo *et al.*, 2010). Post-Grenville rifting produced Neoproterozoic continental plutonic and volcanic sequences (*e.g.*, Fetter and Goldberg, 1995; Aleinikoff *et al.*, 1995; Tollo *et al.*, 2004); unconformable deposition of the intracontinental rift deposits of the Ocoee Supergroup above regional Mesoproterozoic basement (Hadley and Goldsmith, 1963); and the drift sequence sediments of the Chilhowee Group. More recent geochronologic and petrotectonic studies document regional high-grade Middle Ordovician (Taconian) to Devonian metamorphism (Kohn and Malloy, 2004; Moecher *et al.*, 2011), and late Paleozoic low grade regional metamorphism, folding, and ductile faulting (Southworth *et al.*, 2006; Clemons and Moecher, 2009).

Basement in the Dellwood quadrangle of the EGSM is lithologically and structurally complex (Fig. 1.2). Original and subsequent mapping (Hadley and Goldsmith, 1963; Southworth *et al.*, 2005) of the EGSM highlands basement complex in the Cherokee-Dellwood area distinguished biotite gneiss (bgn) and hornblende gneisses (hgn) with metaplutonic orthogneiss nonconformably below Neoproterozoic rift metasediments of the Snowbird Group. Zircon U-Pb SHRIMP geochronology by the USGS confirmed

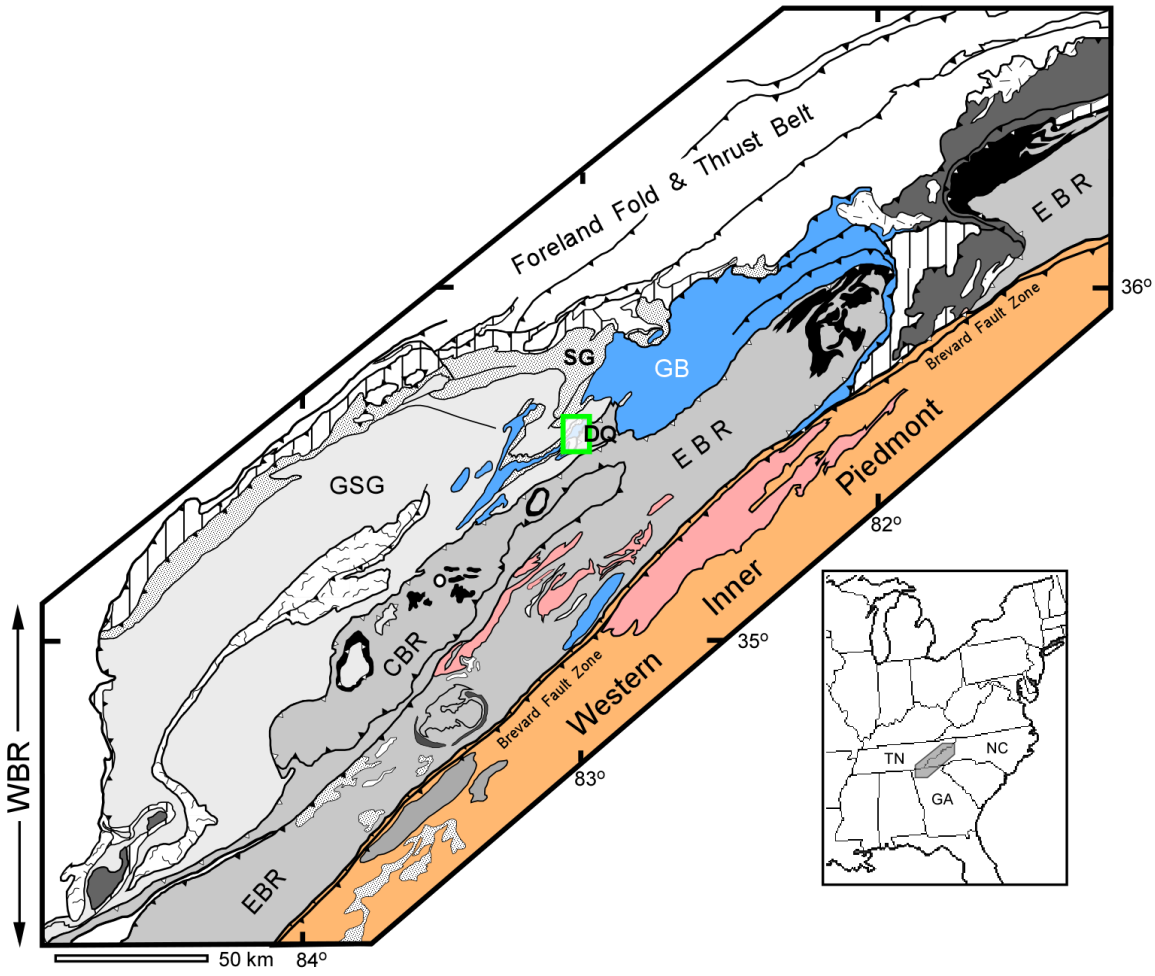

Figure 1.2: Generalized tectonic map of the southern Appalachians: CBR-central Blue Ridge; DQ- Dellwood quad (green rectangle); EBR-eastern Blue Ridge; GB-Grenville basement; GSG-Great Smoky Group; SG-Snowbird Group; WBR-western Blue Ridge;

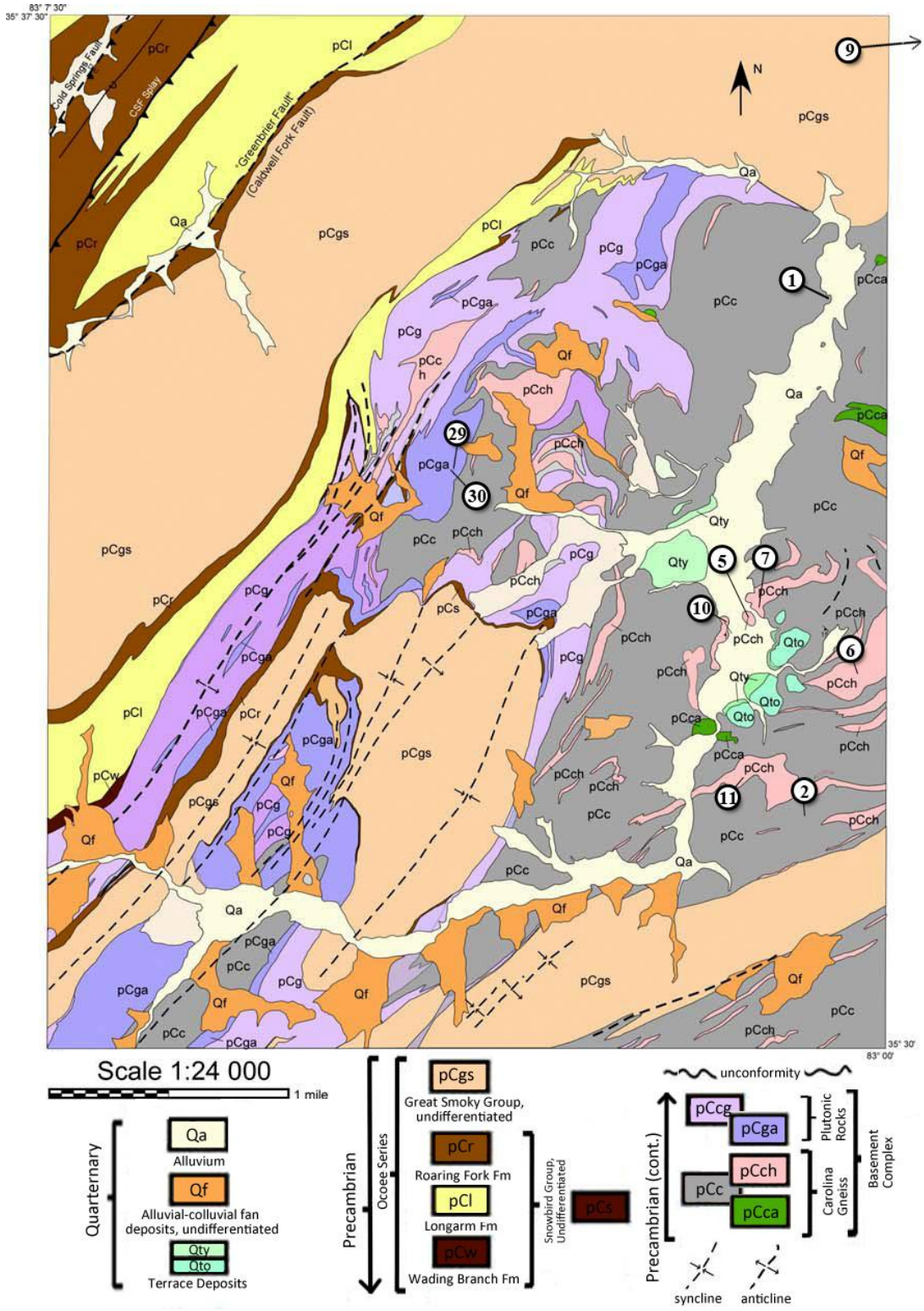

Figure 1.3: Geologic map of the Dellwood 7.5 min. quadrangle, eastern Great Smoky Mountains (Hadley and Goldsmith, 1963). Sample location 9 is located in the Clyde quadrangle (35° 36' 15" N; 82° 57' 26" W). pЄcg-granitoid gneiss, pЄga-augen gneiss, pЄch-hornblende gneiss, pЄc-biotite gneiss, pЄca-amphibolite.

the largely Grenville affinity of the basement complex (magmatic rocks ranging from 1000 to 1180 Ma: Aleinikoff et al., 2006). A considerably older magmatic component (*ca.* 1330 Ma) of hornblende or clinopyroxene tonalitic orthogneiss among rocks mapped as hgn were discovered by previous UK EES graduate students in the Dellwood area (Anderson and Moecher, 2008; Loughry, 2010a; Anderson, 2011). The orthogneiss was discovered to contain intermediate to mafic xenoliths, or mafic enclaves (Anderson and Moecher, 2008), which, if xenoliths, suggest a crustal component older than 1.33 Ga is present in the ESGM basement complex.

Purpose of Study

The orthogneiss of the Dellwood Quadrangle is of uncertain crustal affinity, the biotite gneiss does not have a known protolith and its relation to the Ocoee sequence is uncertain (time equivalent?), and there has been no detailed study of the xenoliths recently discovered within the orthogneiss. Detailed geochemistry and geochronology are necessary to determine the ultimate crustal source of the Dellwood basement complex rocks within the Cartoogechaye terrane, the petrogenesis of the biotite gneiss, and the relationship between the xenoliths and their host rock. The primary objective is analysis of Pb and Sm-Nd isotope compositions, and U-Pb geochronology, in an attempt to understand the intricate relationships among the gneisses in the Dellwood quad, and to provide further constraints on the history of Laurentian accretion and crustal growth during the Grenville orogeny.

The Sunsás Orogen of Amazonia contains magmatic rocks of 1.3-1.0 Ga age with Nd mantle derivation ages (T_{DM}) in excess of 1.6 Ga, which have similar Pb isotope compositions to that of the southern/central Appalachian basement rocks (Fig. 1.4b; Ruiz

et al., 1999; Tohver *et al.*, 2004; Fisher et al., 2010). Considering these similarities, the proposition that the exposed southern/central Appalachian basement was transferred to Laurentia from Amazonia during the Grenville orogeny (Loewy *et al.*, 2003; Tohver *et al.*, 2004), no later than 1.2 Ga, is generally accepted. These studies were based on whole-rock common Pb isotope compositions, which can be problematic due to U mobility, potentially yielding evolved and not initial $^{207}Pb/^{206}Pb$ ratios. Lead isotope analysis of K-feldspar differs from whole-rock Pb isotope analysis in that K-feldspar contains essentially no U and thus the measured Pb isotopic compositions are more accurate measurements of a rock's initial magmatic Pb isotope composition. As other minerals partition U relative to feldspars during crystallization, Pb isotopes will evolve from the initial Pb ratio given by K-feldspar to higher ratios with time. So whole rock Pb values are still useful for discriminating crustal reservoirs. Lead and Sm-Nd isotope compositions, and U-Pb zircon geochronology analysis is required to further test the hypothesis that the basement complex in the ESGM is solely of Amazonian affinity.

The biotite gneiss has nearly identical major and trace element geochemistry to that of the orthogneiss (Loughry, 2010a), but whether it is metasedimentary or metavolcanic has been thus far undetermined. If the biotite gneiss is a highly deformed post-Grenville, Neoproterozoic metaclastic rock (Hatcher *et al.*, 2004; Hatcher *et al.*, 2005) of the same age as the Ocoee Supergroup, it should contain detrital zircon grains derived from other young Neoproterozoic sources in the southern Blue Ridge (e.g., 600-800 Ma), have detrital zircon age spectra dominated by Grenville (1000-1300 Ma) ages with few older ages, and possess similar detrital zircon age patterns as the Ocoee Supergroup (Chakraborty, 2010; Chakraborty et al., 2012) and Ashe metamorphic suite

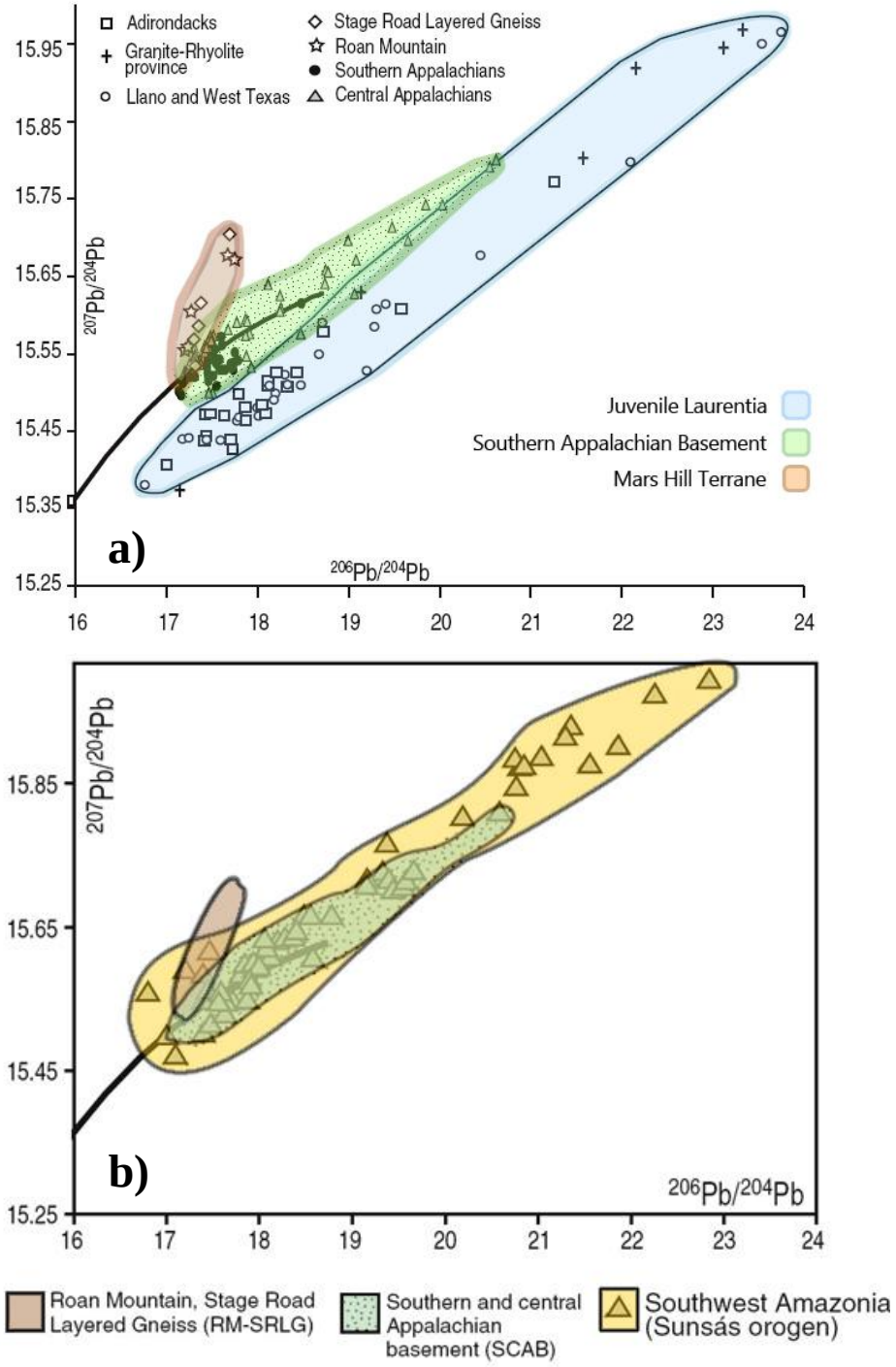

Figure 1.4: Present-day uranogenic ($^{207}Pb/^{204}Pb$ versus $^{206}Pb/^{204}Pb$) Pb isotope compositions from previous studies of Proterozoic igneous rocks of (a) eastern North America and (b) the Sunsás orogen of southwest Amazonia (Ruiz et al., 1999; Tohver et al., 2004) plotted with data from eastern North America. Thick black line is average crustal Pb growth curve (Stacey and Kramers, 1975). Figures modified from (a) Fisher et al. (2010) and (b) Berquist *et al.* (2005).

(Hietpas *et al.*, 2011; Moecher *et al.*, 2011). If it is older (Mesoproterozoic), the youngest detrital zircons it contains would define the oldest depositional age. Detecting all possible age components requires analysis of many zircon grains, which previous ion microprobe studies tended not to do (Bream et al., 2004). Analysis of zircon by rapid LA-ICP-MS methods permits interrogation of more grains and greater likelihood of detecting minor age components.

This study presents new whole-rock Sm-Nd and feldspar Pb isotope compositions from key outcrops of Mesoproterozoic orthogneiss and biotite gneiss in the EGSM in order to further test the Amazonia-Laurentia terrane transfer model. New U-Pb zircon ages are presented and, together with the geochemical data, permit a more detailed view of Grenvillian orogenic development. These geochronologic data will also provide evidence bearing on whether or not the protolith of the biotite gneiss is magmatic or sedimentary. This study provides the first comprehensive isotopic and geochronologic study of Mesoproterozoic basement rocks in the EGSM and the first evidence of a potential Laurentian crustal component in the southern and central Appalachians.

CHAPTER II. ANALYTICAL METHODS

Whole Rock Geochemistry: X-Ray Fluorescence

Whole-rock analysis of major and minor elements was carried out by X-ray fluorescence spectrometry at the Kentucky Geological Survey. Eight representative samples were trimmed of weathered rinds and washed with soap and water. Four other samples, which had been previously collected and powdered by Chakraborty (2010) and Anderson (2011) were also analyzed.

Samples were crushed to coarse gravel sized fragments using a jaw crusher. The collection tray was lined with a plastic trash bag for each sample to avoid contamination. Approximately 90 ml of each sample was powdered using a single puck alumno-silicate shatterbox. The jaw crusher and shatterbox parts were removed and thoroughly cleaned between each sample. Each part was vacuumed and blasted with compressed air. The shatterbox chamber and puck were washed with soap and water. The jaw crusher was cleaned with a wire brush power grinder and wiped with isopropanol. For each sample the shatterbox chamber was pre-contaminated by running a portion of sample, discarding the powder, and cleaning the shatterbox again before loading the sample for collection.

The sample powders were weighed and mixed with 8.0000 g ± 0.5 mg of Fluxite® (90 $Li_2Br_4O_7$: 10 LiF) and 4.0000 g ± 0.5 mg of unknown sample. The mixture was transferred to a platinum crucible and approximately 100 µl of 5.8 M LiBr solution was added. Low dilution lithium tetra-borate fused discs were made from samples using a Katanax K_1 Prime automatic fluxer at a maximum temperature of 1080^{o}C. Cooled discs were labeled with a silver paint marker (titanium bearing) on the backside of the disc to avoid titanium contamination. Fused discs were then analyzed at the Kentucky

Geological Survey X-ray analytical lab on a 4-kW Bruker S4 Pioneer wavelength dispersive X-Ray fluorescence spectrometer. Elemental concentrations were calculated from measured intensities calibrated to various rock standards (AMH-1, multiple BCR-2, multiple DNC-1, G-2, and YG-1).

Whole Rock Sm-Nd and Feldspar Pb Geochemistry

Whole rock analysis of Sm and Nd, and feldspar analysis of common Pb were completed at the Syracuse University Radiogenic Isotope Laboratory. Samples were crushed as above. For whole rock Sm, Nd, and Pb analyses approximately 90 ml of each sample were powdered using a single puck alumino-silicate shatterbox. Care was taken to homogenize the sample and to ensure a representative aliquot was obtained. The puck and chamber of the shatterbox were vacuumed, blasted with compressed air, and washed with soap and water between samples. For each sample the shatterbox chamber was pre-contaminated by running a portion of the sample, discarding the powder, and cleaning the shatterbox again before loading the sample. Seven samples previously collected and powdered by Chakraborty (2010), Loughry (2010), and Anderson (2011) were also analyzed.

Whole rock powders analyzed for Sm and Nd were dissolved in Teflon bombs. Bombs were cleaned by a series of overnight acid rinses in an oven at 160 °C. These three individual rinses were with a 4.8 ml 29 M HF and 0.2 ml HNO_3 mixture, 6 M HCl, and another HF and HNO_3 mixture of the same proportions. Savillex® vials (50 ml) were cleaned by filling the vials with the same 2.4 HF : 1 HNO_3 mixture, capping, and leaving on a hot plate for all three nights.

To prepare the samples for bomb dissolution approximately 0.300 g were weighed into the 50 ml vials. The walls of the vials were rinsed and swirled with HNO_3 to collect all powder. 10 ml of 29 M HF was added to the vial, which was then capped and heated for 24 hrs. Samples were then uncapped and dried to a solid. 2.8 ml of 29 M HF and 0.2 ml of HNO_3 were added to the vials to re-dissolve the powder. This solution was poured into the bombs with approximately 0.1500 g of an enriched $^{149}Sm/^{150}Nd$ spike and another 2.0 ml of 29 M HF. The bombs were heated in the oven at 160 °C for 6 or 7 days.

After the bombs were removed samples were poured back into their respective Savillex® vials. The bombs were rinsed with 29 M HF to ensure the entire aliquot was collected. Samples were dried and dissolved in 6 M HCl over a 12 hr period and then dried again. Samples were heated for 30 min in 5 ml of 6 M HCl and then contents were added to their respective bombs. The bombs were then placed in an oven overnight at 160 °C. Contents were then transferred back into their respective vials and dried. Approximately 10 ml of 6 M HCl was added to the vials, which were then capped and heated for 30 min. After the entire sample was dissolved the contents were transferred into 2 equal volumes in centrifuge tubes and ran in a centrifuge for 6 min at 11 rpm.

Samples were added to cation exchange resin columns. To extract Pb, 6 ml of 2.5 M HCl was passed through the column and collected in a beaker. Columns were rinsed with 94 ml of 2.5 M HCl. 6 M HCl was passed through the columns to collect the heavy rare earth elements. 22 ml of each sample was collected and dried. These aliquots were dissolved in 0.18 M HCl and loaded into the second stage rare earth element cation exchange resin columns. 5 ml were collected for Nd and then the columns were re-equilibrated with 0.5 M HCl and 10-15 ml were collected for Sm. These aliquots were

dried to a solid. Samples were then analyzed on the IsotopX Phoenix thermal ionization mass spectrometer (TIMS) for whole rock Sm and Nd concentrations.

These Sm-Nd data were used to calculate epsilon Nd values at the present time, at the time of crystallization, and at the time of mantle extraction:

$$\varepsilon_{Nd(t)} = \left[\frac{\left(\frac{^{143}Nd}{^{144}Nd}_{sample(t)} \right)}{\left(\frac{^{143}Nd}{^{144}Nd}_{CHUR(t)} \right)} - 1 \right] * 10^4$$

Present day isotopic ratios used for CHUR were $^{147}Sm/^{144}Nd = 0.1967$ and $^{143}Nd/^{144}Nd = 0.512638$ (DePaolo, 1981; Wasserburg *et al.*, 1981). Depleted mantle ages were calculated using the depleted mantle curve of DePaolo (1981).

Seven samples were analyzed for Pb concentration in feldspar. For these analyses the samples were processed through an iron mill after the jaw crusher to produce sand composed of individual minerals. The resulting sand was dry sieved with 250 μm mesh. Precautions were taken to avoid sample contamination. Between each sample the jaw crusher and mill were thoroughly vacuumed, air blasted, and cleaned with isopropanol. Mill discs and jaw crusher plates were removed and cleaned with a vacuum, straight wire brush grinder, and isopropanol. The sieve jar was vacuumed and washed with soap and water. Sieve mesh was discarded after each sample. All worktable surfaces were vacuumed, air blasted, and wiped down with isopropanol and new paper towels were laid down so that the sample never touched any workspace surfaces. The floor was sprayed with water and swept between each sample.

The >250 μm fraction of the samples were run through the Frantz magnetic separator model LB-1 at 0.25 and 1.5 amps. The 1.5 amp non-magnetic portions were

collected and stored. To avoid contamination, all removable parts of the Frantz were washed in soapy water and the rest was vacuumed and wiped with isopropanol between samples. The feldspars were picked using a Leica S8 120 x binocular microscope equipped with a polarizer and analyzer. 20 test grains of each sample were hand-picked and mounted onto a glass slide with carbon tape and examined on the JEOL JXA8600V200 scanning electron microscope at Syracuse University. These grains' compositions were checked by energy dispersive spectrometry to ensure K-feldspar grains could be picked confidently apart from plagioclase, quartz, and other minerals. Some samples did not contain K-feldspar, in which case sodic plagioclase was picked.

Two-hundred feldspar grains from each sample were hand-picked and collected in a petri dish. Care was taken to select the purest and least fractured grains. These picked grains were crushed using a mortar and pestle while submerged in isopropanol. Using a pipette, the powder was transferred into 15 ml Savillex® vials. Isopropanol was then pipetted out of the vial; any remaining isopropanol was evaporated. After the powder was dried each sample went through a series of rinses in acid and water. Each sample bathed in10 ml of HNO_3 in a capped vial on a hot plate for approximately 24 hrs. HNO_3 was pipetted out and then the sample was rinsed with 18 MΩ deionized H_2O. 10 ml of 6 M HCl was added to the vial and was set capped on a hot plate for another 24 hrs. HCl was then pipetted out and the sample was rinsed with distilled H_2O.

This was followed by two half-hour rinses in room-temperature 5% 29 M HF. After each rinse the leach was discarded and the sample rinsed in distilled H_2O.Two 5 min hot leaches in 5% 29 M HF were done for each sample, which were discarded. Three more 10 min hot leaches in 5% 29 M HF were done. For each leach the leachate was

collected in a separate beaker and dried down on a hot plate. After all HF volatilized 15 drops of 0.55 M HBr was added to the aliquot.

Aliquots were run through cation exchange resin columns to extract Pb. Columns were rinsed three times with 6 M HCl. After all HCl was through the column a squirt of distilled H_2O was added to each column. Columns were then equilibrated with 25 drops of 0.55 M HBr. Samples were loaded and processed through the columns. Two sets of 15 drops of 0.55 M HBr, two sets of 25 drops of 0.55M HBr, and two sets of 50 drops of 0.55M HBr were added and drained successively. The collected acid was removed and collection beakers were switched to collect Pb in the original sample in vials. To collect Pb, 20 drops of 6 M HCl were added and then 100 drops of 6 M HCl were added and collected. Feldspar Pb samples were loaded onto rhenium filaments on a VG Sector 54 TIMS.

U-Pb Zircon Geochronology

U-Pb zircon geochronology was carried out by laser ablation-inductively coupled plasma-mass spectrometry (LA-ICP-MS) and sensitive high resolution ion microprobe (SHRIMP-II) analysis. Zircon grains were acquired separated from three samples of biotite gneiss, two augen gneisses, two orthogneisses, one amphibolite, and one xenolith. Two samples were collected by Loughry (2010) and one by Anderson (2011).

Separation of zircon was done at Syracuse University and the University of Kentucky depending on the sample, but methodology was the same in both locations. Samples were crushed into coarse gravel size fragments using a jaw crusher and then milled into fine-grained sand using an iron mill. Sands were dry-sieved using 250 µm mesh. Between each sample the jaw crusher and mill was thoroughly vacuumed, air

blasted, and cleaned with isopropanol. Mill discs and jaw crusher plates were removed and cleaned with a vacuum, straight wire brush grinder, and isopropanol. The sieve jar was vacuumed and washed with soap and water. Sieve cloth was discarded after each sample. After sieving, the < 250 μm fraction was further processed for zircon.

Iron filings from the disc mill and strongly magnetic minerals were removed by agitating the sand with water in a large beaker and swirling a neodymium magnet in the suspended sediment numerous times until the majority of clay sized grains were decanted out of the beaker. The remaining sand was dried and further processed by heavy liquid and magnetic separations.

Heavy minerals were separated using acetylene tetrabromide (TBE; G= 2.96). The sample was loaded into a separatory funnel with TBE and a stopcock under a fume hood. The sand was stirred and heavy minerals were allowed to sink. After all visible heavy minerals were settled, the floating portion was stirred again to release any remaining heavy minerals. This was repeated at 3-5 times or until no more minerals were visibly separated. After a sufficient amount of heavy minerals settled, the stop cock was released allowing deposition of all the heavy minerals into a funnel lined with filter paper. The stopcock was intermittently closed so that TBE-light minerals could be collected in a separate beaker-funnel-filter paper system. After excess TBE was collected for reuse, the resulting mineral separates were rinsed with acetone until all TBE was removed. Thorough cleaning of all glassware and tools was done in between samples with acetone, de-ionized water, and soapy water to avoid contamination. After minerals were segregated by density, a series of magnetic separations was executed to remove magnetic minerals.

Magnetic minerals were removed over several steps using a Frantz Isodynamic Magnetic Separator Model LB-1. Separates were collected for 0.25 amps, 0.5 amps, and 1.5 amps magnetic fractions, and 1.5 amps non-magnetic fractions. Mafic samples were separated by Frantz magnetic separation before acetylene tetrabromide whereas the felsic samples were processed in the reverse order. After a non-magnetic, TBE-heavy aliquot was obtained, samples were run through another heavy liquid separation to purify the zircon population by removing mainly apatite.

All samples were divided via a second heavy liquid separation. Heavy non-magnetic portions were loaded into test tubes with 12 ml of methylene iodide (MI; G= 3.32) and run in an IEC Clinical Centrifuge on setting 1 for 5 min. Centrifuge was shut off and allowed to naturally slow to a stop. Test tubes were then removed and the bottom inch was submerged in liquid nitrogen. After the submerged portion froze, the MI-light elements and remaining MI was decanted into a coffee filter funnel and beaker. After the remaining portion melted the heavy separate was filtered and rinsed with acetone and water until all MI was removed. The heavy and light separates from this stage were collected in plastic petri dishes. Samples with a less pure zircon population were processed through this step twice to increase the population density of zircon.

After sufficient zircon was separated, grains were handpicked and mounted on double-sided sticky tape for LA-ICP-MS and SHRIMP-II analyses. Analysis of biotite gneiss samples was approached as a detrital study, *i.e.* the separate was poured into four squares using a mounting tube from Arizona LaserChron Lab onto a glass slide with double sided tape adhered to the surface. The glass plate was inverted so that excess grains which did not adhere to the surface of the tape would fall off. For all other samples,

fifty zircons were handpicked with a bias towards euhedral grains. These grains were mounted on double-sided tape in rows with three or four samples per mount. After unknowns and standards were picked, zircons were mounted in a 1 inch diameter plastic mounting cylinder with epoxy (5:2 by weight EpoThin® Epoxy Resin 20-8140-032 to EpoThin® Epoxy Hardener 20-8142-016). Resin and hardener were mixed and stirred with a wooden spatula for 5 min and then sonicated for 2 min to remove bubbles. The epoxy mixture was poured into the mounting cylinder and over the sample grains within. If any air bubbles were visible in the epoxy from under a picking microscope they were plucked out with a metal needle. Epoxy was then set to dry 24 hrs.

After solidification the mounts were removed from the tape and roughly polished down to approximate grain cores using wet 2000 grit sandpaper. Afterwards mounts were polished using Buehler® Metadi® 6 μm diamond suspension paste followed by 3 μm and 1 μm diamond compound polishes. Mounts were sonicated in dilute HCl for 1 min and then washed with soap and water after each polishing step.

Except for augen gneiss (agn) sample DEL10-29 and tonalite xenolith (tx) DEL10-7e, all samples were analyzed at the Arizona LaserChron Center at the University of Arizona on the Nu Plasma HR MC-ICPMS (High Resolution - Multi Collector - Inductively Coupled Plasma- Mass Spectrometer). The standard for U-Pb analysis at the Arizona LaserChron Center was Sri Lanka zircon (ID-TIMS age of 563.5±3.2 Ma; Gehrels et al., 2008).

Cathodoluminescence (CL) and backscatter electron (BSE) images were collected at the University of Western Australia for agn-DEL10-30 and hgn-DEL10-7b. BSE and some CL images for other samples were collected at the University of Arizona. BSE and

CL images were used to guide spot locations to specific zones and to avoid imperfections. Mounts were carbon-coated and imaged on the Hitachi 3400N Scanning Electron Microscope (SEM) at the Geo Arizona SEM laboratory. High-resolution BSE images were taken for all samples using the Oxford EDS/EBSD system. CL images (CL) were taken for magmatic samples with the Gatan Chroma CL system. Only BSE images were taken for the biotite gneiss samples but they were of sufficient contrast to reveal grain cores and rims.

Spots for analysis on the HR MC-ICPMS were selected from BSE and CL images to confine the analysis to a homogeneous crystal zone clear of fractures and inclusions. Spot sizes were set at 20 µm for magmatic zircon and at 30 µm for the detrital zircon. Each analysis consisted of a single 12 s non-laser firing integration to collect background intensities, 15 s of laser ablation at 1 integration per second, and 30 s without firing to purge the system of ablated material. Laser firing duration was increased to 20 s for the tx-DEL10-7a small grain sample.

Resulting U-Th-Pb intensity data were reduced using Microsoft Excel *agecalc* (Gehrels et al., 2008) to calculate isotopic concentrations and ratios, apparent ages, and standard errors. Further data reduction to calculate concordia and weighted mean 'best ages' was accomplished with *Isoplot* (Ludwig, 1999) and *agecalc* (Gehrels et al., 2008).

Samples agn-DEL10-30 and hgn-DEL10-7b were mounted with standard BR266 (TIMS age: 559.0 ± 0.3 Ma; Stern 2001) in a 1 inch diameter epoxy plug, polished with the same procedure as aforementioned and analyzed at Curtin University John de Laeter Centre on the Sensitive High Resolution-Ion Micro Probe (SHRIMP-II). Spot sizes on the SHRIMP-II were 20 µm. U-Th-Pb intensity data were reduced using SQUID 2.5 (Ludwig

2009) to calculate isotopic concentrations and ratios, apparent ages, and standard errors. Further data reduction to calculate concordia and weighted mean 'best ages' was accomplished with *Isoplot* (Ludwig, 1999). All isotopic and age data are compiled in Appendix 1.

CHAPTER III. SAMPLE DESCRIPTION AND PETROLOGY

Hand samples and 1 inch drill cores were collected from various locations in Dellwood quadrangle (Fig. 1.3). Thin sections were prepared for petrographic characterization. Mineral modes were collected by point counting using a Hacker Instruments Inc. Swift Model F point counter. For each thin section, 300 points were counted at a horizontal spacing of 1 mm and a vertical spacing of 1 mm, and mineral modes were classified according to normalized to quartz (Q), alkali-feldspar (A), and plagioclase (P) content (Streckeisen, 1975).

Samples were collected from the Dellwood quad with the exception of ASH08-9-1a (Clyde quad), MP04-2 (Lemon Gap quad), and FC08-2 (Fines Creek quad). Other samples analyzed for geochemistry and/or geochronology were collected and described by previous UK EES graduate students (FC08-2: Chakraborty, 2010; bgn-DEL08-2d, bgn-DEL08-2e (Fig. 3.2), hgn-DEL08-6c, hgn-DEL08-7a, and hgn-DEL08-10a: Loughry, 2010; bgn-DEL03-1 (Fig. 3.1b), hgn-DEL04-5, and Max Patch granite (mpg) MP04-2: Anderson, 2011). Sample bgn-ASH08-9-1a (Fig. 3.1a) was provided by D. Moecher. Eight new samples (tonalite xenolith tx-DEL10-7a; hornblende gneiss hgn-DEL10-7b, hgn-DEL10-7e, and hgn-DEL10-11; amphibolite xenoliths amx-DEL10-7c and amx-DEL10-7d; and augen gneiss samples agn-DEL10-29 and agn-DEL10-30) were collected for this study from the basement complex of the Dellwood quadrangle (Fig. 1.3).

The Carolina Gneiss and plutonic rocks comprising the basement complex of the Dellwood quadrangle (Fig. 1.3; Hadley and Goldsmith, 1963) are the main lithologies sampled for this study: hornblende gneiss (pЄch/hgn), biotite gneiss (pЄc/bgn), augen

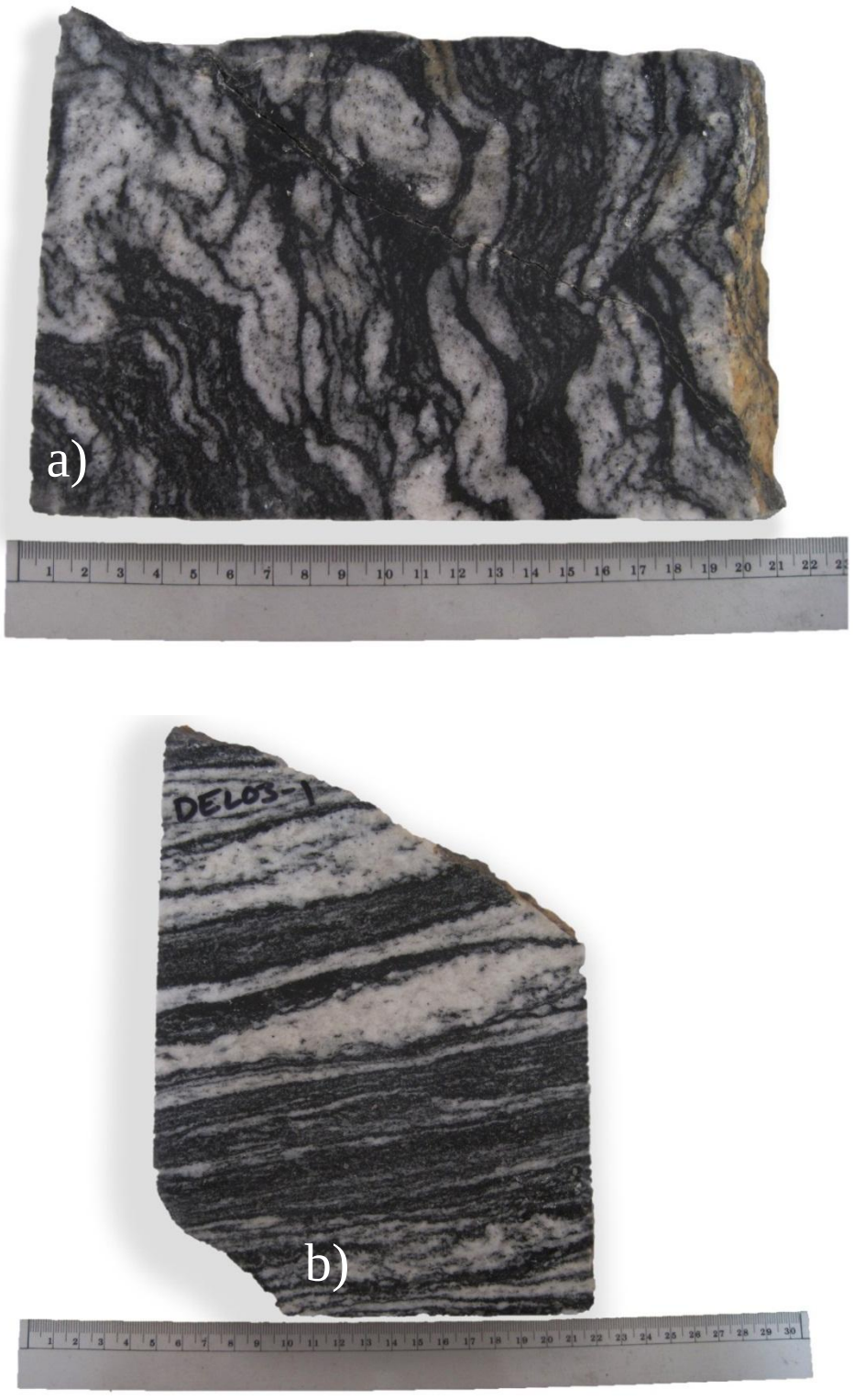

Figure 3.1: Photographs of slabs of biotite gneiss samples (a) ASH08-9-1a and (b) DEL03-1. Ruler units are cm. ASH09-9 cut perpendicular to fold axes, DEL03-1 cut parallel to fold axes.

Figure 3.2: Photograph of slap of biotite gneiss sample DEL08-2e showing leucocratic migmitization defining a folded foliation. Ruler units are cm.

Figure 3.3: Outcrop photograph at Trinity Cove subdivision showing foliated migmatitic biotite gneiss where sample DEL08-2e was collected by Loughry (2010). Rock hammer for scale.

gneiss (pЄga/agn), and amphibolite (pЄca/amx) (Fig. 1.3). The outcrop of hornblende gneiss at the Messer Farm on U.S. Rt. 276-Jonathan Creek Rd. (sample location 7, Fig. 1.3) is of particular interest due to unique igneous relationships between intermediate to mafic xenoliths, and the weakly lineated hornblende gneiss host.

Previous studies provide detailed discussion of petrological, lithological, and structural characteristics of rocks discussed herein (Hadley and Goldsmith, 1963; Merschat and Wiener, 1988; Montes, 1997; Massey and Moecher, 2005; Southworth et al., 2005; Loughry 2010; Anderson 2011). The purpose here is to provide a brief synopsis of the petrology of rocks collected for this study at the thin section to outcrop scale. All samples have experienced regional upper amphibolite facies Middle Ordovician metamorphism and late Paleozoic greenschist facies metamorphism, folding, and mylonitization, but exhibit varying degrees of textural and mineralogic modification as a result of these events. The critical aspect of the Messer Farm locality is that the degree of overprinting appears to be minor compared to all other lithologies and exposures in the EGSM area.

Hornblende Orthogneiss

DEL10-7a:

Cores were taken from an intermediate xenolith enclosed in hornblende orthogneiss (Fig. 3.4) at Messer Farm (Fig. 1.3; location 7). The mineral assemblage is plagioclase + biotite + garnet + hornblende + scapolite. Scapolite commonly occurs as coronas around garnet and plagioclase (Fig. 3.5b). Accessory minerals include apatite, ilmenite, retrograde actinolite, and zircon. Grains display equigranular, granoblastic texture with no apparent foliation (Fig. 3.5a).

Figure 3.4: Outcrop photograph of core holes within the tonalitic xenolith sample DEL10-7a within hornblende gneiss. Garnet amphibolite xenoliths are common. Rock hammer handle for scale.

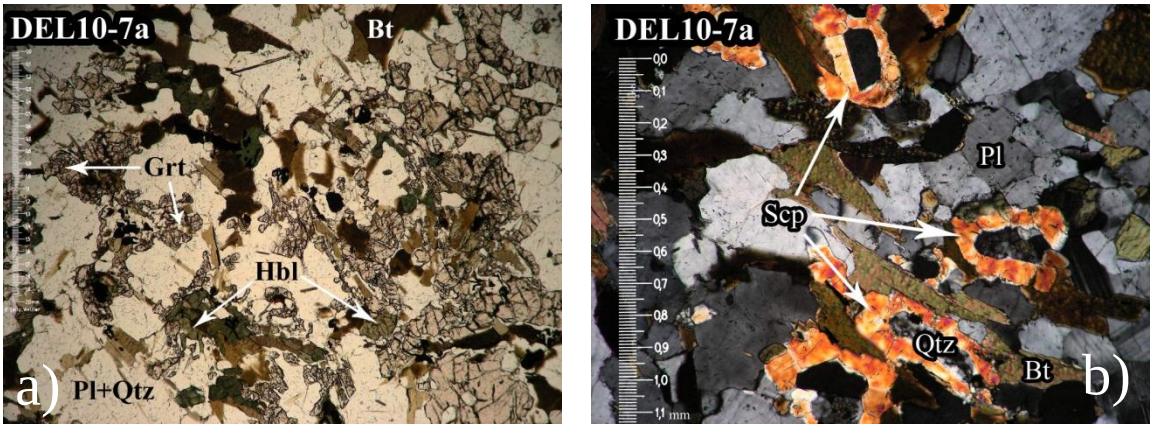

Figure 3.5: Photomicrographs of thin sections of DEL10-7a: a) representative area in plane polarized light (PPL); b) arrows point to scapolite coronas surrounding plagioclase grains in crossed polarized light (XPL).

Figure 3.6: Outcrop photograph of Messer Farm showing the location of samples tx-DEL10-7a, hgn-DEL10-7b, and hgn-DEL10-7e. Sledge hammer for scale.

Figure 3.7: Outcrop photograph of sample location hgn-DEL10-7b. Circles mark drill core locations.

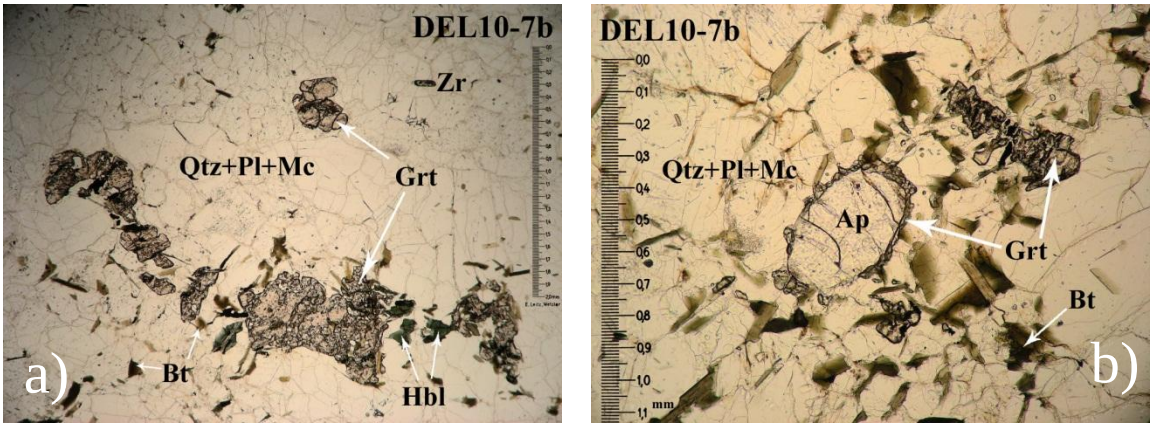

Figure 3.8: Photomicrographs of sample DEL10-7b. (a) and (b): representative areas in PPL.

Scapolite, garnet and some biotite and hornblende are likely to be metamorphic and not part of the original magmatic assemblages. Modal amounts of quartz and plagioclase are 21 % and 79 %, respectively, corresponding to a tonalite.

DEL10-7b:

Cores of metaplutonic orthogneiss host rock for the amphibolite and tonalite xenoliths were taken from Messer Farm (Fig. 1.3; location 7). The core location was selected at the most felsic domain in the outcrop (Fig. 3.7) interpreted to be the best representation of the original orthogneiss protolith. The assemblage is quartz + plagioclase + microcline + biotite (Fig. 3.8) with minor garnet, ilmenite, scapolite, and hornblende. Accessory minerals include apatite, titanite, and zircon. Grains display granoblastic texture with no crystallographical or shape preferred orientation, although a compositional layering (magmatic flow banding?) is apparent in outcrop (Fig. 3.8). Garnet occurs as fine grained anhedral porphyroblasts (Fig. 3.8) and as caronas around apatite (Fig. 3.8b). Modal abundances are 35 % quartz, 35 % plagioclase, and 30 % alkali-feldspar, corresponding to granite.

DEL10-7e:

This sample is another example of metaplutonic orthogneiss collected at the Messer Farm. The sample has a weakly developed lineation and no foliation (Fig. 3.9). The mineral assemblage is quartz + plagioclase + biotite + orthoclase + hornblende + garnet + scapolite (Figs. 3.10a; 3.10b). Accessory minerals include ilmenite, zircon, and apatite. Biotite occurs in aggregates up to 3 mm in diameter (Fig. 3.9c). Modes are 30 % quartz, 50 % plagioclase, and 20 % alkali-feldspar, corresponding to granodiorite.

Figure 3.9: Slab cut parallel to lineation from hornblende gneiss sample DEL10-7e. Ruler units are in cm.

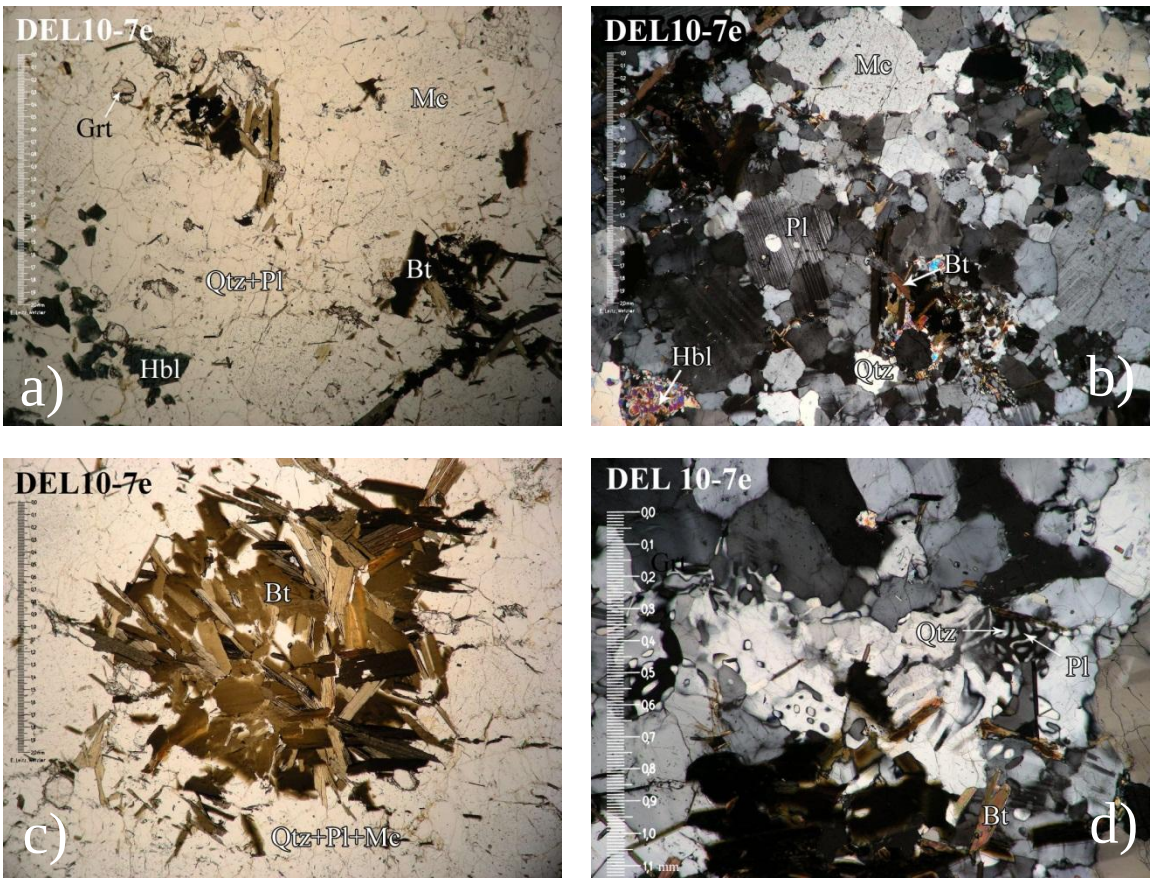

Figure 3.10: Photomicrographs of a thin section from hgn-DEL10-7e: (a) representative area in PPL; (b) representative area in XPL; (c) biotite aggregate from retrograde recrystallization of garnet in PPL; (d) myrmekite texture shown in XPL.

Figure 3.11: Slab sawn from hornblende gneiss sample DEL10-11 showing a distinct compositional banding defining foliation. Ruler units are cm.

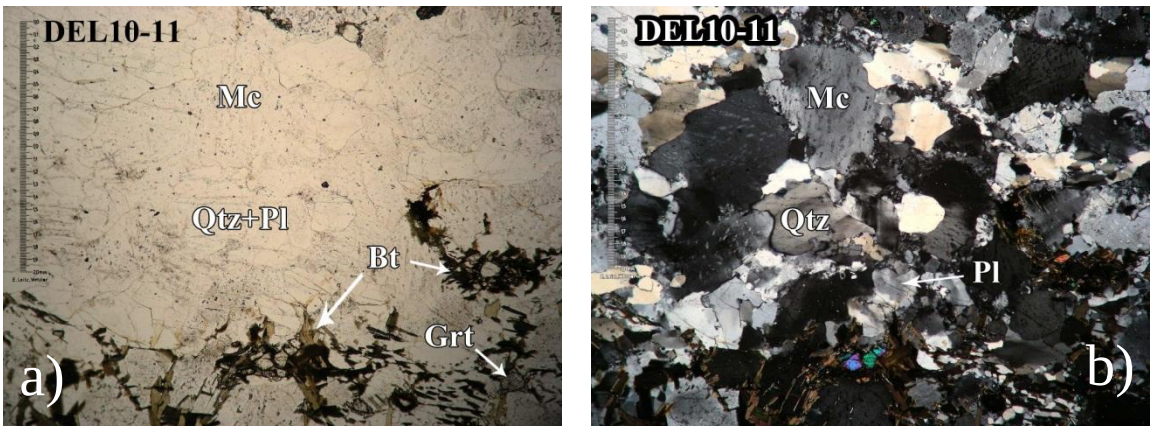

Figure 3.12: Photomicrographs of a thin section from hgn-DEL10-11: (a) representative area in PPL; (b) representative area in XPL.

DEL10-11:

This sample of orthogneiss and was collected from a road cut on Holiday Road in The Preserve subdivision off Route 276 (Jonathan Creek Road; Fig. 1.3; location 11). A prominent foliation is defined by alternating layers of varying mafic mineral content (Fig. 3.11), a mineral assemblage of microcline + quartz + biotite + plagioclase + hornblende + (Figs. 3.12a; 3.12b), and accessory scapolite, apatite, zircon, and garnet. The mode is 37 % quartz, 12 % plagioclase, and 51 % microcline, corresponding to granite.

Amphibolite

DEL10-7c:

Cores of a garnet amphibolite xenolith in orthogneiss at Messer Farm consist of hornblende + plagioclase + garnet + biotite + scapolite (Fig. 3.14a) with accessory zircon, apatite, epidote, ilmenite, and titanite. Garnets appear as mm sized porphyroblasts.

DEL10-7d:

This sample is also a garnet amphibolite xenolith in orthogneiss from Messer Farm (Figs. 3.13 and 3.14b). Hornblende ranges from subhedral to anhedral and occasionally displays oriented inclusions. The mineral assemblage is hornblende + plagioclase + garnet + biotite (Fig. 3.14b) with accessory zircon, apatite, epidote, ilmenite, and titanite. The grain size in DEL10-7d is slightly coarser than DEL10-7c (Fig. 3.14), otherwise the amphibolite xenolith samples are very similar.

Figure 3.13: Photograph of slab of amphibolite DEL10-7d. Ruler units are cm.

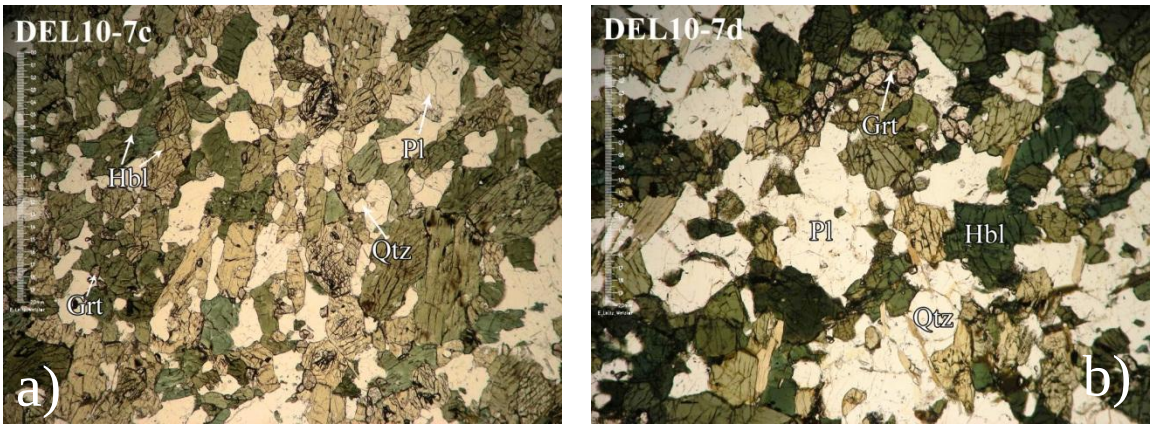

Figure 3.14: Representative photomicrographs in PPL of thin sections from amphibolite samples DEL10-7c (a) and DEL10-7d (b).

Augen Gneiss

DEL10-29:

This sample was collected from a road cut in the Creek Stone subdivision off of Prosperity Ridge (Fig. 1.3; location 29). This sample has a strongly developed protomylonitic foliation with cm-sized microcline porphyroclasts (Figs. 3.15; 3.16a; 3.16b). The mineral assemblage is quartz + microcline + plagioclase + biotite + epidote ± muscovite ± clinopyroxene with accessory apatite, titanite, zircon, allanite (Fig. 3.16c), and scapolite. The mode is 30 % quartz, 40 % plagioclase, and 30 % microcline, corresponding to granite.

DEL10-30:

This sample was collected from a road cut on Prosperity Ridge approximately 0.5 km south of sample DEL10-29 (Fig. 1.3; location 29). The sample has a well-developed foliation defined by flattened porphyroclasts and alternating mafic and felsic layers, and contains cm-sized plagioclase and microcline augen (Fig. 3.15). The mineral assemblage is quartz + plagioclase + microcline + biotite + epidote ± muscovite ± clinopyroxene with accessory apatite, titanite, zircon, and scapolite. Myrmekite texture is present locally (Fig. 3.16f), and biotite is twinned.

Figure 3.15: Photographs of slabs of (a) agn-DEL10-29 and (b) agn-DEL10-30. Ruler units are cm.

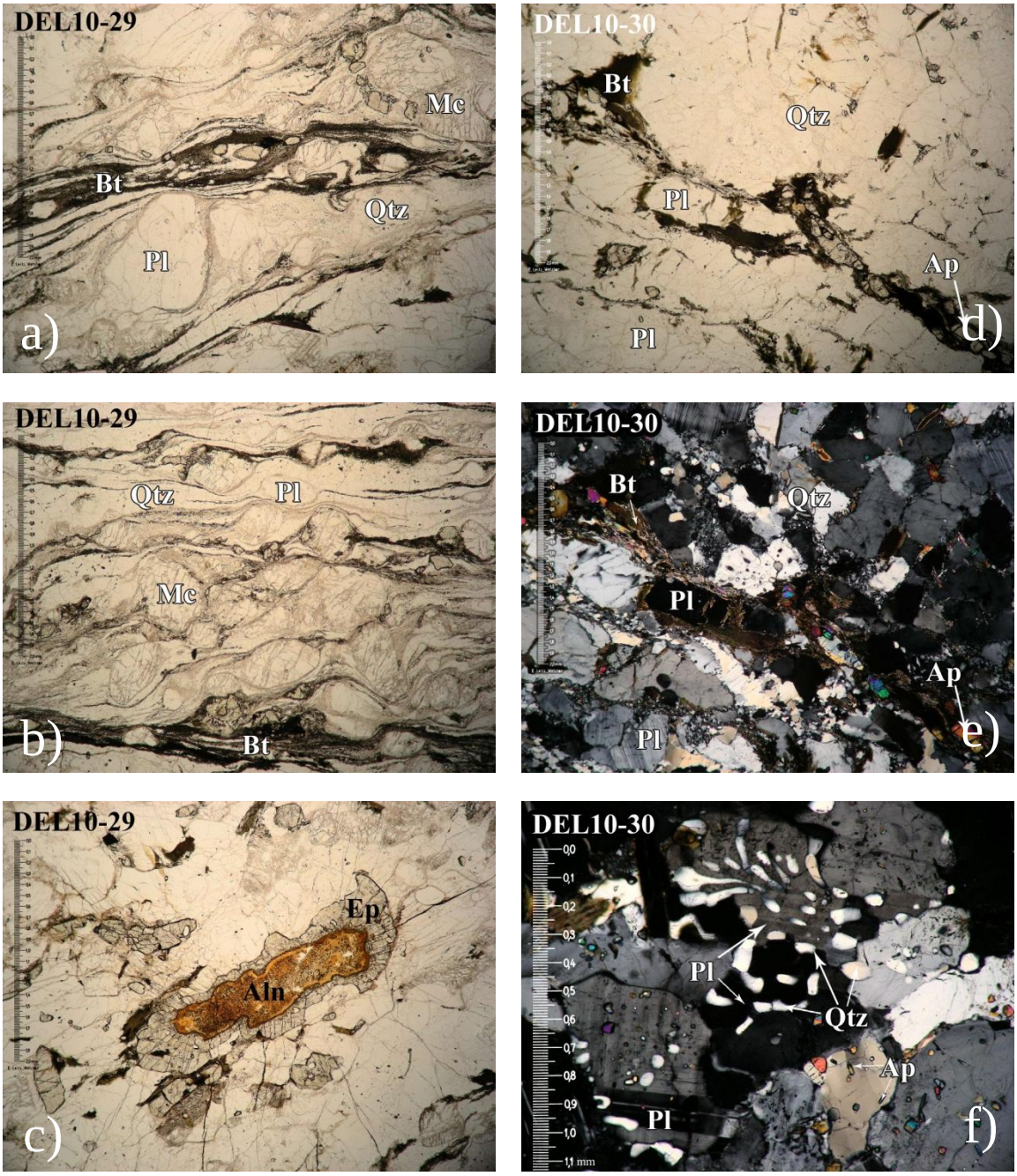

Figure 3.16: Photomicrographs of thin sections from augen gneiss samples DEL10-29 and DEL10-30: (a) representative example in PPL displaying the foliation of the sample; (b) rolled feldspar grains shown in PPL; (c) metamict allanite grain with epidote overgrowth; (d) representative example in PPL; (e) representative example in XPL; (f) myrmekite texture shown in XPL.

CHAPTER IV. RESULTS OF GEOCHEMISTRY

Whole Rock Major Element Geochemistry

Harker variation diagrams display numerous compositional trends (Fig. 4.1). K_2O increases with increasing SiO_2 content whereas Na_2O shows no relationship to SiO_2. CaO, MnO, MgO, TiO_2, Fe_2O_3, P_2O_5, and Al_2O_3 display a general decrease in concentration with increased SiO_2.

Augen gneiss sample DEL10-29 is the most felsic sample and differs from the other augen gneiss DEL10-30 by 12 wt. % SiO_2. There is also a notable difference in SiO_2 among the metaplutonic orthogneisses from Messer Farm. Hgn-DEL10-7b is the most felsic sample, exceeding hgn-DEL10-7e by 7 wt. % SiO_2. Bgn-ASH08-9-1a and tx-DEL10-7a have SiO_2 concentrations near 49 wt. % similar to the amphibolites amx-DEL10-7c and amx-DEL10-7d. These four samples have similar whole rock major element geochemistry, though bgn-ASH08-9-1a has a higher concentration of TiO_2. Agn-DEL10-30 and hgn-DEL10-7e have similar concentrations in SiO_2, K_2O, CaO, and MgO compared to mpg-MP04-2, but are more sodic and aluminous.

Most samples define a calc-alkaline trend (Fig. 4.2). Loughry (2010) reports a tholeiitic trend for the Dellwood quad amphibolites of basaltic composition. The tholeiitic samples in this study may be part of the same magmatic system, but there are insufficient data here to be conclusive.

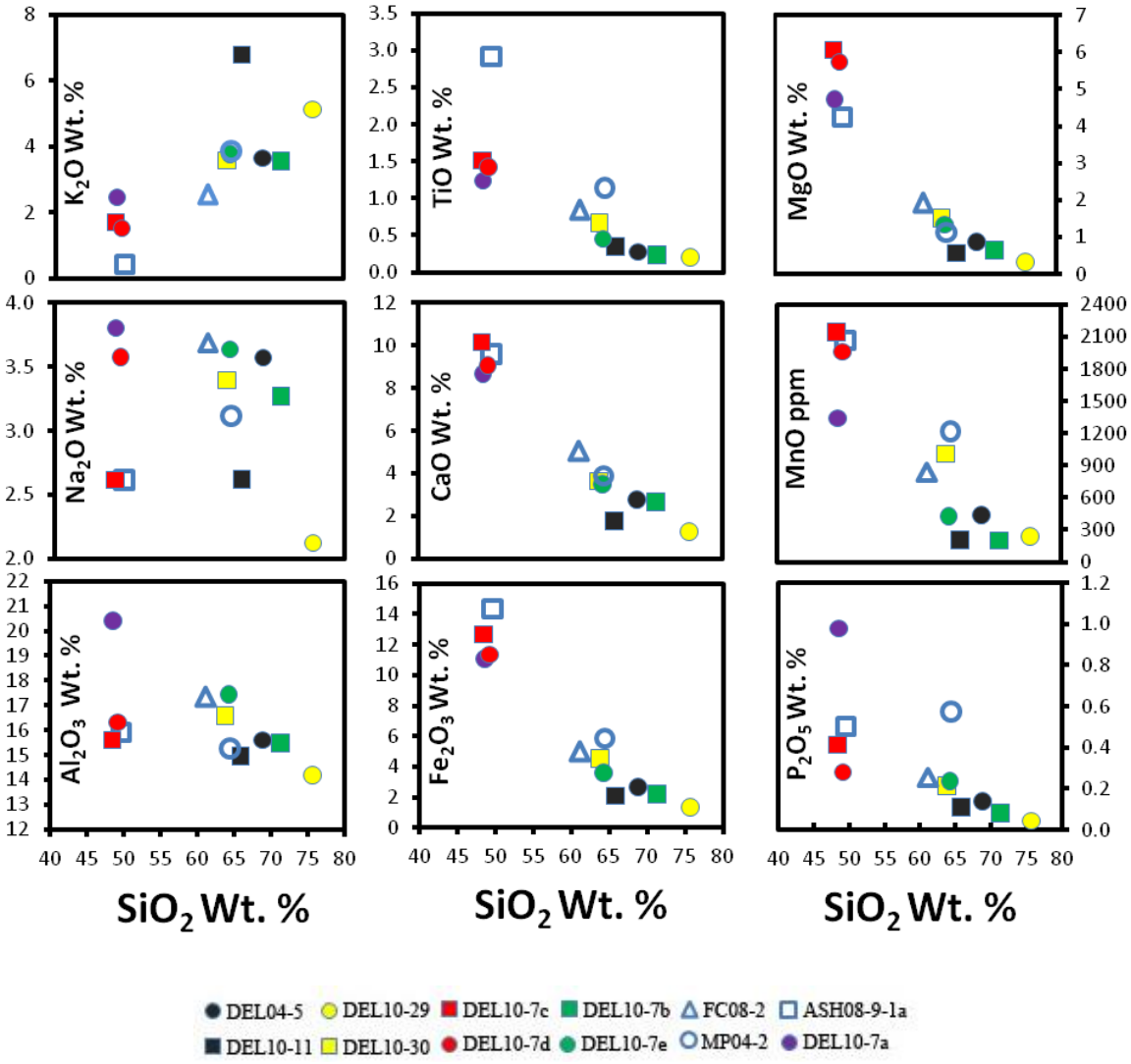

Figure 4.1: Harker variation diagrams for Dellwood area basement lithologies. Colors correspond to lithology: red-amphibolite; yellow-augen gneiss; green-metaplutonic orthogneiss; black-deformed orthogneiss.

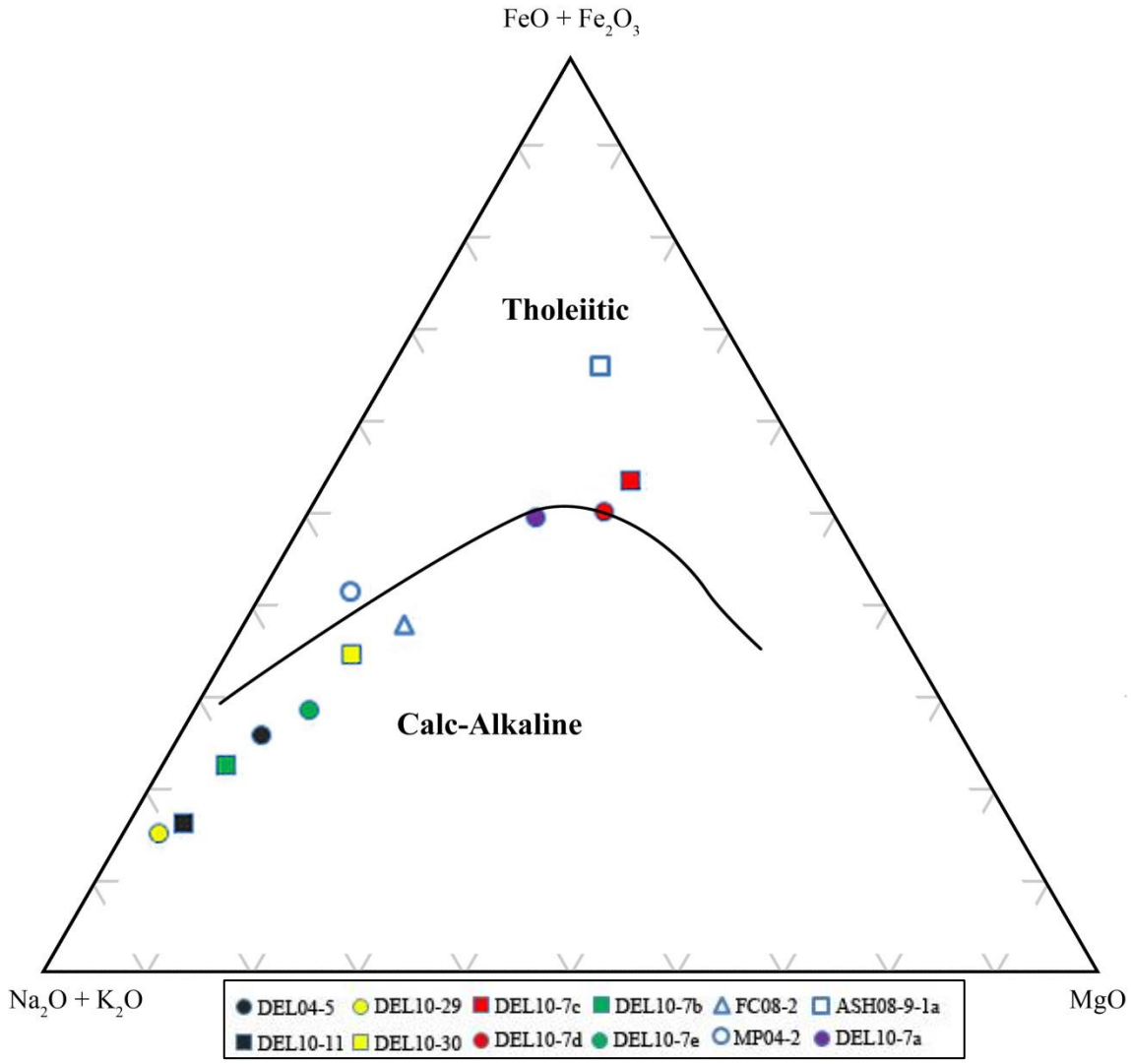

Figure 4.2: AFM diagram of whole rock geochemistry. Symbols are as in Figure 4.1.

Whole Rock Sm and Nd Geochemistry

Epsilon Nd values (ε_{Nd}; DePaolo and Wasserburg, 1976) were calculated and plotted to show the isotopic evolution of Nd in Dellwood samples through time (Fig. 4.3) (Appendix D). Present day values ($\varepsilon_{Nd(0)}$) range from -10 to -21. Biotite gneiss and amphibolite have the least negative $\varepsilon_{Nd(0)}$ values (approximately -10) whereas the orthogneisses and tonalite xenolith have values ranging from -12 to -21. These data evolve back to depleted mantle model ages (T_{DM}) that range from 1.52 (bgn-DEL08-2d and hgn-DEL10-7b) to 1.79 Ga (tx-DEL10-7a). T_{DM} ages are older than their corresponding crystallization ages (1040 to 1342 Ma) by 200 to 650 Ma. At the time of crystallization, ε_{Nd} values range from -3.4 (hgn-DEL10-11) to 2.1 (amx-DEL10-7d). Epsilon evolution trendlines (excluding hgn-DEL10-11, amx-DEL10-7d, bgn-DEL08-2d, and tx-DEL10-7a) converge at a focal point *ca.* 1.25 Ga.

Feldspar Pb Geochemistry

Various lithologies analyzed for feldspar isotopic Pb compositions plot in present day uranogenic Pb space ($^{207}Pb/^{204}Pb$ vs. $^{206}Pb/^{204}Pb$) between arrays defined by the southern and central Appalachian dataset of Fisher et al. (2010) and what they refer to as "juvenile Laurentia" (Fig. 4.4). Only one datum for this study (hgn-DEL10-11) plots above the Stacey and Kramers (1975) two-stage evolution of average crustal Pb, but is not considered anomalous. Most samples overlap a range of values defined by juvenile Laurentia/Granite-Rhyolite province and previous southern and central Appalachian arrays (Fisher *et al.,* 2010). Feldspar in sample tx-DEL10-7a represents the only extreme values, which plot distinctly within the juvenile Laurentian isotopic Pb domain. $^{206}Pb/^{204}Pb$ ratios of all samples range from 16.94 to 17.69. The range in $^{206}Pb/^{204}Pb$

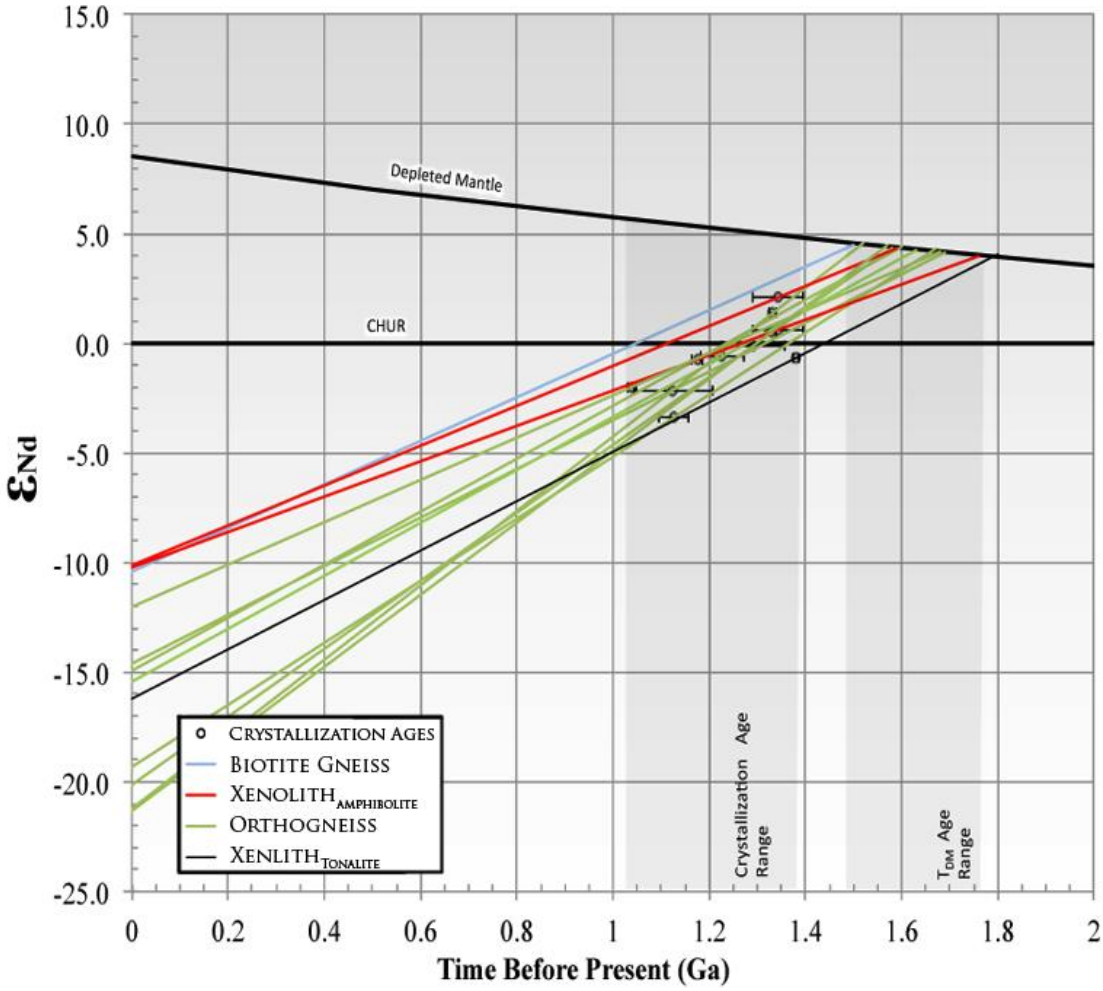

Figure 4.3: Isotopic evolution of Nd (in epsilon units, ε_{Nd}) in Dellwood basement rocks compared to the chondritic uniform reservoir (CHUR) line and depleted mantle growth curve (DePaolo, 1981). The shaded regions highlight the crystallization and T_{DM} age ranges. Individual crystallization ages are labeled by black circles. Age error bars shown are 2σ. The red lines represent amphibolite samples DEL10-7c and DEL10-7d. The blue line represents a metaclastic sample bgn-DEL08-2d, so no crystallization age is displayed.

ratios is much smaller for Dellwood basement than for that of juvenile Laurentia, Amazonia, or other Appalachian data (DeWolf and Mezger, 1994; Tohver *et al.,* 2004; Fisher *et al.,* 2010), though it should be noted that the data set in this study represents fewer samples collected in a much more limited area than other studies used for comparison. These uranogenic Pb values define an array that spans the boundary between juvenile Laurentia (DeWolf and Mezger, 1994; Fisher *et al.,* 2010) and Amazonian data (Fig. 4.4; Tohver *et al.*, 2004). Thorogenic Pb shows a greater differentiation between feldspar and whole rock data in that whole rock data tend to have higher $^{206}Pb/^{204}Pb$ and $^{208}Pb/^{204}Pb$ ratios (Fig. 4.5).

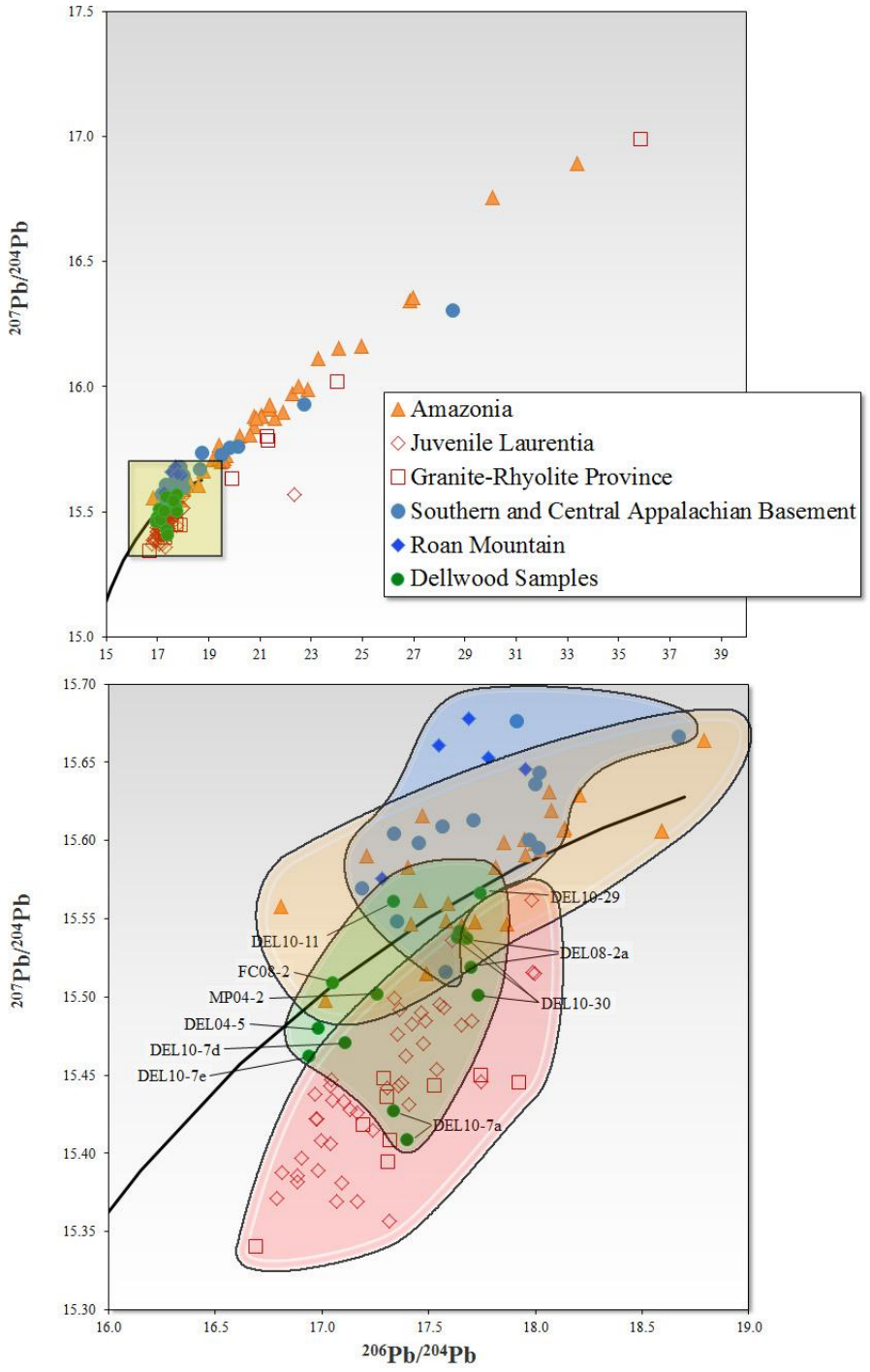

Figure 4.4: Present day uranogenic feldspar Pb isotope compositions of Dellwood area samples compared with previous whole rock (WR) and feldspar data of Proterozoic rocks in eastern North America (Laurentian feldspars: DeWolf and Mezger, 1994; WR Amazonia: Tohver *et al.*, 2004; WR Southern and Central Appalachian Basement and Roan Mountain: Fisher *et al.*, 2010). Red data represent juvenile Laurentian crust, blue data represent exotic Appalachian crust. The black line represents the Stacey and Kramers (1975) average Pb growth curve. The bottom plot is an enlargement of data located within the highlighted field on the upper plot.

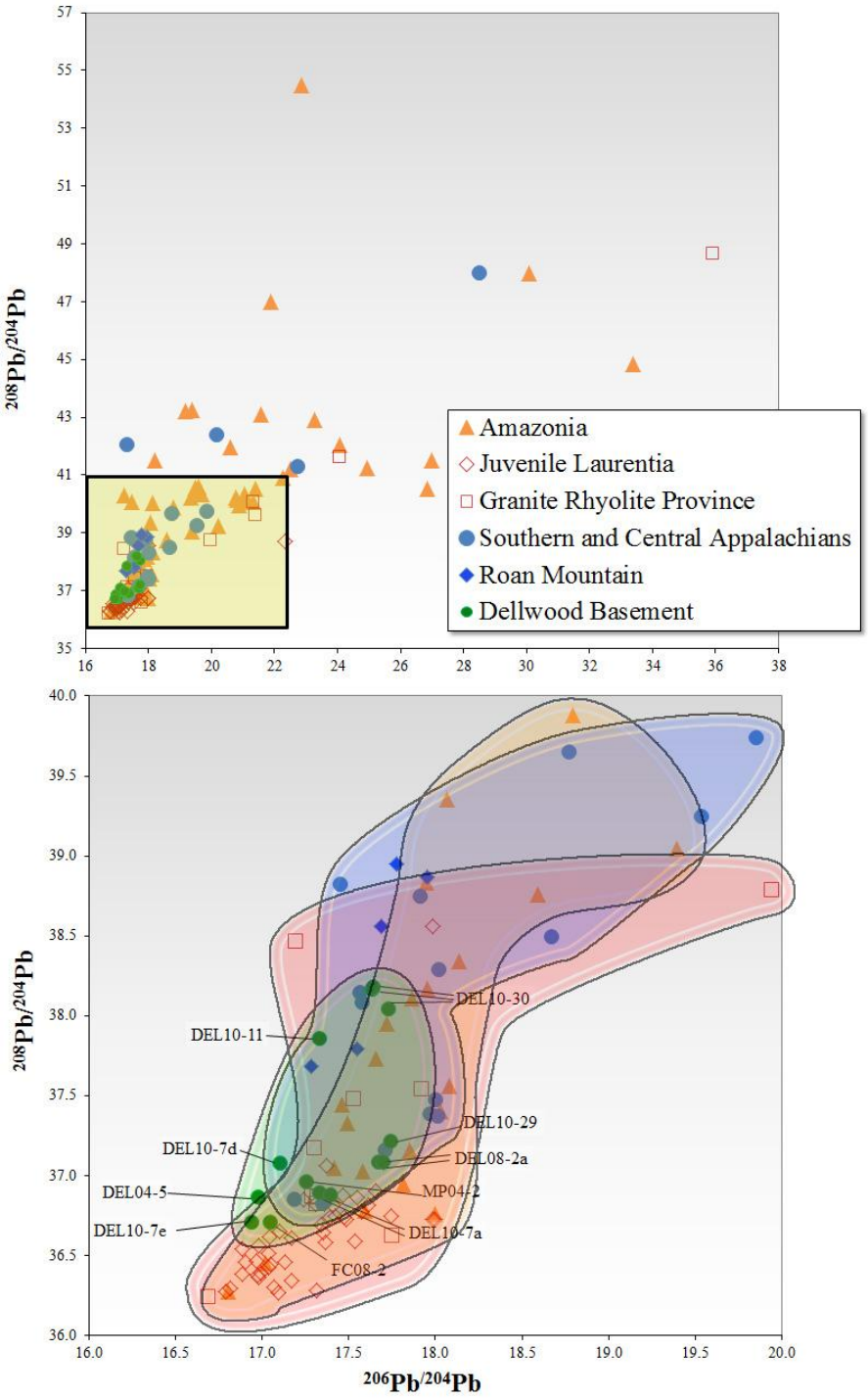

Figure 4.5: Present day thorogenic feldspar Pb isotopic compositions of Dellwood area samples compared with previous whole rock (WR) and feldspar data of Proterozoic rocks in eastern North America (Laurentian feldspars: DeWolf and Mezger, 1994; WR Amazonia: Tohver *et al.*, 2004; WR Southern and Central Appalachian Basement and Roan Mountain: Fisher *et al.*, 2010). Red data represent juvenile Laurentian crust, blue data represent exotic Appalachian crust. The bottom plot is an enlargement of data within the highlighted field on the upper plot.

CHAPTER V. RESULTS OF U-PB ZIRCON GEOCHRONOLOGY

Cores of magmatic zircon for samples hgn-DEL10-7b and agn-DEL10-30 were analyzed to determine magmatic crystallization ages at the Curtin University (Perth, Western Australia) John de Laeter Centre on the Sensitive High Resolution-Ion Micro Probe (SHRIMP-II). Zircon from all other samples was analyzed at the Arizona LaserChron Center at the University of Arizona on the Nu Plasma high resolution-multicollector-inductively coupled mass spectrometer (HR MC-ICPMS). The latter analyses included zircon from biotite gneiss samples ASH08-9-1a, DEL03-1, and DEL08-2e, which were analyzed to determine the nature of the protolith as igneous or sedimentary and their magmatic crystallization ages or detrital zircon age spectra. The cores, intermediate zones, and rims of zircon (interpreted based on CL images as inherited cores, a magmatic growth zone, and a metamorphic growth zone respectively) collected from hgn-DEL10-11 were analyzed to determine the magmatic crystallization ages and metamorphic growth age. Cores from agn-DEL10-29, amx-DEL10-7d, and tx-DEL10-7a were analyzed to determine magmatic crystallization ages.

Description of analytical procedures is found in Chapter II. The cutoff age used to distinguish ‘‘best ages” between $^{206}Pb/^{207}Pb$ and $^{206}Pb/^{238}U$ ages was 900 Ma on the basis that the $^{206}Pb/^{207}Pb$ ages are more precise for older systems whereas the $^{206}Pb/^{238}U$ ages are more precise for younger systems (Gehrels, 2008). Complete geochronologic data (U, Pb, Th contents; isotopic ratios) are compiled in Appendix D.

Augen Gneiss

Zircon from protomylonitic gneisses (agn-DEL10-29 and agn-DEL10-30) were analyzed to determine magmatic crystallization ages. Samples were collected at outcrops approximately 1 km apart, but the textures of zircon grains are significantly different and are expanded on below.

DEL10-29:

Sixteen subhedral to anhedral prismatic zircon grains from this sample were analyzed. Zircon from this sample generally contains fractures, exhibits iron staining, and has pocked edges. Many grains exhibit complex zoning (Fig. 5.1; *e.g.* grains 5, 10, and 14) whereas others exhibit unzoned dull cores (Fig. 5.1; *e.g.* grains 15, 17, and 20). Oscillatory zoning is present (Fig. 5.1 *e.g.* grains 1 and 6) but rare. Luminescent metamorphic rims are ubiquitous. However, these rims are < 20 μm in width and were too narrow to analyze via LA-ICP-MS.

Single spot ages range from approximately 1020 Ma to 1220 Ma. A concordia plot of 10 analyses yields an upper intercept age of 1179 ± 44 Ma (Fig. 5.2; MSWD = 2.0). A weighted mean 'best age' calculation yields a crystallization age of 1175 ± 11 Ma (Fig. 5.2; MSWD = 2.0, probability = 0.044). These two ages agree within error, but the weighted mean age of 1175 ± 11 Ma is more precise and is the proposed age of this sample.

DEL10-30:

Zircon in this sample exhibits more consistent oscillatory zoning than DEL10-29 (Fig. 5.3; grains 103-1, 103-11, 103-4, 103-14, 103-16, and 103-17). Grain 103-13 displays local intermediate resorption by a luminescent zone (Fig. 5.3). Luminescent

Figure 5.1: Cathodoluminescence images of zircon grains from agn-DEL10-29. Rings represent 20 μm LA spot locations. Green ages are analyses with anomalously high ^{204}Pb counts. Yellow ages are analyses with greater than 10 % $^{206}Pb/^{238}U$ error. These analyses were not included in the concordia or probability density plots. Errors are 1σ.

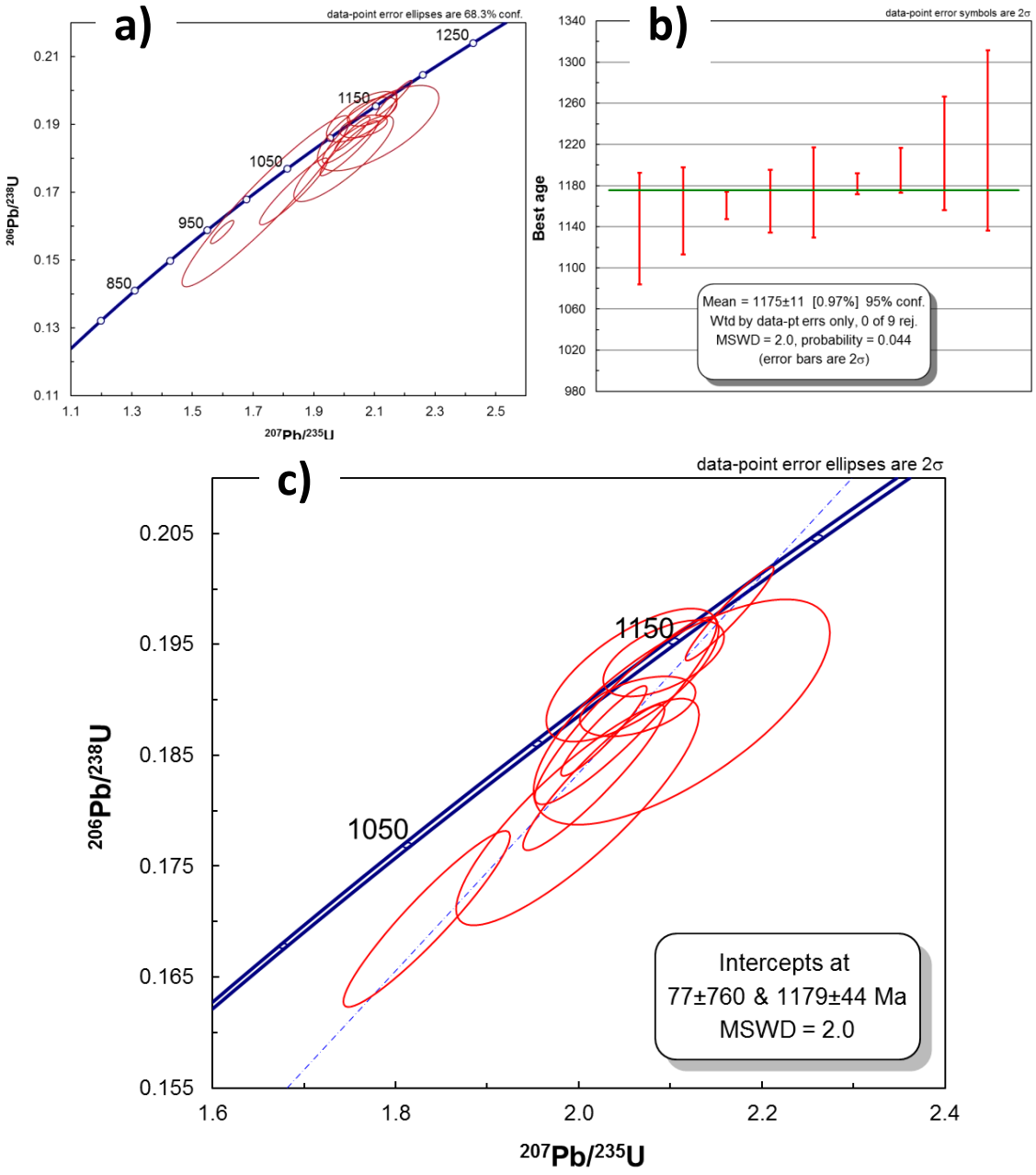

Figure 5.2: Age plots from agn-DEL10-29. All analyses are by LA-ICP-MS. (a) Concordia diagram of all sample data collected; (b) mean 'best age' plot of selected analyses; (c) Concordia diagram of selected analyses and best fit line with proposed upper intercept age.

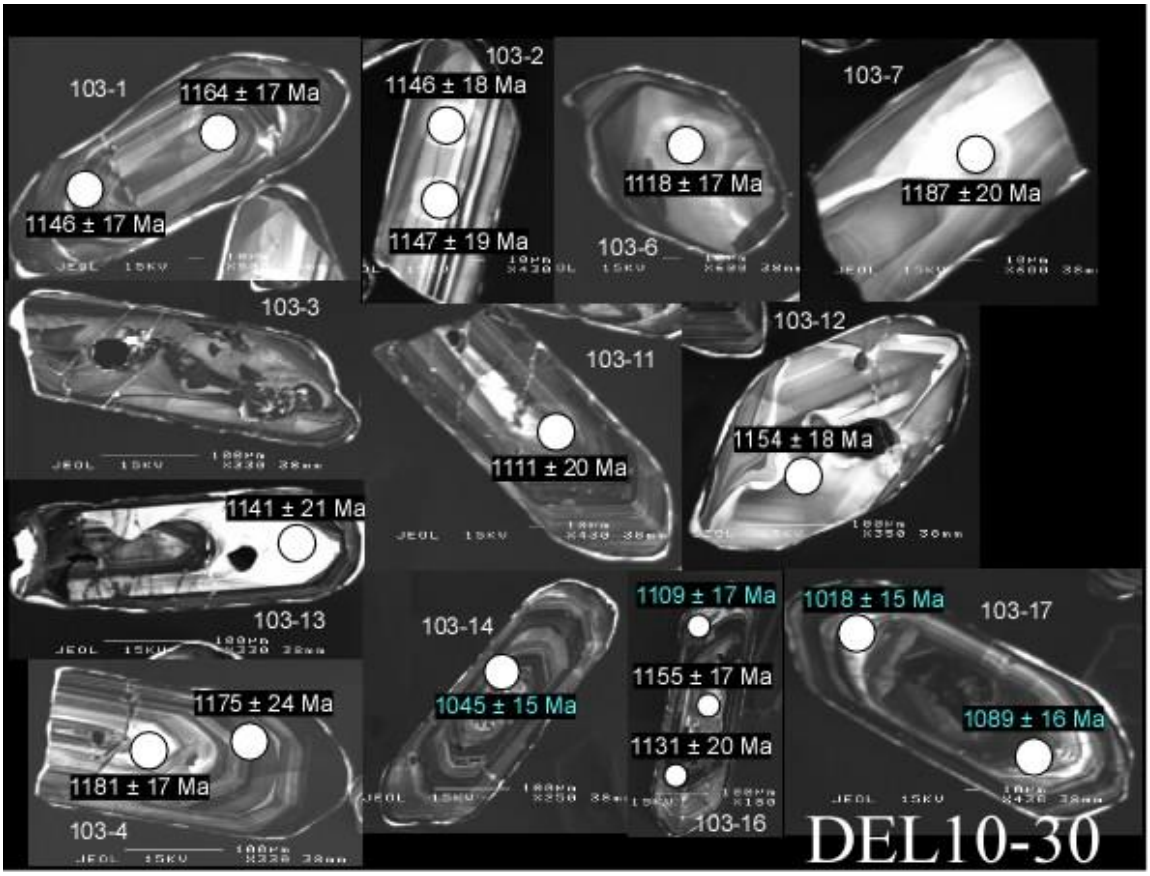

Figure 5.3: Cathodoluminescence images of zircon grains from agn-DEL10-30. Rings represent 30 μm SHRIMP II spot locations. Blue ages are analyses that were not included in the mean age calculation. Errors are 1σ.

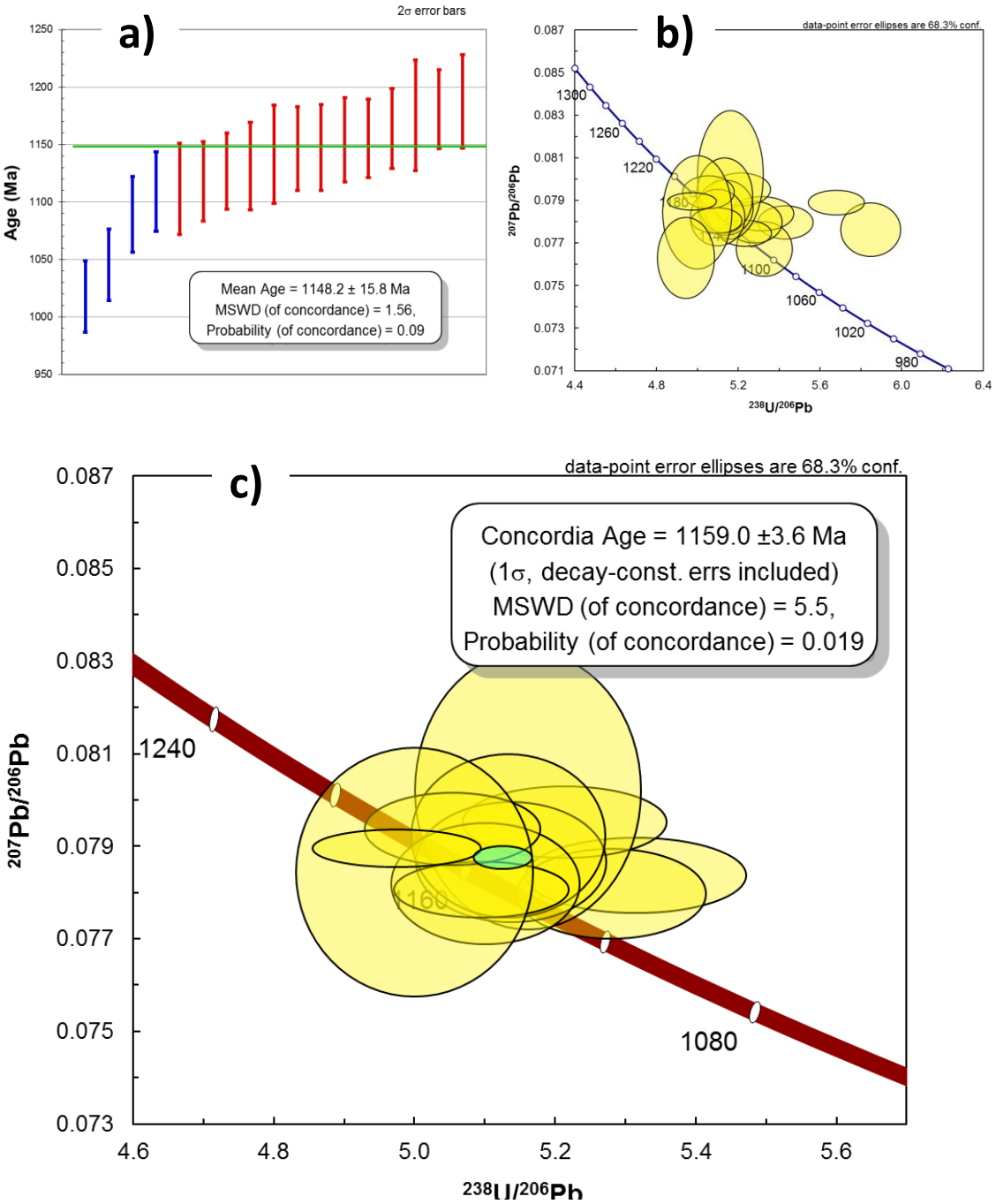

Figure 5.4: Tera-Wasserburg and mean age plots of zircon SHRIMP II analyses from agn-DEL10-30. (a) average 'best age' plot of sample of selected analyses, blue analyses were not included in the calculations; (b) Tera-Wasserburg plot of all data collected; (c) Tera-Wasserburg plot of selected analyses with proposed sample age.

metamorphic rims are ubiquitous. However, these rims are < 20 μm wide and were too narrow to analyze.

Single spot ages range from approximately 1020 Ma to 1190 Ma. A concordia age calculation is 1159 ± 4 Ma (Fig. 5.4; 1σ error, MSWD = 5.5, probability = 0.019). The proposed age is based on a weighted mean age calculation based on $^{206}Pb/^{238}U$ ages, which yielded an age of 1148 ± 15 Ma (Fig. 5.4; 2σ error, MSWD = 1.56, probability = 0.09). The weighted mean age is favored over the concordia age because of a lower MSWD value and a higher probability.

Hornblende Orthogneiss

DEL10-11:

Zircon grains are consistently prismatic and euhedral with very complex zoning patterns implying a complex zircon growth and recrystallization history for this sample. Most grains contain well defined prismatic xenocrystic cores (Fig. 5.5; grains 1, 2, 6, 7, 8, 9, 10, 13, and 16). One grain has an unzoned luminescent xenocrystic core within a second generation oscillatory zoned xenocrystic core (Fig. 5.5; grain 20). Grain 6 exhibits chaotic irregular zoning (Fig. 5.5). Other xenocrystic cores are oscillatory zoned or unzoned. Most cores have thin luminescent rims that appear similar to typical metamorphic rims (Fig. 5.5; grains 2, 4, 8, 9, 10, 14, 15, and 20). Large intermediate non-luminescent (dull) homogeneous zones and large luminescent rims are present in all grains. Ten rims, nine intermediate cores, and eleven xenocrystic cores were analyzed to determine age and growth histories. This sample has an unusually high percentage (40%) of analyses that exhibit more than 5 % reverse discordance, which motivated a larger

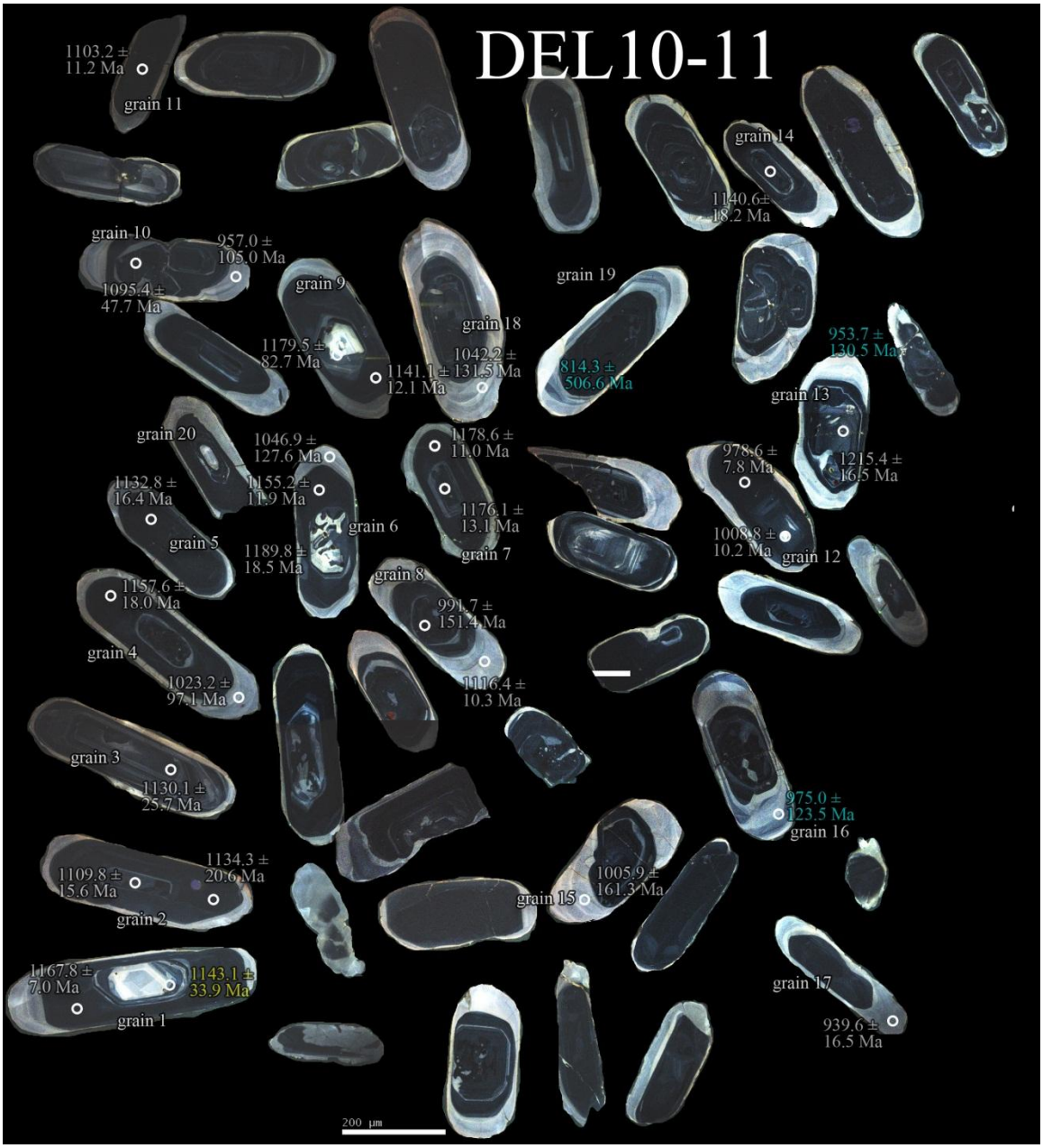

Figure 5.5: Cathodoluminescence images of zircon grains from hgn-DEL10-11. Rings represent 20 µm LA spot locations. Blue ages are analyses with more than 10 % reverse discordance. Yellow ages are analyses with anomalously greater than 10 % $^{206}Pb/^{238}U$ error. These analyses were not included in the concordia or probability density plots. Errors are 1σ.

cutoff of 10 % reverse discordance for single spot ages used in concordia and weighted mean ‘best age’ calculations.

Single spot ages for the bright rim zone range from approximately 810 Ma to 1120 Ma. A concordia age from 7 rim analyses was calculated to be 1038 ± 13 Ma (Fig. 5.6a; 2σ error, MSWD = 2.1). The weighted mean ‘best age’ of the same analyses is 1005 ± 47 Ma (Fig. 5.6b; 2σ error, MSWD = 0.38, probability = 0.89). The proposed age for the rim growth is proposed to be the concordia age of 1038 ± 13 Ma, opposed to the weighted mean ‘best age’, because it has a smaller error.

Intermediate core single spot ages are less consistent than rim analyses and range from approximately 980 Ma to 1180 Ma. A concordia best fit line of 6 analyses for the intermediate cores yields an upper intercept age of 1127 ± 30 Ma (Fig. 5.6c; 2σ error, MSWD = 1.8). The weighted mean ‘best age’ from the same set of analyses is 1160 ± 15 Ma (Fig. 5.6d; 2σ error, MSWD = 7.4, probability = 0.000). The single spot ages of xenocrystic cores range from approximately 990 Ma to 1220 Ma. Some xenocrystic core ages are younger than intermediate core or rim ages from the same grain (Fig. 5.5; grains 1, 2, 7, and 8), which is not possible. Tunneling into another zone is an unlikely explanation since an average age should still produce an age older then the surrounding crystal. More likely these xenocrystic cores were in isotopic equilibrium with younger intermediate zones, producing equivalent crystallization ages within error. Based on an upper intercept concordia age from 8 analyses of xenocrystic cores, the resulting age is 1130 ± 72 Ma (Fig. 5.6e; 2σ error, MSWD = 2.9). A weighted mean ‘best age’ calculation of the same set of analyses yields an age of 1115 ± 51 Ma (Fig. 5.6f; 2σ error, MSWD = 83, probability = 0.000). Concordia intercept ages are more precise and

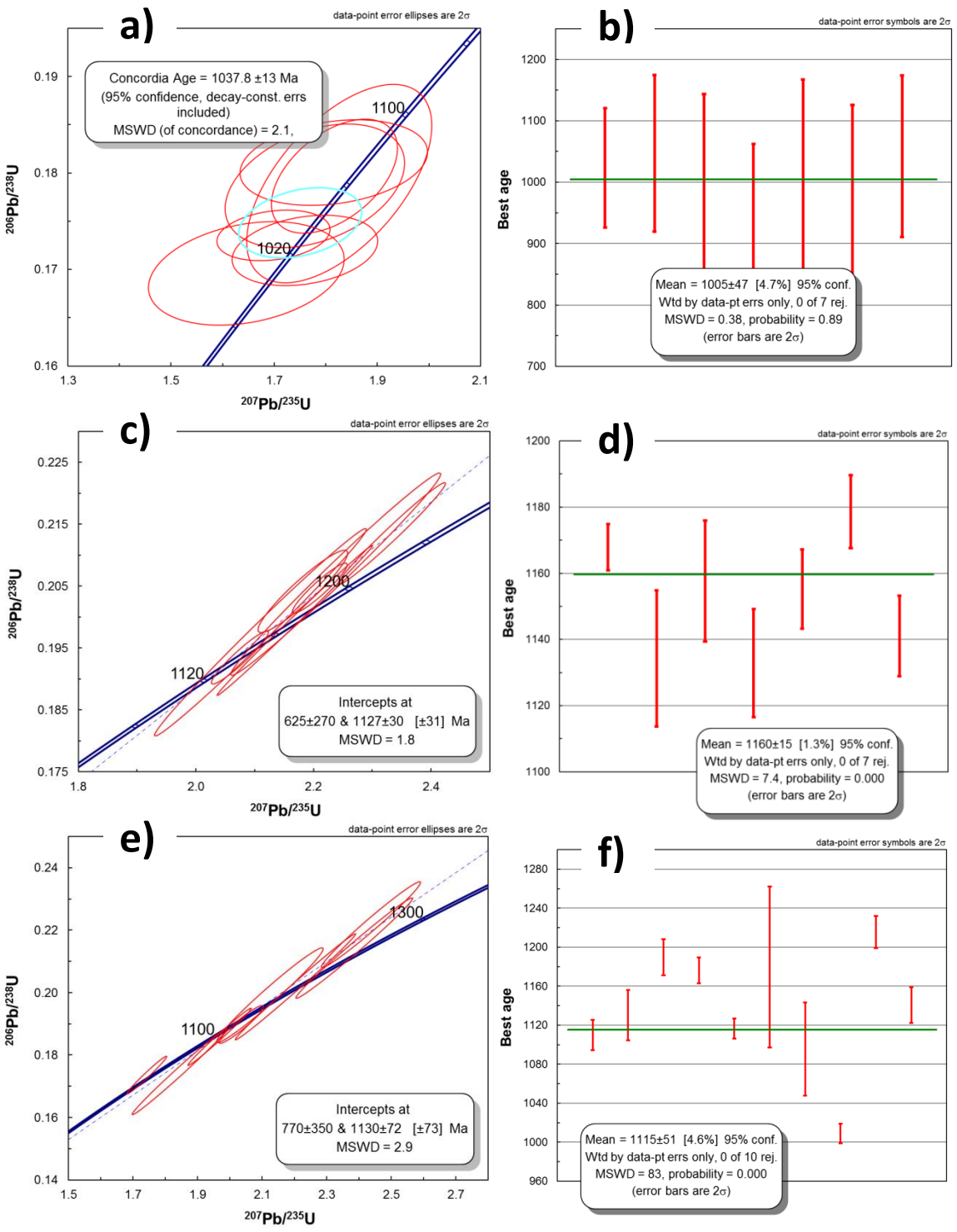

Figure 5.6: Results of LA-ICP-MS analyses showing concordia and mean 'best age' plots of zircon grains from sample hgn-DEL10-11. (a) Concordia age of rims; (b) mean 'best age' of rims; (c) Concordia upper intercept age of intermediate cores; (d) mean 'best age' of intermediate cores; (e) Concordia upper intercept age of inner cores; (f) mean 'best age' of inner cores.

accurate than the weighted mean ages, which have extremely high MSWD values and are poor estimations of core ages. Therefore, 1127 ± 30 Ma and 1130 ± 72 Ma are the proposed ages for the intermediate and xenocrystic core zones respectively.

Hornblende Gneiss and Xenoliths

Zircon from three samples collected at Messer Farm were analyzed to determine the geochronological relationships within the outcrop and to assess the potential of an older crustal component. These samples are tx-DEL10-7a and amx-DEL10-7d (xenoliths), and hgn-DEL10-7b (the host rock).

DEL10-7b: *hornlende gneiss (hgn)*

Zircon grains are consistently euhedral and consist almost entirely of oscillatory zoned cores with a thin luminescent rim (Fig. 5.7). Single spot ages in this sample range from approximately 1020 Ma to 1390 Ma. The Concordia age is 1331 ± 8 Ma (Fig. 5.8; 1σ error, MSWD = 6.6, probability = 0.010), but has a large MSWD value, which motivated the use of a weighted mean age calculation based on $^{206}Pb/^{238}U$ ages as the proposed ages of 1327 ± 17 Ma (Fig. 5.8a; 2σ error, MSWD = 1.4, probability = 0.13).

DEL10-7a: *tonalite xenolith (tx)*

Zircon grains were prepared in two separate mounts. The 7a.1 mount was polished to grain cores and the 7a.2 was (inadvertently) over-polished through the cores. Grain textures between the mounts are similar: both mounts have unzoned crystals (Fig. 5.9; *e.g.* grains 23 and 24) and crystals with zonation characteristic of diorite (Corfu *et al;* 2003; Fig. 5.9; *e.g.* grains 2, 8, and 20). Oscillatory zoning in grains is present but uncommon (fig 5.9; grains 9 and 4). Rims, if present, are thin and in some cases show

Figure 5.7: Cathodoluminescence images of zircon grains from sample hgn-DEL10-7b. Rings represent 20 μm SHRIMP II spot locations. Blue ages were not included in mean age calculation. Errors are 2σ.

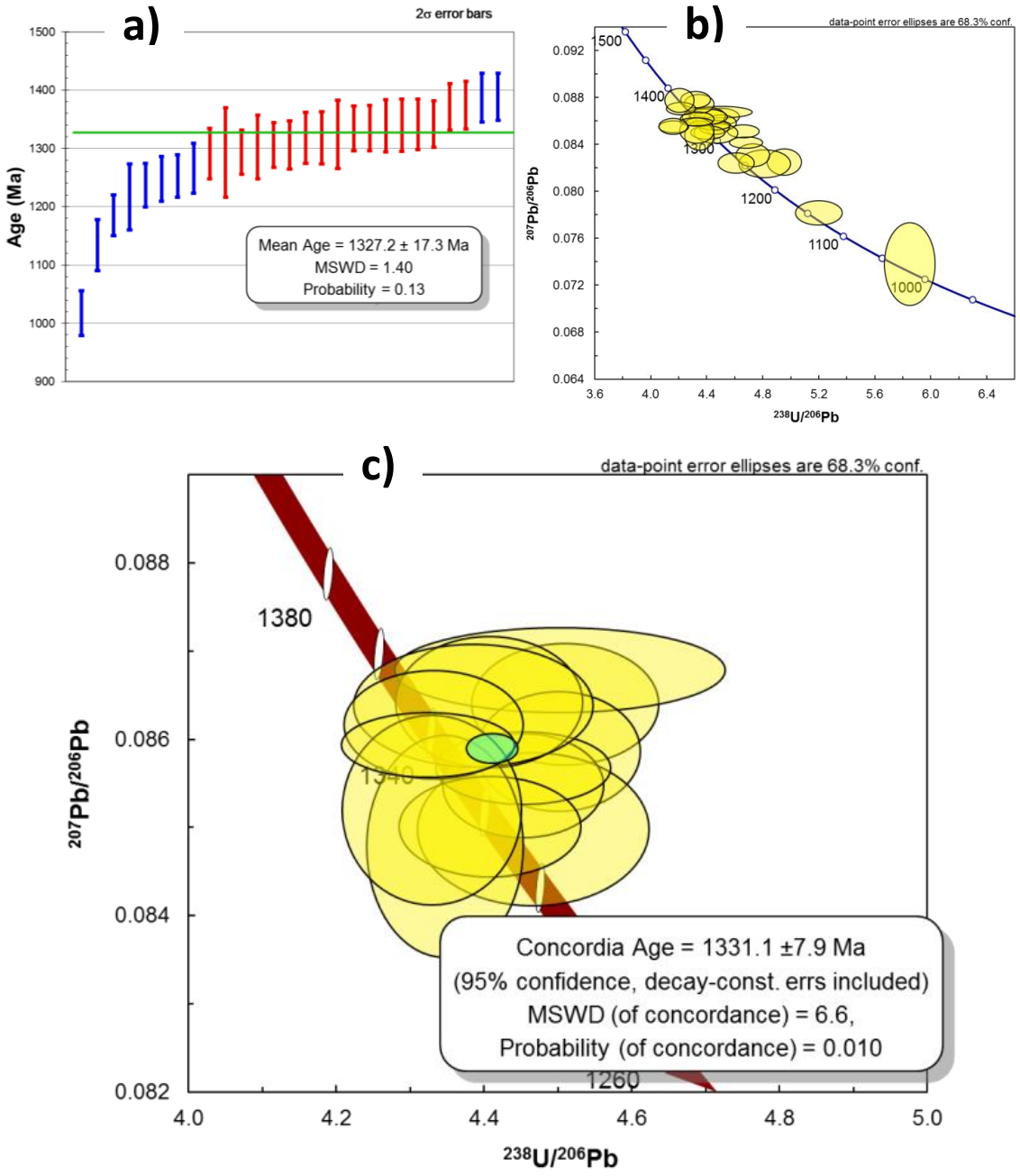

Figure 5.8: SHRIMP II zircon geochronology for hgn-DEL10-7-b. (a) mean 'best age' plot of selected analyses; (b) Tera-Wasserburg plot of all data collected; (c) Tera-Wasserburg plot of least discordant analyses with proposed age of the sample.

local intermediate resorption (Fig.5.9; grains 5, 17, and 23). Grains are generally subhedral with aspect ratios of 2:1 to 3:1.

Single spot ages in 7a.1 range from approximately 1150 Ma to 1440 Ma. The proposed age of this sample based on a mean 'best age' calculation is 1381 ± 6 (Fig. 5.11e; 1σ error, MSWD = 0.31, probability = 0.93). A concordia upper intercept age of 1385 ± 27 Ma (MSDW = 3.1) is within error of the weighted mean age but has a larger MSWD value. Ages in 7a.2 range from approximately 980 Ma to 1360 Ma. A weighted mean 'best age' calculation for selected data from this mount is 1315 ± 18 Ma (Fig. 5.11f; 1σ error, MSWD = 3.2, probability = 0.001). A concordia upper intercept age of 1324 ± 53 (MSWD = 50) is within error of the weighted mean age, but is discounted because of a higher MSWD value.

DEL10-7d: *amphibolite xenolith (amx)*

Zircon grains in this sample are anhedral to euhedral and prismatic. Consistent oscillatory zoning is present in several grains (Fig. 5.12; grains 13, 14, and 2). Other grains have consistent, dull, and unzoned cores (Fig. 5.12; grains 11 and 15). Some grains have patchy and irregular zoning (Fig. 5.12; grains 6, 7, 1, 3, and 8). Luminescent rims are ubiquitous and are typically less than 10 μm though some rims exceed 30 μm (Fig. 5.12; grains 7 and 9)

Single spot ages range from approximately 970 Ma to 1350 Ma. The proposed age of this sample is 1342 ± 53 Ma (Fig.5.13c; 2σ error, MSWD = 2.5) based on a concordia upper intercept. A mean 'best age' calculation yielded an age of 1328 ± 29 Ma (Fig. 5.13; 2σ error, MSWD = 5.6, probability = 0.000), which is within error of the concordia upper intercept age, but is considered to be less accurate because of a high MSWD value.

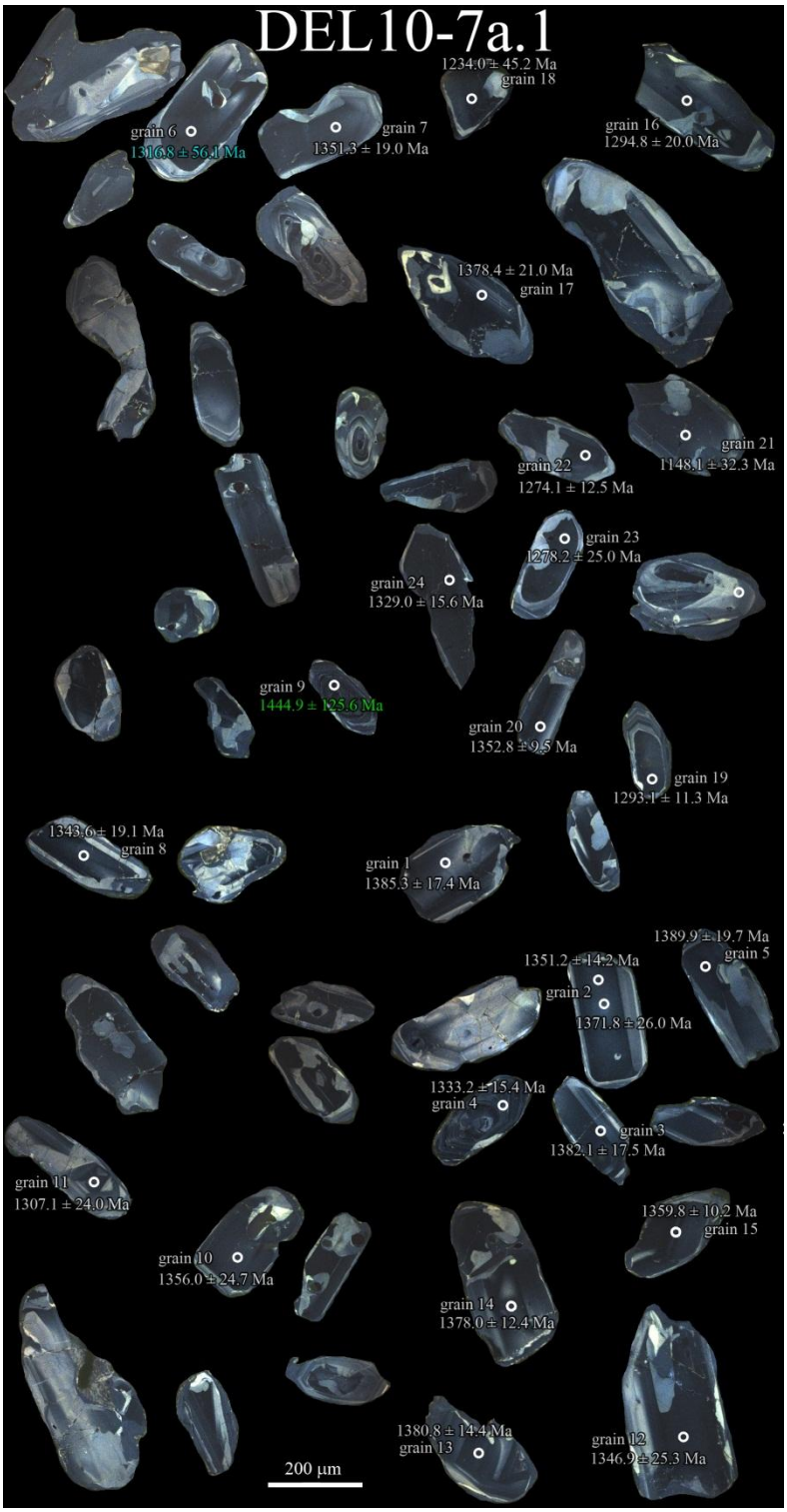

Figure 5.9: Cathodoluminescence images of zircon grains from sample tx-DEL10-7a.1. Rings represent 20 µm LA spot locations. Blue ages are analyses with more than 5 % reverse discordance. Green ages are analyses with anomalously high ^{204}Pb counts. These analyses were not included in the Concordia mean 'best age' plots. Errors are 1σ.

Figure 5.10: Cathodoluminescence images of zircon grains from tx-DEL10-7a.2. Rings represent 20 µm LA spot locations. Errors are 1σ.

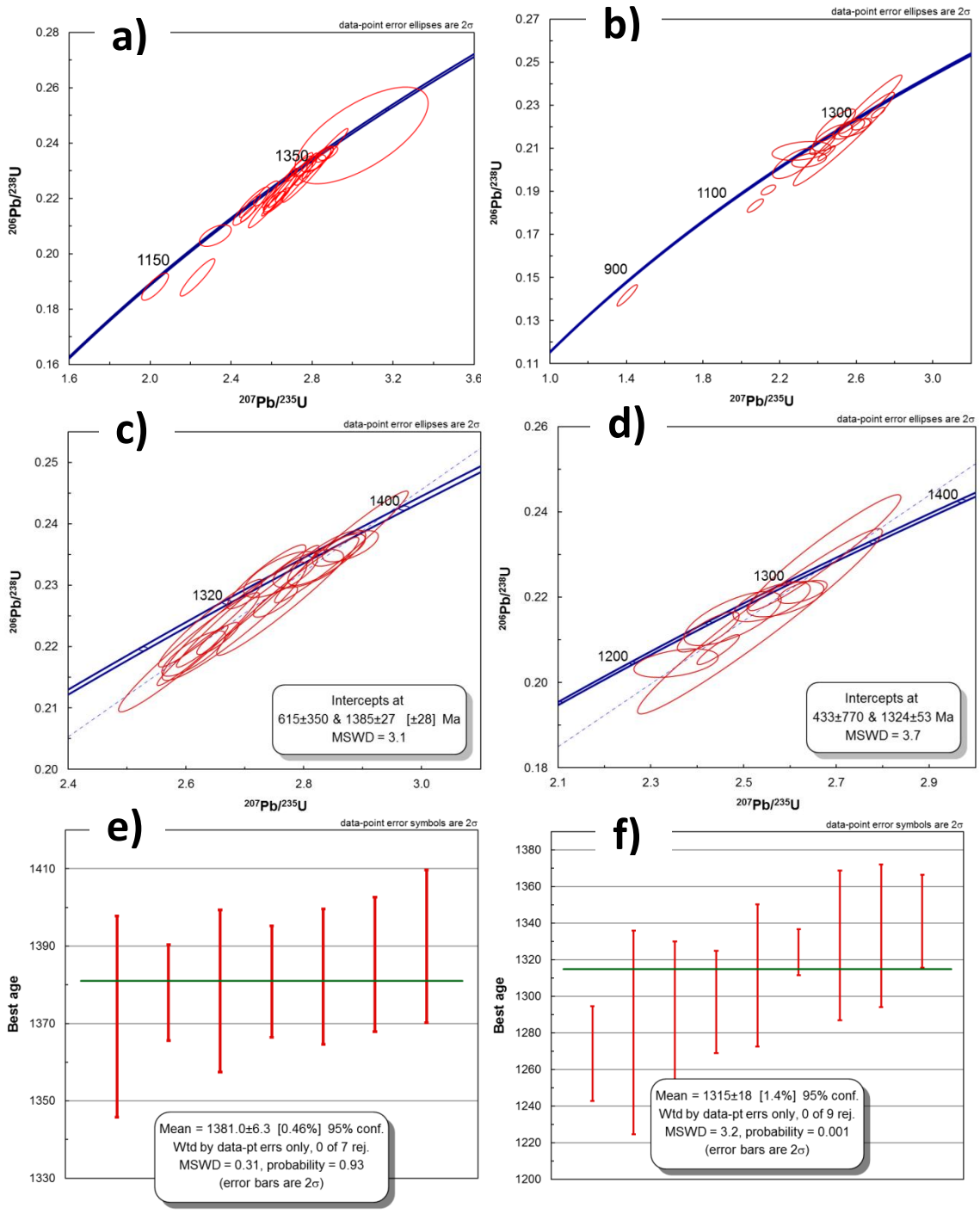

Figure 5.11: Results of LA-ICP-MS showing concordia and mean 'best age' plots of zircon analyses from tx-DEL10-7a. (a) Concordia of all 7a.1 data; (b) Concordia of all 7a.2 data; (c) Concordia upper intercept age of selected analyses from 7a.1; (d) Concordia upper intercept age of selected analyses from 7a.2; (e) mean 'best age' of inner selected analyses from 7a.1; (f) mean 'best age' of selected analyses from 7a.2.

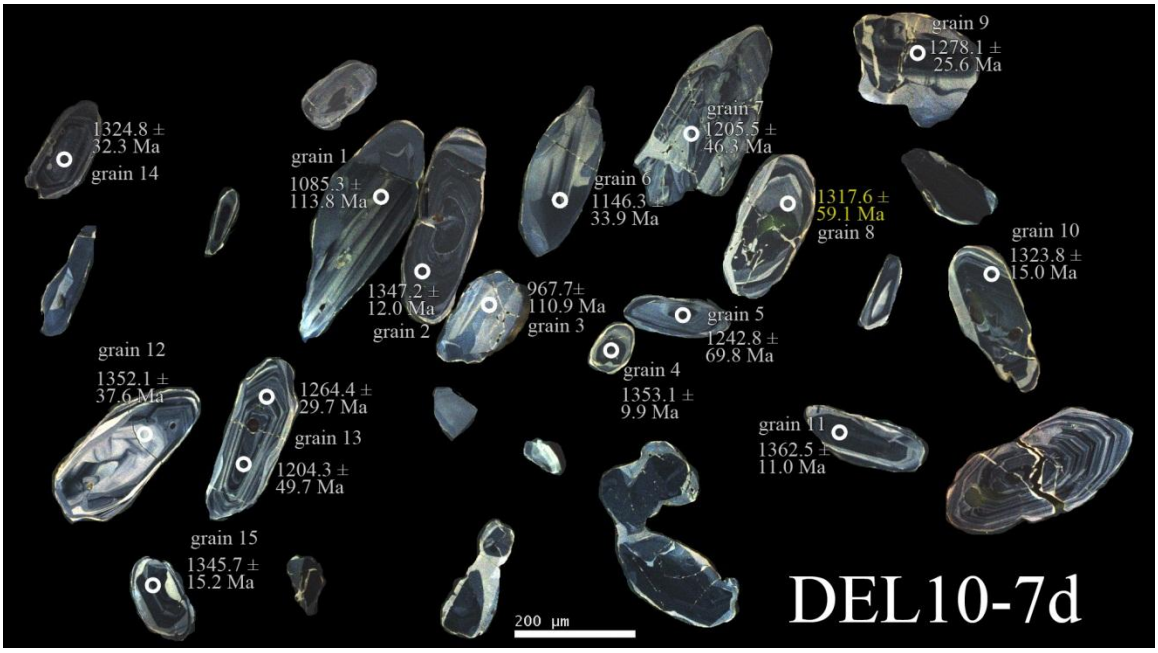

Figure 5.12: Cathodoluminescence images of zircon from amx-DEL10-7d: rings represent 20 µm LA spot locations. The yellow age is an analysis with greater than 10 % $^{206}Pb/^{238}U$ error. This analysis was not included in the Concordia or probability density plots. Errors are 1σ.

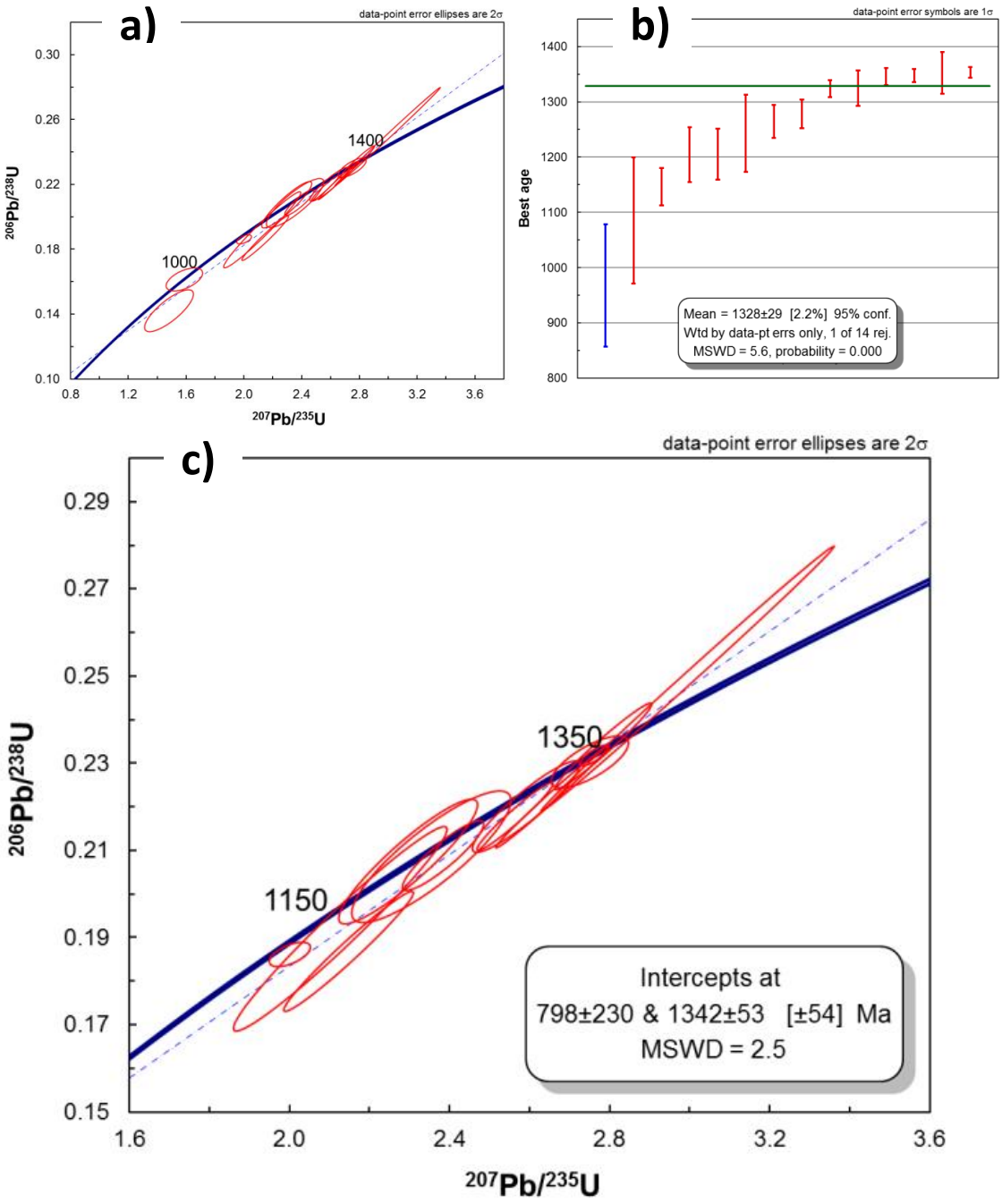

Figure 5.13: Geochronology of amx-DEL10-7d. (a) Concordia plot of all data collected; (b) mean 'best age' plot, blue analysis was omitted from calculations; (c) Concordia plot of selected data and proposed age of the sample.

Migmatitic Biotite Gneiss

A large number of zircon grains were analyzed for samples of biotite gneiss in order to ascertain the protolith character (igneous vs. sedimentary). An igneous rock should have a limited range of (crystallization) ages for zircon cores, whereas a sedimentary rock could exhibit a wide range of (detrital) zircon ages. All zircon analyses were guided by high contrast BSE imaging, which clearly revealed cores of grains. These images guided positioning of the laser to avoid analysis of overlapping growth zones.

ASH08-9-1a:

Cores of fifty-nine zircon grains of variable texture were analyzed. The majority of grains are subangular to well-rounded and equant though there are several prismatic examples (Fig. 5.14; grains 7, 10, 22, and 42). Grain 42 is euhedral with an aspect ratio of approximately 3:1, which is characteristic of leucocratic zircon and is thus interpreted to be a magmatic grain from leucosome formation during partial melting. Dating the leucosome growth age was not a goal of this study, so such grains were generally avoided. Back scatter electron (BSE) images show that cores are generally unzoned though some grains have distinct oscillatory zoning (Fig. 5.14; grains 10, 36, and 51). Some cores are metamict (Fig. 5.14; grains 7 and 19); these tended to occur with dense cracks and pits and were therefore analyzed outside of the core. Metamorphic rims are present and are of varying thickness (2 to 20 μm; e.g. Fig. 5.14; grains 19 and 23). Single spot ages range from approximately 450 Ma to 1850 Ma and occur in five distinct age modes (Fig. 5.17). Ages of all rims and several cores yielded ages *ca.* 460 Ma consistent with Taconian regional metamorphic growth (Fig. 5.17). Other grain morphologies do not clearly correlate to specific age modes. The largest age mode is *ca.* 1330 and there are two

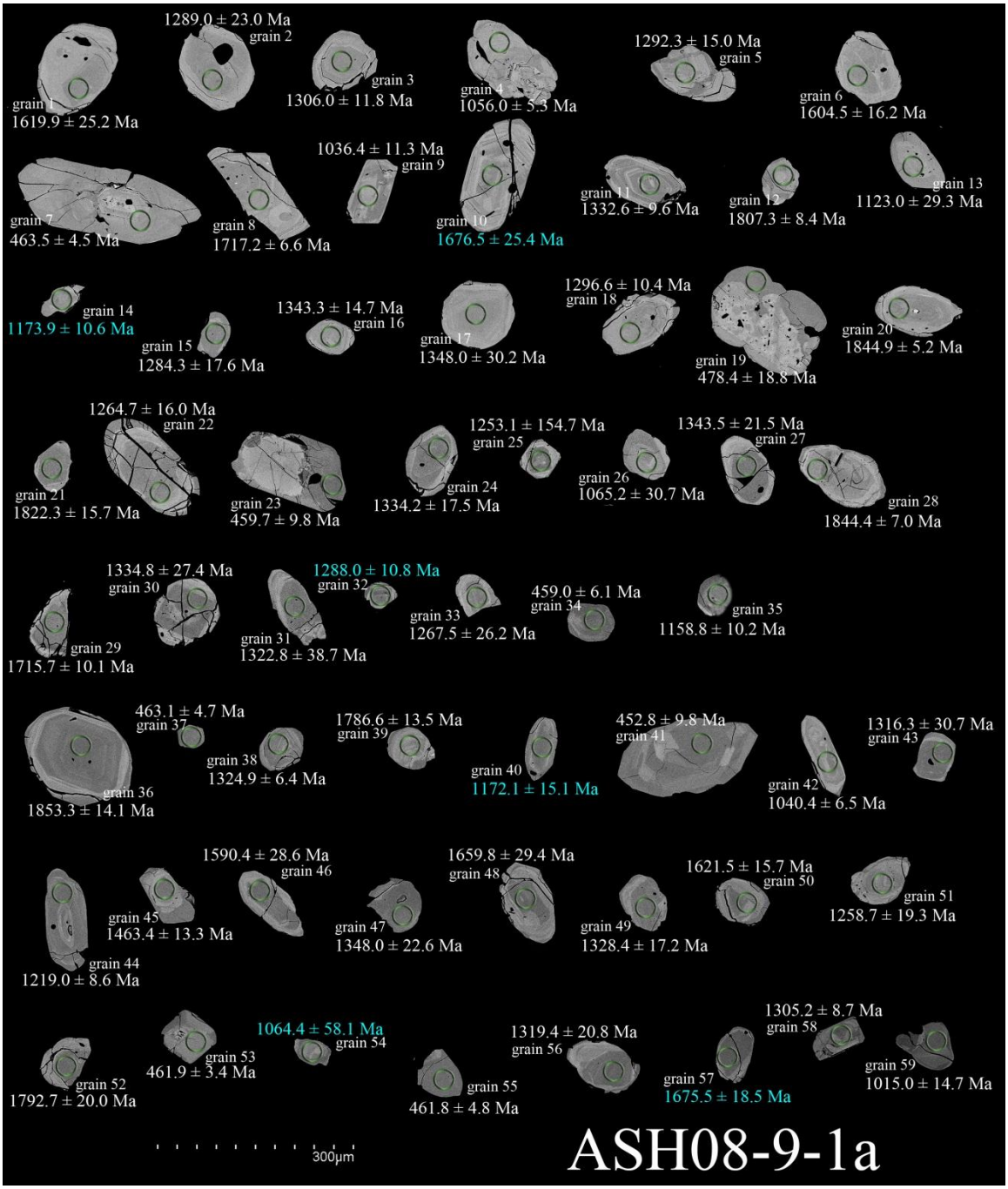

Figure 5.14: Back scatter electron images of all analyzed zircon from bgn-ASH08-9-1a. Green rings represent 30 µm LA spot locations. Blue ages are analyses with more than 5 % reverse discordance and were not included in the Concordia or probability density plots. Errors are 1σ.

distinct older populations *ca.* 1620 and 1840 Ma (Fig. 5.17). The usual Grenville age modes (*ca*. 1050, 1150 Ma) are remarkably poorly represented.

DEL08-2e:

A 1055 ± 65 Ma magmatic age for this sample is proposed by Loughry (2010) based on U-Pb zircon geochronology of ten zircon grains. Cores of 100 prismatic to sub-rounded zircon grains were analyzed for this study. The majority of grains exhibit consistent unzoned growth sectors in BSE. Some grains exhibit anhedral resorbed cores (Fig. 5.15; grains 21, 22, 28, 33, 48, and 62) to euhedral cores (Fig. 5.15; grains 46 and 73). Single spot ages range from approximately 820 Ma to 1860 Ma with two dominant age modes at 1060 Ma and 1180 Ma containing 90 % of the analyses (Fig. 5.17). Grains 24 (1544 ± 10 Ma), 92 (1598 ± 7 Ma), and 41 (1864 ± 10 Ma) are interpreted to represent relict cores of detrital grains preserved through regional Taconian high grade metamorphism, partial melting, and leucosome growth.

DEL03-1:

Two stages of metamorphic rim growth at ~997 ± 18 Ma and ~897 ± 31 Ma are presented for this sample in Anderson (2011, ion microprobe U-Pb zircon ages). The previous study was oriented toward testing the validity of tectonic models with emphasis on Taconic tectonism in the southern Appalachian Blue Ridge so analyzing the rims of zircon or cores of small equant grains was favored. The focus of the current study is to analyze zircon cores to provide insight regarding the presence of multiple Proterozoic age domains, the identity of the protolith of the biotite gneiss, and the evaluation of potential detrital zircon source terranes.

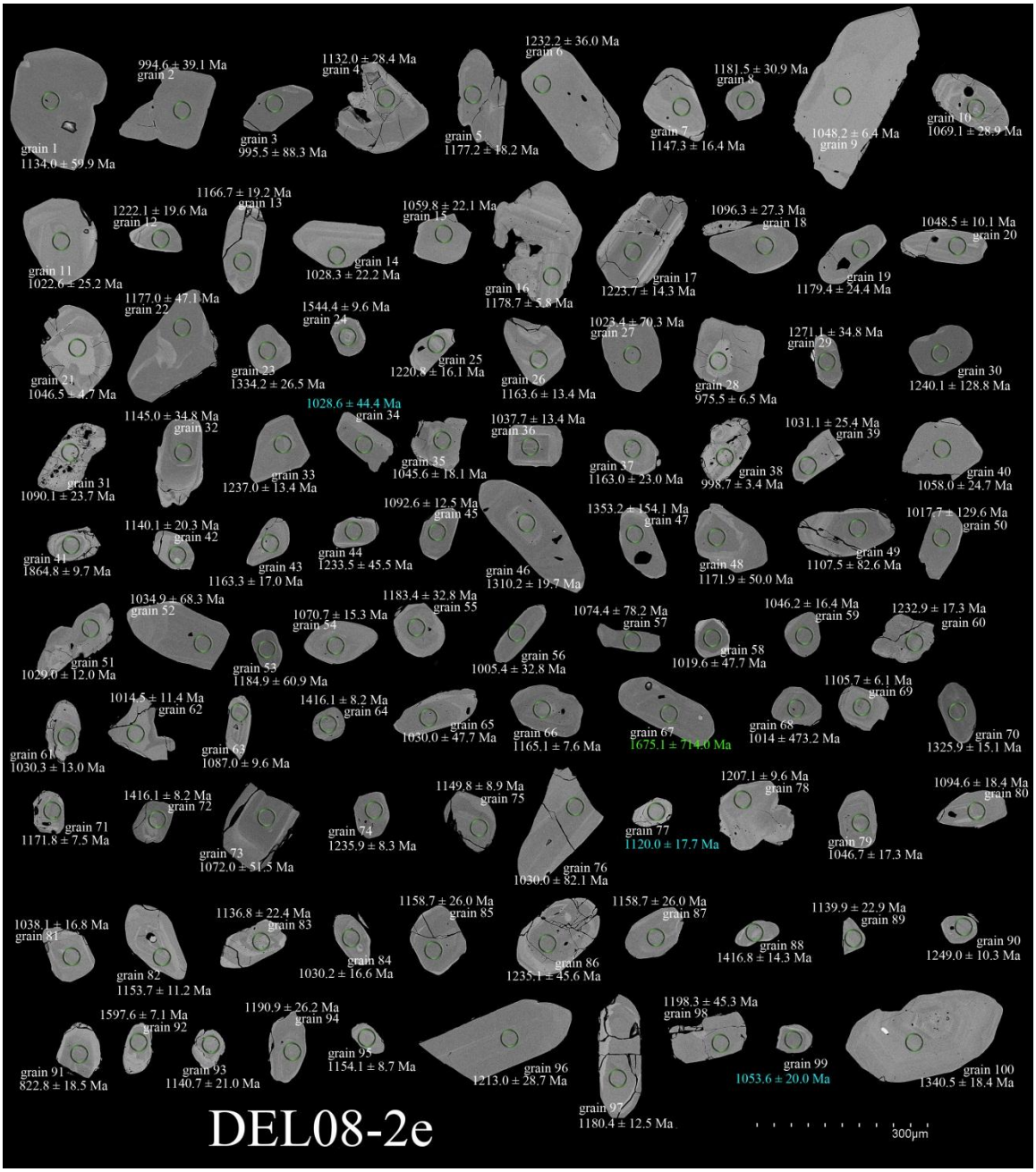

Figure 5.15: Back scatter electron images of all analyzed zircon from bgn-DEL08-2e. Green rings represent 30 µm LA spot locations. Blue ages are analyses with more than 5 % reverse discordance. Green ages are analyses with anomalously high ^{204}Pb counts. These analyses were not included in the Concordia or probability density plots. Errors are 1σ.

Figure 5.16: Back scatter electron images of all analyzed zircon from bgn-DEL03-1. Green rings represent 30 µm analysis spot locations. Blue ages are analyses with more than 5 % reverse discordance. Yellow ages are analyses with greater than 10% $^{206}Pb/^{238}U$ error. These analyses were not included in the concordia or probability density plots. Errors are 1σ.

Cores of 100 zircon grains ranging from well-rounded to prismatic were analyzed. Oscillatory zoning is visible in BSE for several zircon cores (Fig. 5.16; grains 8, 59, 66, 70, 80, 93, and 96) or is otherwise absent. Many grains exhibit large consistent growth zones and homogeneous metamorphic rims (Fig. 5.16; *e.g.* grain 6). Grain cores range from spheroidal (Fig. 5.16; grains 5, 36, 53, 557, 78, 79, 92, 96, and 99) to prismatic (Fig. 5.16; grains 3, 8, 30, 55, 61, 70, 90). Resorption of the core of grain 93 during rim growth is visible. Single spot ages range from approximately 960 Ma to 1970 Ma. Three separate age modes at 1060 Ma, 1360 Ma, and 1780 Ma are present. Remarkably, there are no ages between 1090 Ma and 1150 Ma (Fig. 5.17).

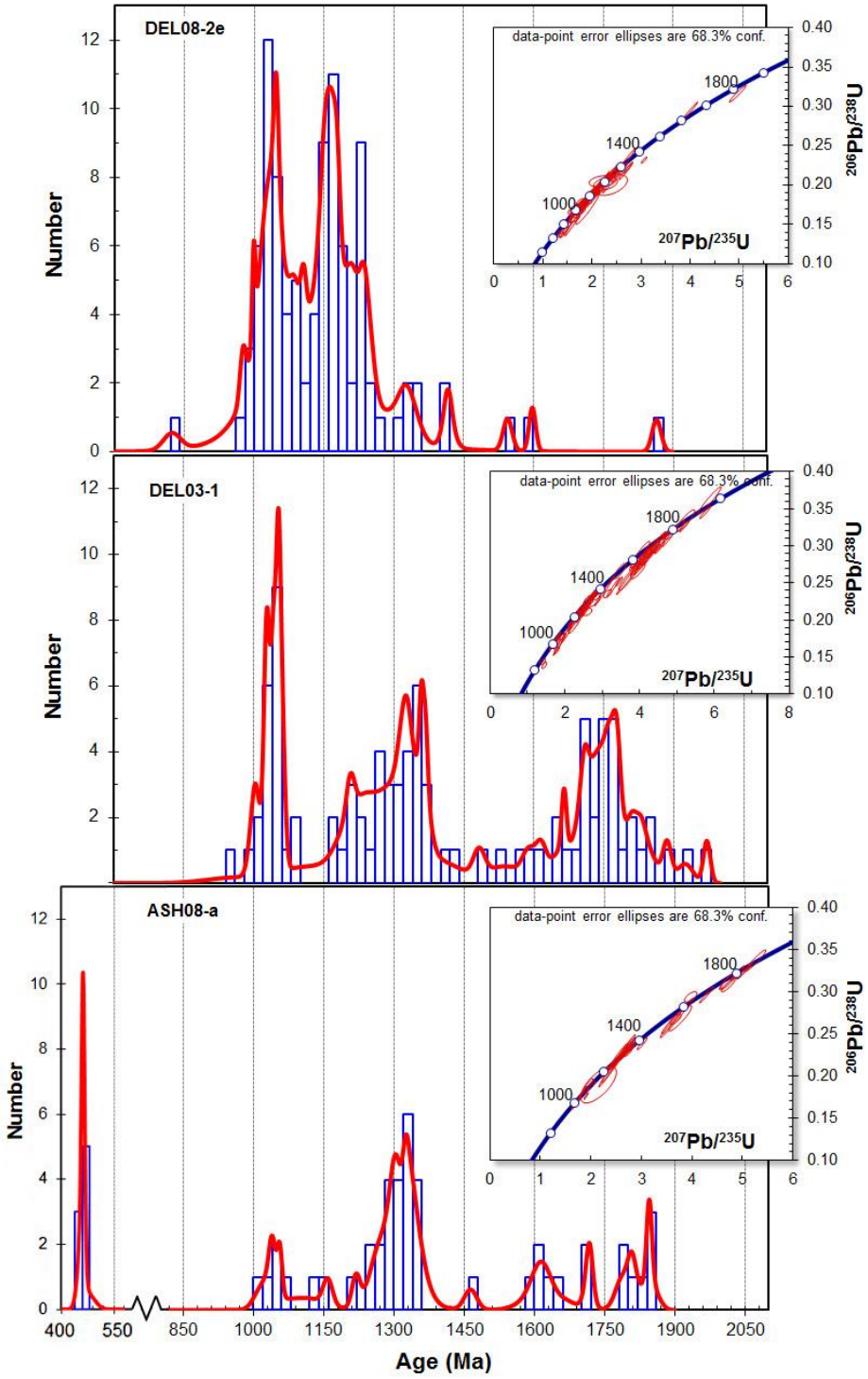

Figure 5.17: Probability density plots of zircon from biotite gneiss samples DEL08-2e, DEL03-1, and ASH08-2. Insets show concordia plots with all analyses. Red line is relative probability age distribution.

CHAPTER VI. DISCUSSION

Biotite Gneiss

The biotite gneiss and enveloping hornblende gneiss exhibit identical major and trace element trends, but lack of igneous textures and widespread (but variable) migmitization in the biotite gneiss makes it difficult to confirm an igneous or sedimentary origin (Loughry, 2010). Three biotite gneiss samples analyzed in this study yielded three distinct zircon age spectra, containing zircon crystallization ages ranging from 1.0 to 1.9 Ga (Figs. 5.17, 6.1). The wide range of zircon ages combined with the rounded to sub-rounded zircon grain shapes (Fig. 5.14-5.17) support the interpretation that the biotite gneiss is a paragneiss. Biotite gneiss sample DEL08-2e has peak populations at 1060 and 1160 Ma, which is similar to that of the Ocoee Supergroup (Bream *et al.*, 2004; Chakraborty, 2010), whereas bgn-DEL03-1 and bgn-ASH08-9-1a have dominant age modes at *ca.* 1330 and 1750 Ma.

U-Pb ion microprobe detrital zircon geochronology of metasandstones, metapelites, and metagraywackes from the central Blue Ridge, Dahlonega gold belt, and eastern Innner Piedmont yield similar Grenville dominated zircon age spectra with distinguishable pre-Grenville zircon populations (1.4 to 1.5 Ga, 1.6 to 1.9 Ga, and 2.7 to 2.9 Ga; Bream *et al.*, 2004). However, zircon ages older than 1.5 Ga are sparse in these areas compared to samples bgn-DEL03-1 and bgn-ASH08-9-1a and no Archean ages are present in Dellwood samples. The Dellwood samples also had 60-100 grains per sample analyzed (compared to 35-75 per sample by Bream *et al.*, 2004) so that if older ages were present, they should have appeared in the Dellwood samples. Samples bgn-DEL03-1 and bgn-ASH08-9-1a contain a large number of 1750 Ma zircon grains and a paucity of

zircon grains with ages in the 1130 to 1180 Ma range. The lack of such Grenville ages is remarkable considering that Grenville zircons dominate detrital zircon age spectra of late Precambrian through Phanerozoic sedimentary rocks in eastern Laurentia.

The older age population of 1750 Ma is interpreted to be related to the 1.8 Ga zircon in the Mars Hill terrane (Carrigan *et al.,* 2003), which has recently been reinterpreted to be detrital (Southworth *et al.,* 2011; Aleinikoff et al., 2012). Bream *et al.* (2004) favor a Laurentian crustal affinity for paragneisses in the southern Appalachian Blue Ridge (note that their study included examples of terranes currently interpreted to be exotic, e.g. Carrigan et al. (2003), as Laurentian sources) and provides a model of deposition of Granite-Rhyolite Province (GRP) components into the same basin as the eroding Grenville orogen. However, ages greater than 1.5 Ga require source(s) older than the GRP.

Detritus can travel thousands of kilometers in modern tectonic systems (Hamilton, 1979). Before the development of land plants in a supercontinent environment such as Rodinia, detrital zircons could be inherited from great distances such as Kalahari, Rio de la Plata, Congo, Amazonia, Baltica, and Laurentia cratons. The closest provinces considered as potential 1.65-1.95 Ga sources for bgn-DEL08-2d and bgn-DEL03-1are: (1) the Laurentian Yavapi province (1.8-1.7 Ga; Whitmeyer and Karlstrom), (2) the Rio Negro-Juruena (1.80-1.55 Ga) belt of Amazonia (Payolla *et al.,* 2002), and (3) the Kheis-Okwa-Magondi belt of Kalahari (2.1-1.75 Ga; Jacobs *et al.,* 2008). An alternative provenance model precludes distant sources and hypothesizes derivation of grains from older crustal components within the Grenville belt. The latter model is favored due to non-existent detritus from younger provinces in between the Grenville Province and

potential distal sources. For example, if Yavapi zircon were deposited in the area of the Grenville province one would expect detritus from the Mazatzal and GRP (1.6-1.7 Ga and 1.35-1.55 Ga respectively; Whitmeyer and Karlstrom, 2010).

The consistency between samples bgn-ASH08-9-1a and bgn-DEL03-1 with data from Bream *et al.,* (2004), with the exception of Archean ages, suggest similar sources of different relative contributions. The inconsistency in age spectra between bgn-DEL08-2d and the other two biotite gneisses indicate that the biotite gneiss mapped as a single unit (Hadley and Goldsmith, 1963) is heterogeneous and may have unique histories despite their geochemical and petrological similarities.

Zircon of Dellwood orthogneisses record several magmatic and metamorphic events in the Mesoproterozoic and Paleoproterozoic. A distinct metamorphic event at 1038 ± 13 Ma is supported by hgn-DEL10-11 zircon rims, which may be associated with the youngest (Ottowan) magmatic age mode at 1060 ± 5 Ma (Tollo *et al.,* 2010). Magmatic ages are present in two groups: a younger Grenvillian event from 1130 to 1180 Ma and an older event at approximately 1330 Ma. The detrital record from the biotite gneiss reflects sources produced during magmatism *ca.* 1030, 1150, and 1330 Ma, and an additional event near 1750 Ma (Fig. 5.17). Sample bgn-DEL08-2e in the southeastern portion of Dellwood quad exhibits major peaks at 1030 and at 1150 Ma and few zircon ages *ca.* 1330 Ma. Although bgn-DEL03-1 shares a peak at 1030 Ma, there are few zircon ages *ca.* 1150 Ma, and instead exhibits a greater zircon population near 1330 Ma. Together these samples encapsulate the entire Grenville period, but their differences suggest potential amalgamation of various terranes within the Dellwood quad or extreme variations between local in sources.

Crustal Affinity

Use of Nd and Pb isotopic systematics allows meaningful correlations to be made between an igneous rock and its potential crustal source. The isotopic evolution of Nd in a rock diverges from the trend of the depleted mantle reservoir at the time of magma generation (DePaolo and Wasserburg, 1976). Resetting of Nd isotopic systematics is considered resistant to crustal processes (*e.g.*, reworking and remelting) and thus enables the distinction to be made between a juvenile heritage (mantle derived) and a source in pre-existing crust (Whitehouse, 1988). Juvenile crust can be identified by the coincidence of zircon U-Pb crystallization ages and depleted mantle model (T_{DM}) ages. However, T_{DM} ages of rocks may represent an average between mixed reservoirs and may yield erroneous conclusions regarding the nature of the source (Arndt and Goldstein, 1987; DeWolf and Mezger, 1994). Interpreting a T_{DM} age as the time of crust extraction requires the assumption that the Sm/Nd ratio has not been modified by exchange of neodymium between isotopically distinct reservoirs. If assimilation between multiple crustal reservoirs took place, then T_{DM} ages would be intermediate between the true mantle derivation ages of the multiple reservoirs. The history (and complexities) of non-juvenile crust requires additional information to assess the Sm and Nd data. To this purpose, complimentary analysis of the U-Th-Pb system is employed to achieve better constraints on the evolution of Grenville basement in the eastern Great Smoky Mountains. The analysis of whole rock and feldspar Pb isotopes enables identification of crustal source (*e.g.* DeWolf and Mezger, 1994; Shina *et al.*, 1996, 1999; Fisher *et al.*, 2010).

Lead isotopes of eastern Laurentia basement rocks define four distinct arrays in uranogenic Pb space: (1) the Granite-Rhyolite province (GRP: Van Schmus *et al.*, 1996;

Fisher *et al.,* 2010); (2) southern and central Appalachian basement (SCAB; Carrigan *et al.,* 2003; Ownby *et al.,* 2004; Hatcher *et al.,* 2004; Berquist *et al.,* 2005; Fisher *et al.,* 2010); (3) Adirondacks and Llano uplift (ALU: DeWolf and Mezger, 1994; Smith *et al.,* 1997; Cameron and Ward, 1998; Shina and McLelland, 1999; Roller, 2004), and (4) the Roan Mountain-Stage Road layered gneiss (Shina *et al.,* 1996; Carrigan *et al.,* 2003; Ownby *et al.,* Fisher *et al.,* 2010).

To identify a Laurentian crustal affinity (*e.g.* Hatcher, 1989; Whitmeyer and Karlstrom, 2007), Pb isotope compositions should overlap values for juvenile Laurentian sources such as the GRP or ALU (Fisher *et al.,* 2010) and Nd isotope data should yield T_{DM} ages that are close to the U-Pb zircon crystallization age (within 100 Ma; Van Schmus *et al.,* 1996). In the case of an exotic origin (Carrigan *et al.,* 2003; Loewy *et al.,* 2003; Tohver *et al.,* 2004, 2005; Berquist *et al.,* 2005; Fisher *et al.,* 2010), Pb isotope compositions should overlap that of the Amazonian trend and T_{DM} ages should be significantly older than U-Pb zircon ages (greater than 100 Ma). A third possibility is that the evolution of Grenville basement included crustal mixing between juvenile Laurentian crust (*e.g.,* GRP) and exotic crust (*e.g.* Hatcher *et al.,* 2004). In this scenario the expected result would be averaged T_{DM} ages and Pb isotope compositions that are intermediate between exotic (Amazonian) and native (GRP and Grenville province) crust.

The model of a solely Grenvillian mantle-derived juvenile magmatic history for SCAB was deemed unsupportable by Fisher *et al.* (2010) based on T_{DM} ages of 1.43 to 1.88 Ga (Carrigan *et al.,* 2003; Ownby *et al.,* 2004; Fisher *et al.,* 2010), which are considerably older than their U-Pb magmatic crystallization ages of 1.0 to 1.3 Ga (400 to 500 Ma younger than their T_{DM} ages; Fig. 6.1). The T_{DM} ages for Dellwood gneisses

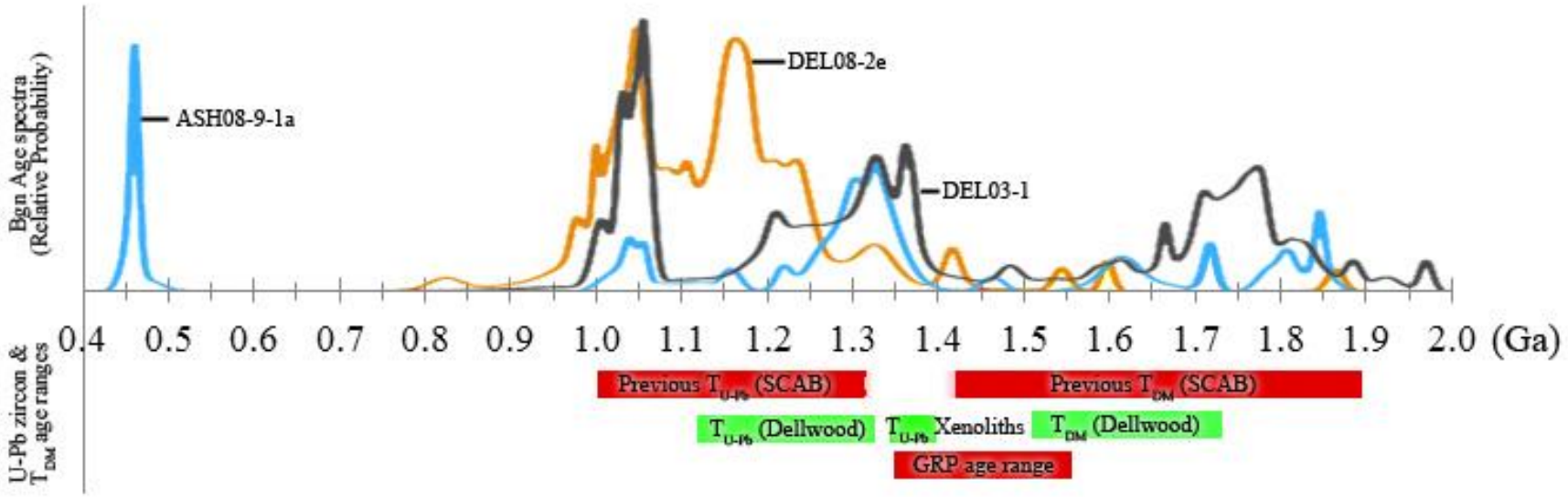

Figure 6.1: Timeline summarizing geochronological data relevant to the evolution of eastern Great Smoky Mountain basement. Curves above x-axis represent U-Pb zircon age spectra of biotite gneiss samples. Scale bars below x-axis represent time frames of U-Pb zircon and T_{DM} ages for previous studies (red) in the southern and central Appalachians (SCAB) and Dellwood basement rocks (green). Granite Rhyolite Province (GRP) is juvenile crust therefore the scale bar represents both U-Pb zircon and T_{DM} ages.

range from 1.5 to 1.8 Ga (Fig. 4.3) and are likewise older than their respective U-Pb zircon ages (200-650 Ma; Fig. 6.1). These Nd isotope data tentatively identify the orthogneisses in Dellwood and their included amphibolite and tonalite xenoliths as non-juvenile, which is in agreement with previous work in the SCAB.

Comparison of T_{DM} ages and detrital zircon age data from the biotite gneiss samples suggests mixing of Nd isotope reservoirs (Fig. 6.1). The age peaks in the detrital zircon age spectra are interpreted as the ages of crust that was incorporated into present day basement during the Greville orogeny (*ca.* 1030, 1150, 1330, and 1750 Ma). However, T_{DM} ages 1500 to 1790 Ma mostly span an age range that is poorly represented by the detrital data. This is interpreted as mixing of Nd isotopic reservoirs between *ca.* 1780 Ma and younger crust. The samples with older T_{DM} ages thus represent relatively less contaminated crust and therefore tx-DEL10-7a (T_{DM} age-1790 Ma) is considered to be representative of the original *ca.* 1750 Ma crustal reservoir. The ideas of crustal mixing and tx-DEL10-7a representing an uncontaminated source are further supported by Pb isotope chemistry.

Lead isotopic compositions presented herein partially overlap juvenile arrays of the GRP/ALU, SCAB, and Amazonia (Fig. 4.4). Caution must be employed while comparing feldspar Pb and whole rock Pb data. However, feldspar and whole rock Pb isotope data are considered to be comparable based on the similarity of previous juvenile whole rock (GRP; Fisher *et al.*, 2010) and juvenile feldspar ratios (Juvenile Laurentia; DeWolf and Mezger, 1994; Fig. 4.4). Feldspar Pb data from Dellwood gneisses define an array that overlaps both the SCAB/Amazonia (Tohver *et al.*, 2004; Fisher *et al.*, 2010) and juvenile Laurentia arrays (Fig. 4.4; DeWolf and Mezger, 1994; Fisher et al., 2010).

This implies a Pb contribution from both juvenile and exotic sources for the majority of Dellwood samples and thus crustal mixing between Laurentia and Amazonia must have occurred. One outlier (tx-DEL10-7a) has significantly lower $^{207}Pb/^{204}Pb$ compared to all other Dellwood samples and plots within the approximate center of the juvenile Laurentia array (Fig. 4.4). This suggests that tx-DEL10-7a has a crustal heritage that is less contaminated (by assimilation of exotic crust) as the rest of Dellwood and SCAB.

Another unique aspect about tx-DEL10-7a is its age. The proposed U-Pb zircon magmatic crystallization age is 1381 ± 6 Ma, which is significantly older than the majority of surrounding Grenville crust (1.06 to 1.33 Ga; Tollo *et al.,* 2010). Fisher *et al.* (2010) report a 1381 ±27 U-Pb age datum for a drill core of granitic basement from central Tennessee in the eastern GRP (T_{DM} age of 1.45 Ga). The xenolith has a Pb isotope composition that is distinctly Laurentian and a crystallization age coeval with adjacent juvenile Laurentian crust (GRP; Fig. 6.1). This suggests tx-DEL10-7a is Laurentian in heritage, but the 1.79 Ga T_{DM} age of tx-DEL10-7a compared to its crystallization age of *ca.* 1.38 Ga precludes the possibility that tx-DEL10-7a is juvenile and is differentiated from the GRP on this basis. Tx-DEL10-7a is the only rock that displays both non-juvenile and Laurentian characteristics and therefore represents a unique crustal source previously unidentified in the Blue Ridge.

The interpretation of all the data is that incipient Grenville magmatism occurred *ca.* 1380 Ma beginning with melting of a Laurentian source (*ca.* 1750-1800 Ma) that did not mix with another crustal reservoir. This is supported by the xenolith with a Laurentian Pb signature and a non-juvenile/unmixed Nd signature. Subsequent magmatism ca. 1330 Ma incorporated multiple crustal components of both Laurentian

and Amazonian affinity, which is supported by mixing of Pb isotope reservoirs (Fig. 4.4) and mixed T_{DM} ages (Fig. 6.1) in the majority of Dellwood gneisses.

Amphibolite sample amx-DEL10-7d is proposed to be 1342 ± 53 Ma, which is also older than the typical Grenville age range (although precision is poor). It is proposed that amphibolite in the Dellwood area is a portion of an ancient accretionary complex related to subduction (Ryan *et al.*, 2005). If subduction of oceanic lithosphere emplaced these amphibolite bodies it is natural to expect juvenile lithosphere nearby. The presence of exotic, Laurentian, and oceanic crust together in the same location would require that present day outcrops within the Dellwood area were proximal to the Laurentia-Amazonia continent-continent suture zone. The U-Pb zircon age for the host rock for these xenoliths is 1331 ± 8 Ma, which agrees with nearby Dellwood samples (Loughry, 2010; Anderson, 2011), and the oldest magmatic pulse in the Blue Ridge (Tollo *et al.*, 2010). The outcrop is geochemically consistent with surrounding Carolina Gneiss (Loughry, 2010; Anderson, 2011) but is petrologically unique due to preserved igneous textures. It may be the case that crustal components similar to tx-DEL10-7a existed within other areas of the southern Appalachians, but evidence of such relicts has been convoluted by multiple phases of high grade metamorphism, anatexis, and deformation. The lack of outcrop in the southern Appalachians also makes it difficult to delimit the spatial extent of such a crustal component.

Conclusions

1. Although its bulk chemistry is similar to spatially associated orthogneisses (Loughry, 2008), the wide range of zircon ages from 0.85 to 1.97 Ga is most consistent with the biotite gneiss being a metaclastic rock. The map unit has a

non-unique provenance as shown by the strikingly variable detrital zircon age spectra among the three samples that are mapped as one basement unit (Hadley and Goldsmith, 1963; Southworth et al., 2005; Merchat and Cattanach, 2010). The youngest detrital zircon age obtained (0.85 Ga) for the biotite gneiss suggests it is a latest Mesoproterozoic-earliest Neoproterozoic sediment, and not a distal, time-equivalent unit of the intracontinental rift Ocoee Supergroup, which is clearly late Neoproterozoic in age (Aleinikoff et al., 2010; Chakbraborty et al., 2012).

2. Multiple old crustal components of native and exotic Laurentian affinity contributed to the evolution of the Dellwood basement. This is supported by detrital U-Pb zircon data from the biotite paragneiss that exhibits a large number of ages between 1.60 and 1.95 Ga and a xenolith of 1.38 Ga age within 1.33 Ga orthogneiss.

3. The xenolith tx-DEL10-7a represents the first evidence of a Laurentian component in the EGSM basement. However, this sample is not correlative with other Laurentian crustal regimes (GRP/ALU) because of its non-juvenile Nd isotope signature. Tx-DEL10-7a is interpreted as a relict of 1.79 Ga Laurentian crust that contributed to Grenville development of the eastern Great Smoky Mountains basement.

4. T_{DM} ages for all Dellwood samples between *ca*. 1.5 and 1.7 Ga represent an age range that is poorly represented in the detrital zircon age data (Fig. 6.1). These ages suggests mixing between crustal reservoirs during Grenville orogenesis.

5. Lead isotopic compositions that overlap Laurentian and Amazonian arrays are the strongest evidence supporting a model of mixing between juvenile Laurentian and exotic Amazonian crustal components.

Future Work

Remaining questions related to this research include the degree of mixing, the proportion of Amazonian and Laurentian crustal components, and the mechanism by which the proposed mixing occurred. Whole rock isotopic Pb analyses should be included in future work to confirm that feldspar Pb isotope compositions presented herein and whole rock Pb compositions of previous studies (Tohver *et al.*, 2004; Fisher *et al.*, 2010) are comparable. U-Pb zircon geochronology should be employed to analyze the age(s) of the various sized amphibolite masses (dm- to km-scale masses; Loughry, 2010) which may represent remnants of oceanic lithosphere within a potential Laurentia-Amazonia suture zone.

Further geochronological studies of biotite gneiss with higher sampling density would be useful in determining which zircon age spectra are dominant in the biotite gneiss. This would provide insight to the relative contribution of older crustal components. Hf isotope analysis of ca. 1.3 to 1.9 Ga detrital zircon in biotite gneiss may be able to resolve more precisely the affinity of crustal components in the EGSM basement.

The Ocoee Supergroup represents material eroded from Grenville basement *e.g.* Dellwood basement. Feldspar Pb analyses of the Ocoee Supergroup may be able to describe the crustal affinity of large portions of basement that are no longer present.

CHAPTER VII. APPENDICES

Appendix A: Whole Rock X-Ray Fluorescence Spectrometric Analysis

Sample	ASH08-9-1a	DEL04-5	DEL10-11	DEL10-29	DEL10-30	DEL10-7a	DEL10-7b	DEL10-7c	DEL10-7d	DEL10-7e	FC08-2	MP04-2
Quadrangle Lithology	Clyde bgn	Dellwood Hgn	Dellwood hgn	Dellwood agn	Dellwood agn	Dellwood tx	Dellwood hgn	Dellwood amx	Dellwood amx	Dellwood hgn	Fines Creek hgn	Lemon Gap mpg
SiO_2 (wt.%)	49.59	68.77	65.82	75.63	63.76	48.52	71.27	48.38	49.16	64.19	61.10	64.40
TiO_2 (wt.%)	2.92	0.27	0.34	0.20	0.67	1.24	0.23	1.51	1.42	0.45	0.84	1.14
Al_2O_3 (wt.%)	15.91	15.60	14.95	14.18	16.58	20.41	15.49	15.61	16.31	17.45	17.32	15.25
Fe_2O_3 (wt.%)	14.33	2.69	2.08	1.33	4.55	11.09	2.19	12.66	11.34	3.59	4.99	5.85
MgO (wt.%)	4.25	0.88	0.56	0.33	1.51	4.71	0.64	6.06	5.73	1.33	1.93	1.13
CaO (wt.%)	9.60	2.77	1.77	1.27	3.64	8.68	2.67	10.15	9.08	3.48	5.03	3.88
Na_2O (wt.%)	2.61	3.57	2.62	2.12	3.39	3.80	3.27	2.61	3.58	3.63	3.69	3.12
K_2O (wt.%)	0.42	3.65	6.79	5.12	3.58	2.45	3.55	1.70	1.51	3.78	2.53	3.86
P_2O_5 (wt.%)	0.50	0.14	0.11	0.04	0.21	0.98	0.08	0.41	0.28	0.24	0.26	0.57
MnO ppm	2068	441	204	239	1009	1343	202	2142	1961	430	842	1218
LOI	0.20	0.35	0.32	1.99	0.82	0.63	0.33	0.64	0.80	0.52	0.78	0.40
Total	100.54	98.73	95.39	102.23	98.81	102.64	99.74	99.95	99.42	98.70	98.54	99.73

bgn-biotite gneiss; hgn-hornblende gneiss; agn-augen gneiss; tx-tonalite xenolith; amx-amphibolite xenolith; mpg-Max Patch Granite

Appendix B: Feldspar Pb TIMS Analysis

Sample	Leach #	206Pb 204Pb	±	207Pb 204Pb	±	208Pb 204Pb	±	208Pb 206Pb	±	207Pb 206Pb	Lithology
FC08-02	4	17.051	0.018	15.509	0.017	36.707	0.040	N.A.	N.A.	N.A.	Hgn
Del08-2a	3	17.678	0.016	15.537	0.014	37.083	0.033	N.A.	N.A.	N.A.	Bgn
Del08-2a	4	17.699	0.017	15.519	0.015	37.082	0.035	N.A.	N.A.	N.A.	Bgn
Del10-7a	3	17.337	0.041	15.427	0.034	36.890	0.085	N.A.	N.A.	N.A.	tx
Del10-7a	4	17.400	0.066	15.409	N.A.	36.879	N.A.	N.A.	N.A.	N.A.	tx
Del04-5	4	16.982	0.009	15.480	0.008	36.861	0.021	N.A.	N.A.	N.A.	hgn
Del10-7e	4	16.940	0.007	15.462	0.007	36.705	0.017	N.A.	N.A.	N.A.	hgn
Del10-7d	4	17.109	0.030	15.471	0.027	37.074	0.064	N.A.	N.A.	N.A.	amx
Del10-11	4	17.335	0.005	15.561	0.005	37.852	0.013	N.A.	N.A.	N.A.	hgn
MPO4-2	4	17.257	0.031	15.502	0.030	36.959	0.031	2.142	0.003	0.898	mpg
DEL10-29	3	17.742	0.030	15.567	0.030	37.209	0.030	2.097	0.005	0.877	agn
DEL10-30	3	17.635	0.016	15.538	0.016	38.164	0.017	2.164	0.004	0.881	agn
DEL10-30	4	17.730	0.056	15.501	0.055	38.039	0.057	2.145	0.003	0.874	agn

bgn-biotite gneiss; hgn-hornblende gneiss; agn-augen gneiss; tx-tonalite xenolith; amx-amphibolite xenolith; mpg-max patch granite
N.A.- not available

Appendix C: Whole Rock Sm and Nd TIMS (Analytical Uncertainty)

A significant degree of uncertainty is involved when calculating T_{DM} ages. Various estimates of the Sm-Nd isotopic evolution of the depleted mantle have been proposed (DePaolo, 1981; Goldstein et al. 1984; Nelson and DePaolo, 1984; Michard et al., 1985; Liew and McCulloch, 1985). Variation among the models results in differences of up to 300 Ma T_{DM} ages for the same sample (Arndt and Goldstein, 1987). The model of DePaolo (1981) is the most widely cited and was chosen for this study on that basis. Regardless of model, analytical error produces a range of possible T_{DM} ages. Fisher (2006) approximates the uncertainty by assuming an error of ± 0.000005 for measured $^{144}Nd/^{143}Nd$ and 0.4 % error in $^{147}Sm/^{143}Nd$ (Patchett and Kouvo, 1986). Based on these assumptions T_{DM} age uncertainties increase with increasing Sm/Nd. Crustal Sm/Nd typically range from 0.07 to 0.14 (0.06 to 1.33 in this study) and associated T_{DM} age errors increase exponentially (concave up) from approximately 12 to 52 Ma.

Appendix D: Whole Rock Sm and Nd TIMS Analysis

Sample	Age (Ma)	± (Ma) 2σ	Nd (ppm)	Sm (ppm)	147Sm 144Nd	143Nd 144Nd	± 2σ	$\varepsilon_{Nd}(0)$	143Nd 144Nd (T)	$\varepsilon_{Nd}(T)$	T_{DM} (Ga)†	Ϫ (Ma)††	$\varepsilon_{Nd}(DM)$
Del04-5	1145	70	20.9	3.64	0.1053	0.511859	6	-15.2	0.510939	0.4	1.66	331	4.3
Del08-10a	1125	83	39.1	7.13	0.1103	0.511891	2	-14.6	0.511186	-2.1	1.69	568	4.2
Del08-2d	N.A.	N.A.	42.5	8.40	0.1194	0.512106	3	-10.4	N.A.	N.A.	1.52	N.A.	4.7
Del08-6c	1227	45	32.1	5.43	0.1023	0.511846	3	-15.4	0.511054	-0.6	1.64	408	4.4
Del08-7a	1292	65	26.0	3.26	0.0757	0.511606	3	-20.1	0.510970	-0.1	1.59	294	4.5
Del10-7a	1381	6	53.7	9.68	0.1090	0.511809	6	-16.2	0.510821	-0.7	1.79	4	4.0
Del10-11	1175	30	28.2	4.03	0.0864	0.511649	3	-19.3	0.511184	-3.4	1.67	538	4.3
Del10-29	1175	11	8.3	1.14	0.1023	0.511872	13	-14.9	0.511121	-0.8	1.60	426	4.5
Del10-7b	1331	8	9.2	0.98	0.0645	0.511552	3	-21.2	0.510919	1.3	1.52	192	4.7
Del10-7c	1342	53	24.6	5.45	0.1337	0.512114	3	-10.2	0.510905	0.6	1.76	420	4.0
Del10-7d	1342	53	30.3	6.30	0.1256	0.512118	2	-10.1	0.510905	2.1	1.60	257	4.5
Del10-7e	1331	8	23.0	2.61	0.0686	0.511546	4	-21.3	0.510919	0.5	1.57	240	4.5
MP04-2	1050	N.A.	82.7	14.7	0.1072	0.512008	6	-12.3	0.511269	-0.3	1.48	434	4.8
FC08-2	1040	8	30.9	6.21	0.1214	0.512022	2	-12.0	0.511296	-2.0	1.68	642	4.2

N.A.- not available

*: Preferred magmatic ages of zircon geochronology from Loughry (2010).

**: Preferred magmatic age of zircon geochronology from Chakraborty (2010).

†: Depleted mantle model ages (T_{DM}) calculated using present day $^{143}Nd/^{144}Nd$=0.512638 and $^{147}Sm/^{144}Nd$=0.1967 for CHUR (DePaolo, 1981) and $^{143}Nd/^{144}Nd$=0.513047 (DePaolo, 1981) and $^{147}Sm/^{144}Nd$=0.2165 for depleted mantle

††: T_{DM} and crystallization age difference

Appendix E: LA-ICP-MS U-Pb Zircon Geochronology

ASH08-9-1a (biotite gneiss)				Isotope ratios							Apparent ages (Ma)								
Analysis	U (ppm)	206Pb 204Pb	U/Th	206Pb* 207Pb*	± (%)	207Pb* 235U*	± (%)	206Pb* 238U	± (%)	error corr.	206Pb* 238U*	± (Ma)	207Pb* 235U	± (Ma)	206Pb* 207Pb*	± (Ma)	'best age' (Ma)	± (Ma)	Conc (%)
ASH08A-1	101	97288	1.9	10.0224	1.4	3.6788	2.0	0.2674	1.4	0.73	1527.6	19.7	1566.8	15.8	1619.9	25.2	1619.9	25.2	94.3
ASH08A-2	145	34404	1.3	11.9265	1.2	2.5194	9.5	0.2179	9.4	0.99	1270.9	108.6	1277.6	69.1	1289.0	23.0	1289.0	23.0	98.6
ASH08A-3	141	67037	1.2	11.8226	0.6	2.7209	2.4	0.2333	2.3	0.97	1351.8	27.7	1334.2	17.5	1306.0	11.8	1306.0	11.8	103.5
ASH08A-4	778	1518464	56.7	13.4163	0.3	1.7829	0.9	0.1735	0.9	0.96	1031.3	8.5	1039.2	6.0	1056.0	5.3	1056.0	5.3	97.7
ASH08A-5	378	80224	1.2	11.9063	0.8	2.5351	2.1	0.2189	2.0	0.93	1276.1	22.9	1282.2	15.5	1292.3	15.0	1292.3	15.0	98.7
ASH08A-6	448	186928	3.9	10.1056	0.9	3.5886	3.4	0.2630	3.3	0.97	1505.3	44.7	1547.0	27.3	1604.5	16.2	1604.5	16.2	93.8
ASH08A-7	272	35535	165.3	17.8774	1.7	0.5749	2.0	0.0745	1.0	0.50	463.5	4.5	461.2	7.3	449.8	37.9	463.5	4.5	103.0
ASH08A-8	439	217942	1.2	9.5090	0.4	4.2473	1.5	0.2929	1.5	0.97	1656.1	21.3	1683.2	12.4	1717.2	6.6	1717.2	6.6	96.4
ASH08A-9	447	138846	5.2	13.5475	0.6	1.8247	3.2	0.1793	3.1	0.98	1063.1	30.4	1054.4	20.7	1036.4	11.3	1036.4	11.3	102.6
ASH08A-11	237	119033	1.0	11.6617	0.5	2.7294	1.5	0.2308	1.5	0.95	1338.9	17.7	1336.5	11.5	1332.6	9.6	1332.6	9.6	100.5
ASH08A-12	348	262206	1.4	9.0516	0.5	4.8993	1.9	0.3216	1.8	0.97	1797.7	28.5	1802.1	15.8	1807.3	8.4	1807.3	8.4	99.5
ASH08A-13	634	84333	12.8	12.9754	1.5	2.0080	2.3	0.1890	1.8	0.78	1115.8	18.8	1118.2	15.9	1123.0	29.3	1123.0	29.3	99.4
ASH08A-15	219	214258	2.3	11.9551	0.9	2.4714	6.9	0.2143	6.8	0.99	1251.6	77.9	1263.7	49.9	1284.3	17.6	1284.3	17.6	97.5
ASH08A-16	258	39301	2.0	11.5970	0.8	2.7378	1.8	0.2303	1.6	0.90	1335.9	19.3	1338.8	13.2	1343.3	14.7	1343.3	14.7	99.4
ASH08A-17	125	204942	1.3	11.5690	1.6	2.7228	2.2	0.2285	1.5	0.70	1326.4	18.3	1334.7	16.2	1348.0	30.2	1348.0	30.2	98.4
ASH08A-18	288	88081	0.9	11.8799	0.5	2.6053	2.2	0.2245	2.1	0.97	1305.5	24.8	1302.1	15.9	1296.6	10.4	1296.6	10.4	100.7
ASH08A-19	184	39242	80.3	17.3786	3.2	0.6112	5.2	0.0770	4.1	0.79	478.4	18.8	484.3	20.0	512.4	70.4	478.4	18.8	93.4
ASH08A-20	252	199467	0.7	8.8655	0.3	5.0283	1.7	0.3233	1.7	0.99	1805.9	26.5	1824.1	14.5	1844.9	5.2	1844.9	5.2	97.9
ASH08A-21	85	57876	1.2	8.9772	0.9	4.7241	1.9	0.3076	1.7	0.89	1728.8	25.8	1771.5	16.0	1822.3	15.7	1822.3	15.7	94.9
ASH08A-22	332	168750	5.0	12.0762	0.8	2.4650	2.4	0.2159	2.3	0.94	1260.2	26.2	1261.8	17.6	1264.7	16.0	1264.7	16.0	99.6
ASH08A-23	117	35058	88.2	17.1798	4.7	0.5932	5.2	0.0739	2.2	0.43	459.7	9.8	472.9	19.5	537.6	101.8	459.7	9.8	85.5
ASH08A-24	139	119437	1.5	11.6518	0.9	2.7229	2.0	0.2301	1.8	0.89	1335.1	21.9	1334.7	15.1	1334.2	17.5	1334.2	17.5	100.1
ASH08A-25	219	3585	1.0	12.1481	7.9	2.1517	10.9	0.1896	7.5	0.69	1119.1	77.3	1165.6	75.8	1253.1	154.7	1253.1	154.7	89.3
ASH08A-26	428	190767	4.8	13.3551	1.5	1.9440	3.4	0.1883	3.1	0.90	1112.2	31.3	1096.4	23.0	1065.2	30.7	1065.2	30.7	104.4
ASH08A-27	84	35922	1.3	11.5961	1.1	2.8064	2.2	0.2360	1.9	0.86	1366.0	23.0	1357.2	16.3	1343.5	21.5	1343.5	21.5	101.7

Appendix E: LA-ICP-MS U-Pb Zircon Geochronology (cont.)

ASH08-9-1a (biotite gneiss cont.)				Isotope ratios							Apparent ages (Ma)								
Analysis	U (ppm)	206Pb 204Pb	U/Th	206Pb* 207Pb*	± (%)	207Pb* 235U*	± (%)	206Pb* 238U	± (%)	error corr.	206Pb* 238U*	± (Ma)	207Pb* 235U	± (Ma)	206Pb* 207Pb*	± (Ma)	'best age' (Ma)	± (Ma)	Conc (%)
ASH08A-28	291	152795	1.5	8.8684	0.4	5.0464	2.1	0.3246	2.1	0.98	1812.1	32.5	1827.1	17.8	1844.4	7.0	1844.4	7.0	98.2
ASH08A-29	268	136951	1.7	9.5167	0.5	4.3623	1.1	0.3011	0.9	0.86	1696.7	14.1	1705.2	9.0	1715.7	10.1	1715.7	10.1	98.9
ASH08A-30	124	64251	0.9	11.6479	1.4	2.7923	2.5	0.2359	2.1	0.82	1365.3	25.3	1353.5	18.7	1334.8	27.4	1334.8	27.4	102.3
ASH08A-31	72	25386	1.7	11.7203	2.0	2.7423	2.8	0.2331	1.9	0.70	1350.7	23.7	1340.0	20.8	1322.8	38.7	1322.8	38.7	102.1
ASH08A-33	198	123876	1.4	12.0587	1.3	2.5257	5.5	0.2209	5.3	0.97	1286.6	61.7	1279.5	39.7	1267.5	26.2	1267.5	26.2	101.5
ASH08A-34	356	113489	73.6	17.9430	1.7	0.5671	2.2	0.0738	1.4	0.63	459.0	6.1	456.1	8.0	441.7	37.9	459.0	6.1	103.9
ASH08A-35	822	164112	9.9	12.7438	0.5	1.9072	1.5	0.1763	1.4	0.94	1046.6	13.8	1083.6	10.1	1158.8	10.2	1158.8	10.2	90.3
ASH08A-36	70	62862	0.9	8.8244	0.8	5.2602	2.6	0.3367	2.5	0.95	1870.6	40.3	1862.4	22.2	1853.3	14.1	1853.3	14.1	100.9
ASH08A-37	253	63778	94.8	17.6985	2.3	0.5802	2.5	0.0745	1.1	0.42	463.1	4.7	464.6	9.3	472.1	50.0	463.1	4.7	98.1
ASH08A-38	546	287576	1.1	11.7077	0.3	2.6403	1.8	0.2242	1.8	0.98	1304.0	21.0	1311.9	13.3	1324.9	6.4	1324.9	6.4	98.4
ASH08A-39	741	308679	1.6	9.1550	0.7	4.7427	2.5	0.3149	2.4	0.95	1764.8	36.6	1774.8	20.8	1786.6	13.5	1786.6	13.5	98.8
ASH08A-41	122	21157	105.3	17.5589	5.8	0.5714	6.2	0.0728	2.2	0.36	452.8	9.8	458.9	22.8	489.7	127.3	452.8	9.8	92.5
ASH08A-42	721	215101	2.8	13.5203	0.3	1.7502	3.0	0.1716	3.0	0.99	1021.0	28.0	1027.2	19.3	1040.4	6.5	1040.4	6.5	98.1
ASH08A-43	148	93383	1.6	11.7597	1.6	2.7877	2.6	0.2378	2.0	0.79	1375.0	25.0	1352.2	19.2	1316.3	30.7	1316.3	30.7	104.5
ASH08A-44	221	82621	2.2	12.3611	0.4	2.2751	2.2	0.2040	2.2	0.98	1196.6	23.7	1204.6	15.6	1219.0	8.6	1219.0	8.6	98.2
ASH08A-45	231	185709	3.3	10.8923	0.7	3.0176	2.1	0.2384	2.0	0.95	1378.3	25.2	1412.1	16.4	1463.4	13.3	1463.4	13.3	94.2
ASH08A-46	218	126312	2.3	10.1821	1.5	3.9779	2.1	0.2938	1.4	0.67	1660.3	20.3	1629.7	16.8	1590.4	28.6	1590.4	28.6	104.4
ASH08A-47	356	153451	2.2	11.5690	1.2	2.8414	1.9	0.2384	1.5	0.78	1378.4	18.0	1366.5	14.0	1348.0	22.6	1348.0	22.6	102.3
ASH08A-48	106	53964	1.3	9.8095	1.6	3.7695	4.0	0.2682	3.7	0.92	1531.6	50.7	1586.3	32.4	1659.8	29.4	1659.8	29.4	92.3
ASH08A-49	170	92434	1.0	11.6869	0.9	2.6812	1.9	0.2273	1.7	0.89	1320.2	20.1	1323.3	14.1	1328.4	17.2	1328.4	17.2	99.4
ASH08A-50	362	589738	2.6	10.0140	0.8	3.6985	5.8	0.2686	5.7	0.99	1533.8	78.4	1571.0	46.4	1621.5	15.7	1621.5	15.7	94.6
ASH08A-51	447	386221	2.6	12.1133	1.0	2.4194	2.1	0.2126	1.8	0.88	1242.4	20.8	1248.4	15.0	1258.7	19.3	1258.7	19.3	98.7
ASH08A-52	83	55702	0.8	9.1245	1.1	4.7331	2.6	0.3132	2.4	0.91	1756.5	36.5	1773.1	21.9	1792.7	20.0	1792.7	20.0	98.0
ASH08A-53	672	50039	65.8	17.6279	1.2	0.5811	1.4	0.0743	0.8	0.55	461.9	3.4	465.1	5.2	481.0	25.7	461.9	3.4	96.0
ASH08A-55	219	34278	69.6	17.6255	2.7	0.5810	2.9	0.0743	1.1	0.38	461.8	4.8	465.1	10.7	481.3	58.7	461.8	4.8	96.0

Appendix E: LA-ICP-MS U-Pb Zircon Geochronology (cont.)

ASH08-9-1a (biotite gneiss cont.)				Isotope ratios							Apparent ages (Ma)								
Analysis	U (ppm)	206Pb 204Pb	U/Th	206Pb* 207Pb*	± (%)	207Pb* 235U*	± (%)	206Pb* 238U	± (%)	error corr.	206Pb* 238U*	± (Ma)	207Pb* 235U	± (Ma)	206Pb* 207Pb*	± (Ma)	'best age' (Ma)	± (Ma)	Conc (%)
ASH08A-56	143	49012	0.6	11.7412	1.1	2.6479	2.3	0.2255	2.0	0.88	1310.8	23.9	1314.1	16.8	1319.4	20.8	1319.4	20.8	99.3
ASH08A-58	543	186738	0.4	11.8275	0.5	2.6161	1.1	0.2244	1.0	0.92	1305.1	12.1	1305.2	8.2	1305.2	8.7	1305.2	8.7	100.0
ASH08A-59	413	63702	10.4	13.6913	0.7	1.6361	1.2	0.1625	1.0	0.80	970.5	8.6	984.2	7.6	1015.0	14.7	1015.0	14.7	95.6
DEL03-1 (biotite gneiss)				Isotope ratios							Apparent ages (Ma)								
Analysis	U (ppm)	206Pb 204Pb	U/Th	206Pb* 207Pb*	± (%)	207Pb* 235U*	± (%)	206Pb* 238U	± (%)	error corr.	206Pb* 238U*	± (Ma)	207Pb* 235U	± (Ma)	206Pb* 207Pb*	± (Ma)	'best age' (Ma)	± (Ma)	Conc (%)
DEL03-1-1	166	73046	1.4	12.0535	1.1	2.2516	3.1	0.1968	2.9	0.93	1158.3	31.0	1197.3	22.0	1268.4	21.8	1268.4	21.8	91.3
DEL03-1-2	530	173414	35.4	13.8142	0.4	1.6148	0.9	0.1618	0.8	0.88	966.7	7.2	976.0	5.7	996.9	8.7	996.9	8.7	97.0
DEL03-1-3	110	62353	1.8	9.3765	0.6	4.5920	1.6	0.3123	1.5	0.92	1751.9	22.6	1747.8	13.3	1742.9	11.3	1742.9	11.3	100.5
DEL03-1-4	110	70356	1.2	8.9466	0.6	4.7722	2.4	0.3097	2.3	0.97	1739.0	35.3	1780.0	20.0	1828.5	10.2	1828.5	10.2	95.1
DEL03-1-5	126	68558	1.3	11.6574	1.1	2.5917	2.1	0.2191	1.8	0.84	1277.2	20.6	1298.3	15.5	1333.3	22.0	1333.3	22.0	95.8
DEL03-1-6	31	11750	1.6	9.5607	1.9	4.1716	2.6	0.2893	1.8	0.70	1637.8	26.2	1668.5	21.3	1707.2	34.2	1707.2	34.2	95.9
DEL03-1-7	218	10032	9.1	13.1528	2.0	1.4547	2.9	0.1388	2.0	0.71	837.7	16.0	911.8	17.3	1095.8	40.4	1095.8	40.4	76.4
DEL03-1-8	694	217357	1.6	13.4114	0.2	1.7913	1.3	0.1742	1.3	0.98	1035.4	12.4	1042.3	8.6	1056.8	4.9	1056.8	4.9	98.0
DEL03-1-9	113	49409	1.3	11.6725	0.6	2.6390	1.2	0.2234	1.0	0.83	1299.9	11.3	1311.6	8.5	1330.8	12.4	1330.8	12.4	97.7
DEL03-1-10	315	214311	1.5	11.6841	0.5	2.4591	3.9	0.2084	3.9	0.99	1220.2	42.8	1260.1	28.1	1328.8	9.7	1328.8	9.7	91.8
DEL03-1-11	444	182461	3.4	8.2673	0.4	5.7613	1.7	0.3455	1.6	0.97	1912.8	27.2	1940.6	14.7	1970.4	7.4	1970.4	7.4	97.1
DEL03-1-12	92	62468	0.9	9.0474	1.1	4.7971	1.6	0.3148	1.3	0.76	1764.2	19.4	1784.4	13.8	1808.1	19.4	1808.1	19.4	97.6
DEL03-1-13	235	233245	3.0	11.1329	2.6	2.6118	3.0	0.2109	1.5	0.50	1233.5	16.9	1304.0	22.0	1421.8	49.3	1421.8	49.3	86.8
DEL03-1-14	269	179500	2.7	11.9053	0.8	2.4857	1.2	0.2146	0.8	0.72	1253.4	9.6	1267.9	8.4	1292.4	15.6	1292.4	15.6	97.0
DEL03-1-15	897	256111	1.5	13.5125	0.3	1.7962	1.5	0.1760	1.4	0.98	1045.2	13.9	1044.1	9.6	1041.6	5.5	1041.6	5.5	100.3

Appendix E: LA-ICP-MS U-Pb Zircon Geochronology (cont.)

DEL03-1 (biotite gneiss cont.)				Isotope ratios							Apparent ages (Ma)								
Analysis	U (ppm)	206Pb 204Pb	U/Th	206Pb* 207Pb*	± (%)	207Pb* 235U*	± (%)	206Pb* 238U	± (%)	error corr.	206Pb* 238U*	± (Ma)	207Pb* 235U	± (Ma)	206Pb* 207Pb*	± (Ma)	'best age' (Ma)	± (Ma)	Conc (%)
DEL03-1-16	536	107091	5.6	12.3691	1.1	1.8618	6.0	0.1670	5.9	0.98	995.7	54.8	1067.6	39.9	1217.7	21.2	1217.7	21.2	81.8
DEL03-1-17	324	158677	4.6	10.3180	1.7	3.1469	2.3	0.2355	1.5	0.66	1363.2	18.9	1444.2	17.9	1565.6	32.6	1565.6	32.6	87.1
DEL03-1-18	94	44961	2.1	11.5841	1.7	2.8058	2.8	0.2357	2.2	0.79	1364.5	27.4	1357.1	21.1	1345.5	33.4	1345.5	33.4	101.4
DEL03-1-19	739	179468	4.3	13.5115	0.3	1.7159	0.8	0.1681	0.7	0.94	1001.9	6.7	1014.5	4.9	1041.7	5.3	1041.7	5.3	96.2
DEL03-1-20	406	127315	10.6	13.2524	2.8	1.7712	3.6	0.1702	2.2	0.63	1013.4	21.0	1035.0	23.2	1080.7	56.0	1080.7	56.0	93.8
DEL03-1-21	191	55566	0.7	11.7866	0.8	2.6470	1.6	0.2263	1.4	0.88	1314.9	16.5	1313.8	11.7	1311.9	14.8	1311.9	14.8	100.2
DEL03-1-22	124	118535	1.3	12.0407	1.5	2.3826	1.9	0.2081	1.1	0.60	1218.5	12.5	1237.4	13.3	1270.4	29.0	1270.4	29.0	95.9
DEL03-1-23	2542	78063	6.0	12.0741	2.1	2.4499	3.1	0.2145	2.3	0.73	1252.9	25.8	1257.4	22.5	1265.0	41.6	1265.0	41.6	99.0
DEL03-1-24	101	57990	1.1	9.2807	1.8	3.9600	3.3	0.2666	2.7	0.84	1523.3	37.2	1626.0	26.5	1761.7	32.6	1761.7	32.6	86.5
DEL03-1-25	138	52726	1.4	9.5118	0.9	4.3313	2.6	0.2988	2.4	0.94	1685.4	35.8	1699.3	21.2	1716.6	16.3	1716.6	16.3	98.2
DEL03-1-26	540	466297	1.1	9.7846	0.3	3.8458	1.0	0.2729	0.9	0.96	1555.6	12.9	1602.4	7.9	1664.5	5.2	1664.5	5.2	93.5
DEL03-1-27	147	193594	1.2	9.4338	1.2	4.1645	2.8	0.2849	2.5	0.90	1616.2	36.4	1667.1	23.0	1731.7	22.0	1731.7	22.0	93.3
DEL03-1-28	1057	379047	4.6	13.6230	0.4	1.7247	0.9	0.1704	0.8	0.91	1014.3	7.6	1017.8	5.7	1025.1	7.4	1025.1	7.4	98.9
DEL03-1-29	251	129707	0.8	11.7542	0.6	2.7136	2.3	0.2313	2.2	0.96	1341.5	26.8	1332.2	17.1	1317.3	12.3	1317.3	12.3	101.8
DEL03-1-30	83	39367	2.1	11.8488	2.4	2.2872	5.4	0.1965	4.8	0.90	1156.7	51.3	1208.3	38.1	1301.7	45.9	1301.7	45.9	88.9
DEL03-1-31	116	144694	1.0	8.8801	0.9	5.0676	1.8	0.3264	1.6	0.88	1820.8	25.8	1830.7	15.6	1842.0	15.8	1842.0	15.8	98.8
DEL03-1-32	175	41439	3.6	14.0820	2.9	1.4115	3.4	0.1442	1.8	0.54	868.2	14.8	893.8	20.2	957.8	58.7	957.8	58.7	90.6
DEL03-1-33	180	23122	1.2	12.6346	1.8	1.9417	2.5	0.1779	1.7	0.69	1055.7	16.5	1095.6	16.5	1175.8	35.3	1175.8	35.3	89.8
DEL03-1-34	190	30501	1.2	11.8758	1.4	2.4638	2.5	0.2122	2.0	0.82	1240.6	23.1	1261.5	18.0	1297.3	27.5	1297.3	27.5	95.6
DEL03-1-35	53	55923	1.0	8.8170	1.5	5.2218	3.3	0.3339	3.0	0.90	1857.3	47.7	1856.2	28.1	1854.9	26.3	1854.9	26.3	100.1
DEL03-1-36	267	52081	2.0	10.1904	0.7	3.3052	3.5	0.2443	3.4	0.98	1408.9	43.1	1482.3	27.1	1588.9	13.0	1588.9	13.0	88.7
DEL03-1-37	878	442262	23.6	13.7586	0.3	1.6457	2.1	0.1642	2.0	0.99	980.2	18.6	987.9	13.1	1005.1	7.0	1005.1	7.0	97.5
DEL03-1-38	536	241047	7.6	11.5512	1.6	2.6764	1.9	0.2242	0.9	0.50	1304.1	11.2	1322.0	14.1	1350.9	31.8	1350.9	31.8	96.5
DEL03-1-39	431	276292	1.2	10.0505	0.6	3.4538	1.7	0.2518	1.6	0.94	1447.5	21.2	1516.7	13.7	1614.7	11.1	1614.7	11.1	89.6
DEL03-1-40	232	117553	1.8	9.3647	0.8	4.2986	5.3	0.2920	5.3	0.99	1651.3	76.5	1693.1	43.8	1745.2	14.3	1745.2	14.3	94.6

Appendix E: LA-ICP-MS U-Pb Zircon Geochronology (cont.)

DEL03-1 (biotite gneiss cont.)				Isotope ratios							Apparent ages (Ma)								
Analysis	U (ppm)	206Pb 204Pb	U/Th	206Pb* 207Pb*	± (%)	207Pb* 235U*	± (%)	206Pb* 238U	± (%)	error corr.	206Pb* 238U*	± (Ma)	207Pb* 235U	± (Ma)	206Pb* 207Pb*	± (Ma)	'best age' (Ma)	± (Ma)	Conc (%)
DEL03-1-41	114	47352	2.7	12.1942	1.2	2.0516	4.3	0.1814	4.2	0.96	1074.9	41.2	1132.8	29.5	1245.6	23.4	1245.6	23.4	86.3
DEL03-1-44	78	107237	1.6	9.9125	1.4	4.0131	4.3	0.2885	4.1	0.94	1634.1	58.6	1636.9	35.0	1640.4	26.5	1640.4	26.5	99.6
DEL03-1-45	243	134667	5.6	11.4525	0.6	2.5819	3.3	0.2145	3.2	0.98	1252.5	36.3	1295.5	23.8	1367.5	12.5	1367.5	12.5	91.6
DEL03-1-46	163	80647	2.6	10.5531	1.6	3.4760	3.0	0.2660	2.6	0.85	1520.7	35.1	1521.8	24.0	1523.3	29.9	1523.3	29.9	99.8
DEL03-1-47	121	125389	1.9	9.2018	0.4	4.7401	1.5	0.3163	1.5	0.96	1771.9	23.0	1774.4	12.9	1777.3	7.8	1777.3	7.8	99.7
DEL03-1-49	340	60049	8.5	13.7379	0.7	1.7229	1.4	0.1717	1.2	0.88	1021.3	11.7	1017.1	9.1	1008.1	13.8	1008.1	13.8	101.3
DEL03-1-50	165	89501	0.8	11.5758	0.9	2.8241	2.0	0.2371	1.8	0.89	1371.6	21.7	1362.0	14.8	1346.8	17.4	1346.8	17.4	101.8
DEL03-1-51	212	206951	2.0	12.0589	1.2	2.3812	4.5	0.2083	4.3	0.97	1219.5	48.1	1237.0	32.1	1267.5	22.5	1267.5	22.5	96.2
DEL03-1-52	213	104369	2.2	9.5559	0.4	3.8919	2.4	0.2697	2.3	0.98	1539.4	32.1	1612.0	19.3	1708.1	7.8	1708.1	7.8	90.1
DEL03-1-53	286	170272	2.6	11.4645	4.7	2.7250	5.4	0.2266	2.6	0.49	1316.6	31.5	1335.3	39.9	1365.5	90.1	1365.5	90.1	96.4
DEL03-1-55	810	273144	1.0	11.5049	0.2	2.8343	3.4	0.2365	3.4	1.00	1368.5	42.4	1364.7	25.9	1358.7	4.5	1358.7	4.5	100.7
DEL03-1-56	134	76119	2.0	9.1974	0.6	4.5698	3.1	0.3048	3.0	0.98	1715.2	45.1	1743.8	25.5	1778.2	11.1	1778.2	11.1	96.5
DEL03-1-57	840	424240	2.4	11.4507	0.3	2.7894	0.9	0.2317	0.9	0.96	1343.2	11.0	1352.7	7.0	1367.8	5.0	1367.8	5.0	98.2
DEL03-1-58	327	245553	1.1	9.3759	1.7	4.2323	4.9	0.2878	4.6	0.94	1630.5	66.6	1680.3	40.4	1743.0	30.8	1743.0	30.8	93.5
DEL03-1-59	777	162627	1.9	13.4407	0.4	1.7761	1.8	0.1731	1.7	0.97	1029.4	16.3	1036.7	11.5	1052.4	8.1	1052.4	8.1	97.8
DEL03-1-60	1179	284169	7.3	13.5843	0.3	1.7083	1.3	0.1683	1.3	0.98	1002.8	11.9	1011.7	8.4	1030.9	5.7	1030.9	5.7	97.3
DEL03-1-61	111	7104	0.8	12.6514	2.4	1.8555	4.9	0.1703	4.2	0.87	1013.5	39.7	1065.4	32.2	1173.2	47.7	1173.2	47.7	86.4
DEL03-1-62	411	272051	2.2	10.7838	0.6	3.0527	5.5	0.2388	5.5	0.99	1380.2	68.0	1420.9	42.2	1482.4	12.2	1482.4	12.2	93.1
DEL03-1-63	927	124781	2.1	13.4387	0.2	1.8539	0.8	0.1807	0.8	0.97	1070.8	7.8	1064.8	5.3	1052.7	3.7	1052.7	3.7	101.7
DEL03-1-64	920	325910	2.2	13.3606	0.3	1.8737	1.0	0.1816	0.9	0.96	1075.5	9.3	1071.8	6.5	1064.4	5.6	1064.4	5.6	101.0
DEL03-1-66	1032	423292	1.6	13.4325	0.3	1.8027	1.0	0.1756	1.0	0.96	1043.0	9.3	1046.5	6.6	1053.6	6.0	1053.6	6.0	99.0
DEL03-1-67	115	137146	1.0	9.1500	0.9	4.4640	1.6	0.2962	1.3	0.83	1672.6	19.5	1724.3	13.2	1787.6	16.2	1787.6	16.2	93.6
DEL03-1-68	291	96016	1.5	12.2740	0.9	2.1433	2.1	0.1908	1.9	0.91	1125.7	19.5	1162.9	14.4	1232.9	17.3	1232.9	17.3	91.3
DEL03-1-69	738	295140	2.5	13.4914	0.2	1.7775	1.1	0.1739	1.1	0.98	1033.7	10.5	1037.3	7.3	1044.7	5.0	1044.7	5.0	98.9
DEL03-1-70	193	14359	1.1	12.5785	1.0	2.1295	1.4	0.1943	0.9	0.67	1144.5	9.7	1158.4	9.4	1184.6	19.9	1184.6	19.9	96.6

Appendix E: LA-ICP-MS U-Pb Zircon Geochronology (cont.)

DEL03-1 (biotite gneiss cont.)				Isotope ratios							Apparent ages (Ma)								
Analysis	U (ppm)	206Pb 204Pb	U/Th	206Pb* 207Pb*	± (%)	207Pb* 235U*	± (%)	206Pb* 238U	± (%)	error corr.	206Pb* 238U*	± (Ma)	207Pb* 235U	± (Ma)	206Pb* 207Pb*	± (Ma)	'best age' (Ma)	± (Ma)	Conc (%)
DEL03-1-71	135	89781	1.4	9.4517	0.6	4.2453	2.1	0.2910	2.0	0.95	1646.6	29.0	1682.8	17.2	1728.3	11.4	1728.3	11.4	95.3
DEL03-1-74	120	82435	1.5	9.5321	0.8	3.7814	6.9	0.2614	6.9	0.99	1497.1	91.9	1588.8	55.6	1712.7	14.2	1712.7	14.2	87.4
DEL03-1-75	961	478526	1.8	13.4003	0.3	1.7965	0.9	0.1746	0.8	0.95	1037.4	8.0	1044.2	5.7	1058.4	5.3	1058.4	5.3	98.0
DEL03-1-76	131	25283	1.9	11.5652	1.1	2.5410	2.6	0.2131	2.4	0.90	1245.5	27.0	1283.9	19.2	1348.6	21.7	1348.6	21.7	92.4
DEL03-1-78	156	110353	1.2	9.3056	0.6	4.1719	4.9	0.2816	4.9	0.99	1599.2	69.1	1668.5	40.3	1756.8	11.7	1756.8	11.7	91.0
DEL03-1-79	189	165678	1.7	8.6700	0.5	5.2003	1.6	0.3270	1.6	0.95	1823.8	24.9	1852.7	14.0	1885.2	8.9	1885.2	8.9	96.7
DEL03-1-80	98	105054	1.3	8.4840	0.9	5.8723	3.5	0.3613	3.4	0.96	1988.5	57.9	1957.1	30.4	1924.2	16.5	1924.2	16.5	103.3
DEL03-1-81	80	7809	1.1	11.2077	1.9	2.8639	2.5	0.2328	1.6	0.64	1349.1	19.4	1372.5	18.7	1409.0	36.5	1409.0	36.5	95.8
DEL03-1-82	181	99529	2.2	9.6114	0.8	4.0716	2.1	0.2838	2.0	0.93	1610.6	27.9	1648.6	17.2	1697.5	14.5	1697.5	14.5	94.9
DEL03-1-83	1160	372483	13.7	13.6102	0.3	1.6962	0.9	0.1674	0.8	0.94	998.0	7.6	1007.1	5.6	1027.0	6.2	1027.0	6.2	97.2
DEL03-1-84	216	26768	1.5	12.4450	0.9	2.2974	2.1	0.2074	1.9	0.90	1214.7	21.3	1211.5	15.1	1205.7	18.0	1205.7	18.0	100.8
DEL03-1-85	735	138734	2.1	13.5451	0.5	1.7455	1.3	0.1715	1.2	0.94	1020.2	11.3	1025.5	8.3	1036.7	9.2	1036.7	9.2	98.4
DEL03-1-86	152	218689	1.4	11.7247	0.6	2.6649	2.3	0.2266	2.2	0.96	1316.7	26.1	1318.8	16.9	1322.1	12.4	1322.1	12.4	99.6
DEL03-1-87	727	282975	10.1	13.5787	0.5	1.6887	1.6	0.1663	1.5	0.96	991.7	14.2	1004.3	10.3	1031.7	9.5	1031.7	9.5	96.1
DEL03-1-88	240	109351	2.8	9.2804	0.5	4.1182	1.1	0.2772	1.0	0.90	1577.2	13.3	1657.9	8.6	1761.8	8.3	1761.8	8.3	89.5
DEL03-1-89	270	440283	1.6	9.2078	0.5	4.7151	1.4	0.3149	1.4	0.95	1764.7	21.1	1769.9	12.1	1776.1	8.4	1776.1	8.4	99.4
DEL03-1-90	117	142349	2.3	11.9049	2.0	2.5840	3.3	0.2231	2.6	0.80	1298.3	30.8	1296.1	24.1	1292.5	38.9	1292.5	38.9	100.4
DEL03-1-91	270	127256	4.5	11.5043	0.6	2.5908	1.1	0.2162	1.0	0.86	1261.6	11.0	1298.0	8.2	1358.8	11.2	1358.8	11.2	92.8
DEL03-1-92	219	93274	1.6	9.8085	1.0	3.8715	2.3	0.2754	2.1	0.91	1568.2	29.0	1607.8	18.6	1660.0	17.9	1660.0	17.9	94.5
DEL03-1-93	615	237458	2.3	13.6128	0.2	1.7470	1.0	0.1725	1.0	0.97	1025.7	9.0	1026.0	6.3	1026.7	4.6	1026.7	4.6	99.9
DEL03-1-95	384	109743	14.8	12.4380	0.4	2.1850	1.6	0.1971	1.5	0.96	1159.7	15.9	1176.3	10.9	1206.8	8.5	1206.8	8.5	96.1
DEL03-1-96	141	224716	2.2	9.0397	0.5	4.5425	1.9	0.2978	1.9	0.96	1680.5	27.6	1738.8	16.1	1809.7	9.7	1809.7	9.7	92.9
DEL03-1-97	118	31992	2.1	12.2556	1.4	1.7973	2.3	0.1598	1.9	0.80	955.4	16.6	1044.5	15.2	1235.8	27.4	1235.8	27.4	77.3
DEL03-1-98	851	331771	1.5	13.4509	0.2	1.8132	0.8	0.1769	0.8	0.96	1049.9	7.8	1050.2	5.5	1050.8	4.5	1050.8	4.5	99.9
DEL03-1-99	63	42449	1.0	9.5521	1.7	3.6997	4.6	0.2563	4.3	0.93	1470.9	56.4	1571.3	37.0	1708.8	31.9	1708.8	31.9	86.1
DEL03-1-100	287	234574	1.3	9.2955	0.7	4.3272	2.0	0.2917	1.9	0.93	1650.1	27.3	1698.5	16.6	1758.8	13.2	1758.8	13.2	93.8

Appendix E: LA-ICP-MS U-Pb Zircon Geochronology (cont.)

DEL08-2e (biotite gneiss)				Isotope ratios							Apparent ages (Ma)								
Analysis	U (ppm)	206Pb 204Pb	U/Th	206Pb* 207Pb*	± (%)	207Pb* 235U*	± (%)	206Pb* 238U	± (%)	error corr.	206Pb* 238U*	± (Ma)	207Pb* 235U	± (Ma)	206Pb* 207Pb*	± (Ma)	'best age' (Ma)	± (Ma)	Conc (%)
DEL082E-1	52	37085	1.2	12.9035	3.0	2.0234	4.1	0.1894	2.8	0.68	1117.9	29.0	1123.4	28.1	1134.0	59.9	1134.0	59.9	98.6
DEL082E-2	103	66559	1.7	13.8301	1.9	1.6358	2.2	0.1641	1.0	0.45	979.4	8.8	984.1	13.6	994.6	39.1	994.6	39.1	98.5
DEL082E-3	37	11137	1.3	13.8235	4.3	1.6843	5.0	0.1689	2.4	0.48	1005.9	22.4	1002.6	31.6	995.5	88.3	995.5	88.3	101.0
DEL082E-4	220	89599	3.5	12.9163	1.4	1.9613	2.3	0.1837	1.9	0.79	1087.3	18.7	1102.3	15.8	1132.0	28.4	1132.0	28.4	96.0
DEL082E-5	297	162024	1.5	12.6258	0.9	2.1064	1.8	0.1929	1.5	0.85	1137.0	15.7	1150.9	12.2	1177.2	18.2	1177.2	18.2	96.6
DEL082E-6	117	48042	2.2	12.2784	1.8	2.3443	2.4	0.2088	1.6	0.65	1222.2	17.4	1225.8	17.2	1232.2	36.0	1232.2	36.0	99.2
DEL082E-7	253	142411	3.3	12.8179	0.8	1.9997	1.8	0.1859	1.6	0.89	1099.1	16.2	1115.4	12.2	1147.3	16.4	1147.3	16.4	95.8
DEL082E-8	146	46486	0.8	12.5987	1.6	2.1803	2.1	0.1992	1.4	0.67	1171.1	15.1	1174.8	14.7	1181.5	30.9	1181.5	30.9	99.1
DEL082E-9	825	618376	1.6	13.4686	0.3	1.7864	0.9	0.1745	0.8	0.94	1036.9	8.1	1040.5	5.9	1048.2	6.4	1048.2	6.4	98.9
DEL082E-10	343	9482	3.0	13.3294	1.4	1.6077	2.2	0.1554	1.7	0.76	931.3	14.4	973.2	13.7	1069.1	28.9	1069.1	28.9	87.1
DEL082E-11	227	64523	2.4	13.6402	1.2	1.7181	1.7	0.1700	1.1	0.67	1012.0	10.5	1015.3	10.8	1022.6	25.2	1022.6	25.2	99.0
DEL082E-12	170	48171	2.8	12.3414	1.0	2.3782	1.3	0.2129	0.8	0.63	1244.1	9.2	1236.1	9.2	1222.1	19.6	1222.1	19.6	101.8
DEL082E-13	214	137130	3.6	12.6926	1.0	2.1430	1.3	0.1973	0.9	0.69	1160.7	9.9	1162.8	9.3	1166.7	19.2	1166.7	19.2	99.5
DEL082E-14	219	72079	3.3	13.6017	1.1	1.7601	1.4	0.1736	0.9	0.63	1032.1	8.6	1030.9	9.2	1028.3	22.2	1028.3	22.2	100.4
DEL082E-15	172	71316	8.6	13.3914	1.1	1.7682	1.4	0.1717	0.8	0.60	1021.7	7.7	1033.9	8.9	1059.8	22.1	1059.8	22.1	96.4
DEL082E-16	631	156120	2.4	12.6166	0.3	2.0824	0.8	0.1905	0.8	0.94	1124.3	8.0	1143.0	5.7	1178.7	5.8	1178.7	5.8	95.4
DEL082E-17	145	77589	1.9	12.3314	0.7	2.4188	3.3	0.2163	3.2	0.97	1262.4	36.4	1248.2	23.4	1223.7	14.3	1223.7	14.3	103.2
DEL082E-18	157	51164	4.4	13.1495	1.4	1.8790	2.8	0.1792	2.5	0.87	1062.6	24.0	1073.7	18.6	1096.3	27.3	1096.3	27.3	96.9
DEL082E-19	107	63388	0.8	12.6120	1.2	2.1928	1.8	0.2006	1.3	0.71	1178.4	13.5	1178.8	12.3	1179.4	24.4	1179.4	24.4	99.9
DEL082E-20	294	190928	2.2	13.4669	0.5	1.8448	2.6	0.1802	2.5	0.98	1068.0	24.6	1061.6	16.8	1048.5	10.1	1048.5	10.1	101.9
DEL082E-21	1377	602457	8.9	13.4797	0.2	1.7442	1.2	0.1705	1.2	0.98	1015.0	11.3	1025.0	7.9	1046.5	4.7	1046.5	4.7	97.0
DEL082E-22	86	57762	4.9	12.6274	2.4	2.1329	2.8	0.1953	1.5	0.52	1150.2	15.4	1159.5	19.3	1177.0	47.1	1177.0	47.1	97.7
DEL082E-23	143	94998	2.9	11.6518	1.4	2.5233	3.3	0.2132	3.0	0.91	1246.1	33.7	1278.8	23.8	1334.2	26.5	1334.2	26.5	93.4
DEL082E-24	415	134906	1.7	10.4353	0.5	3.0624	1.2	0.2318	1.1	0.91	1343.8	13.5	1423.3	9.4	1544.4	9.6	1544.4	9.6	87.0

Appendix E: LA-ICP-MS U-Pb Zircon Geochronology (cont.)

DEL08-2e (biotite gneiss cont.)				Isotope ratios							Apparent ages (Ma)								
Analysis	U (ppm)	206Pb 204Pb	U/Th	206Pb* 207Pb*	± (%)	207Pb* 235U*	± (%)	206Pb* 238U	± (%)	error corr.	206Pb* 238U*	± (Ma)	207Pb* 235U	± (Ma)	206Pb* 207Pb*	± (Ma)	'best age' (Ma)	± (Ma)	Conc (%)
DEL082E-25	387	126222	3.2	12.3494	0.8	2.1157	1.5	0.1895	1.2	0.83	1118.7	12.6	1153.9	10.2	1220.8	16.1	1220.8	16.1	91.6
DEL082E-26	377	118341	2.9	12.7126	0.7	2.1841	5.3	0.2014	5.3	0.99	1182.7	56.7	1176.0	36.9	1163.6	13.4	1163.6	13.4	101.6
DEL082E-27	75	24279	1.6	13.6349	3.5	1.7415	3.8	0.1722	1.5	0.40	1024.3	14.4	1024.0	24.5	1023.4	70.3	1023.4	70.3	100.1
DEL082E-28	1333	230994	4.5	13.9601	0.3	1.5968	3.1	0.1617	3.1	0.99	966.0	27.9	968.9	19.5	975.5	6.5	975.5	6.5	99.0
DEL082E-29	106	25726	1.9	12.0365	1.8	2.5694	2.2	0.2243	1.3	0.58	1304.6	15.2	1292.0	16.1	1271.1	34.8	1271.1	34.8	102.6
DEL082E-30	53	20741	1.2	12.2290	6.6	2.2765	7.1	0.2019	2.6	0.37	1185.6	28.6	1205.0	50.0	1240.1	128.8	1240.1	128.8	95.6
DEL082E-31	1531	29790	7.0	13.1905	1.2	1.7873	2.9	0.1710	2.6	0.91	1017.5	24.5	1040.8	18.6	1090.1	23.7	1090.1	23.7	93.3
DEL082E-32	147	6783	2.8	12.8328	1.7	1.9860	2.8	0.1848	2.2	0.79	1093.4	22.6	1110.8	19.2	1145.0	34.7	1145.0	34.7	95.5
DEL082E-33	223	214969	1.9	12.2483	0.7	2.4374	1.8	0.2165	1.7	0.93	1263.5	19.7	1253.7	13.3	1237.0	13.4	1237.0	13.4	102.1
DEL082E-35	362	168598	4.4	13.4857	0.9	1.3950	1.9	0.1364	1.7	0.88	824.5	12.8	886.8	11.1	1045.6	18.1	1045.6	18.1	78.9
DEL082E-36	293	76901	1.5	13.5388	0.7	1.7420	1.1	0.1711	0.9	0.81	1017.9	8.8	1024.2	7.4	1037.7	13.4	1037.7	13.4	98.1
DEL082E-37	227	102434	1.6	12.7166	1.2	2.0949	2.0	0.1932	1.7	0.82	1138.7	17.2	1147.1	13.9	1163.0	23.0	1163.0	23.0	97.9
DEL082E-38	1221	165830	13.9	13.8020	0.2	1.5751	8.2	0.1577	8.2	1.00	943.8	71.7	960.4	50.8	998.7	3.4	998.7	3.4	94.5
DEL082E-39	239	133071	3.4	13.5828	1.3	1.4562	2.4	0.1435	2.0	0.85	864.2	16.3	912.4	14.3	1031.1	25.4	1031.1	25.4	83.8
DEL082E-40	210	99791	3.0	13.4036	1.2	1.7981	1.7	0.1748	1.1	0.68	1038.5	11.0	1044.8	11.0	1058.0	24.7	1058.0	24.7	98.2
DEL082E-41	332	368037	1.8	8.7687	0.5	4.9689	2.3	0.3160	2.2	0.97	1770.2	34.1	1814.0	19.2	1864.8	9.7	1864.8	9.7	94.9
DEL082E-42	282	86079	4.4	12.8641	1.0	1.8570	6.1	0.1733	6.0	0.99	1030.0	57.1	1065.9	40.2	1140.1	20.3	1140.1	20.3	90.3
DEL082E-43	259	102326	1.2	12.7150	0.9	2.1487	5.6	0.1981	5.6	0.99	1165.3	59.4	1164.6	39.1	1163.3	17.0	1163.3	17.0	100.2
DEL082E-44	65	35242	2.4	12.2703	2.3	2.3600	2.8	0.2100	1.5	0.54	1228.9	16.9	1230.6	19.7	1233.5	45.5	1233.5	45.5	99.6
DEL082E-45	118	68885	2.8	13.1743	2.1	1.8213	3.4	0.1740	2.7	0.80	1034.2	25.8	1053.2	22.3	1092.6	41.2	1092.6	41.2	94.7
DEL082E-46	218	124695	1.8	11.7972	1.0	2.5483	8.6	0.2180	8.5	0.99	1271.5	98.3	1285.9	62.6	1310.2	19.7	1310.2	19.7	97.0
DEL082E-47	125	16310	2.7	11.5375	8.0	2.3925	9.1	0.2002	4.4	0.48	1176.4	47.0	1240.4	65.2	1353.2	154.1	1353.2	154.1	86.9
DEL082E-48	58	19290	3.1	12.6597	2.5	2.1260	3.6	0.1952	2.5	0.71	1149.5	26.5	1157.3	24.6	1171.9	50.0	1171.9	50.0	98.1
DEL082E-49	96	65785	1.0	13.0761	4.1	1.8771	4.4	0.1780	1.4	0.33	1056.2	14.1	1073.1	29.0	1107.5	82.6	1107.5	82.6	95.4
DEL082E-50	34	10441	2.1	13.6731	6.4	1.6895	6.9	0.1675	2.5	0.37	998.6	23.5	1004.6	43.9	1017.7	129.6	1017.7	129.6	98.1

Appendix E: LA-ICP-MS U-Pb Zircon Geochronology (cont.)

DEL08-2e (biotite gneiss cont.)				Isotope ratios							Apparent ages (Ma)								
Analysis	U (ppm)	206Pb 204Pb	U/Th	206Pb* 207Pb*	± (%)	207Pb* 235U*	± (%)	206Pb* 238U	± (%)	error corr.	206Pb* 238U*	± (Ma)	207Pb* 235U	± (Ma)	206Pb* 207Pb*	± (Ma)	'best age' (Ma)	± (Ma)	Conc (%)
DEL082E-51	517	222859	8.1	13.5968	0.6	1.6770	1.5	0.1654	1.4	0.92	986.6	12.5	999.8	9.5	1029.0	12.0	1029.0	12.0	95.9
DEL082E-52	102	38261	1.8	13.5573	3.4	1.7699	4.0	0.1740	2.1	0.53	1034.3	20.2	1034.5	25.9	1034.9	68.3	1034.9	68.3	99.9
DEL082E-53	63	28910	1.3	12.5772	3.1	2.1214	3.6	0.1935	2.0	0.54	1140.3	20.4	1155.8	25.2	1184.9	60.9	1184.9	60.9	96.2
DEL082E-54	221	110081	3.6	13.3187	0.8	1.8049	1.2	0.1743	0.9	0.76	1036.0	8.4	1047.2	7.6	1070.7	15.3	1070.7	15.3	96.8
DEL082E-55	243	42207	2.4	12.5864	1.7	2.0307	3.5	0.1854	3.1	0.88	1096.3	31.0	1125.8	23.8	1183.4	32.8	1183.4	32.8	92.6
DEL082E-56	143	54535	2.7	13.7564	1.6	1.7179	1.8	0.1714	0.8	0.42	1019.8	7.1	1015.2	11.4	1005.4	32.8	1005.4	32.8	101.4
DEL082E-57	55	28760	2.7	13.2943	3.9	1.6393	4.4	0.1581	2.1	0.47	946.0	18.2	985.5	27.8	1074.4	78.2	1074.4	78.2	88.0
DEL082E-58	76	49494	1.4	13.6605	2.4	1.7231	2.6	0.1707	1.0	0.39	1016.1	9.2	1017.2	16.4	1019.6	47.7	1019.6	47.7	99.7
DEL082E-59	51	15504	2.0	13.4819	5.4	1.7714	5.5	0.1732	1.3	0.23	1029.8	12.3	1035.0	36.0	1046.2	108.9	1046.2	108.9	98.4
DEL082E-59	400	90547	14.3	13.7719	0.8	1.5987	1.4	0.1597	1.1	0.80	955.0	9.7	969.7	8.5	1003.1	16.4	1003.1	16.4	95.2
DEL082E-61	427	70795	3.4	13.5881	0.6	1.6877	1.5	0.1663	1.4	0.91	991.8	12.7	1003.9	9.7	1030.3	13.0	1030.3	13.0	96.3
DEL082E-62	642	373411	2.1	13.6950	0.6	1.6737	1.5	0.1662	1.4	0.93	991.4	12.8	998.6	9.5	1014.5	11.4	1014.5	11.4	97.7
DEL082E-63	612	148518	2.2	13.2109	0.5	1.9772	3.4	0.1894	3.4	0.99	1118.4	34.6	1107.8	23.0	1087.0	9.6	1087.0	9.6	102.9
DEL082E-64	413	372023	2.7	11.1657	0.4	2.7343	2.0	0.2214	1.9	0.98	1289.4	22.7	1337.8	14.8	1416.1	8.2	1416.1	8.2	91.1
DEL082E-65	107	25277	1.7	13.5905	2.4	1.7287	2.6	0.1704	1.2	0.45	1014.3	11.2	1019.3	17.0	1030.0	47.7	1030.0	47.7	98.5
DEL082E-66	472	229395	1.3	12.7032	0.4	2.0732	0.9	0.1910	0.8	0.91	1126.8	8.5	1140.0	6.2	1165.1	7.6	1165.1	7.6	96.7
DEL082E-68	119	20180	2.2	13.6951	2.3	1.4604	5.7	0.1451	5.2	0.91	873.2	42.6	914.2	34.4	1014.5	47.2	1014.5	47.2	86.1
DEL082E-69	693	139389	2.4	13.0883	0.3	1.8821	0.9	0.1787	0.9	0.95	1059.6	8.7	1074.8	6.3	1105.7	6.1	1105.7	6.1	95.8
DEL082E-70	237	138858	3.5	11.7016	0.8	2.5126	1.2	0.2132	0.9	0.76	1246.1	10.3	1275.7	8.7	1325.9	15.1	1325.9	15.1	94.0
DEL082E-71	499	219284	2.9	12.6605	0.4	2.1711	1.2	0.1994	1.1	0.95	1171.9	12.3	1171.8	8.4	1171.8	7.5	1171.8	7.5	100.0
DEL082E-72	516	140107	3.5	12.3124	2.5	1.9148	8.4	0.1710	8.0	0.95	1017.5	75.2	1086.3	55.9	1226.7	49.6	1226.7	49.6	82.9
DEL082E-73	106	45647	2.2	13.3099	2.6	1.8565	3.3	0.1792	2.1	0.63	1062.7	20.6	1065.7	21.9	1072.0	51.5	1072.0	51.5	99.1
DEL082E-74	289	193574	3.5	12.2554	0.4	2.2923	0.9	0.2038	0.8	0.89	1195.5	9.2	1209.9	6.7	1235.9	8.3	1235.9	8.3	96.7
DEL082E-75	402	245998	2.6	12.8015	0.5	2.1053	1.1	0.1955	1.1	0.92	1150.9	11.1	1150.6	7.9	1149.8	8.9	1149.8	8.9	100.1
DEL082E-76	47	44086	1.4	13.5906	4.1	1.8063	4.5	0.1780	1.9	0.42	1056.3	18.4	1047.7	29.3	1030.0	82.1	1030.0	82.1	102.6

Appendix E: LA-ICP-MS U-Pb Zircon Geochronology (cont.)

DEL08-2e (biotite gneiss cont.)				Isotope ratios							Apparent ages (Ma)								
Analysis	U (ppm)	206Pb 204Pb	U/Th	206Pb* 207Pb*	± (%)	207Pb* 235U*	± (%)	206Pb* 238U	± (%)	error corr.	206Pb* 238U*	± (Ma)	207Pb* 235U	± (Ma)	206Pb* 207Pb*	± (Ma)	'best age' (Ma)	± (Ma)	Conc (%)
DEL082E-78	299	165803	1.6	12.4364	0.5	2.2207	0.7	0.2003	0.5	0.71	1177.0	5.2	1187.6	4.8	1207.1	9.6	1207.1	9.6	97.5
DEL082E-79	244	362633	1.4	13.4788	0.9	1.7498	3.2	0.1711	3.1	0.96	1017.9	29.1	1027.1	20.7	1046.7	17.3	1046.7	17.3	97.3
DEL082E-80	387	41309	1.8	13.1610	0.9	1.8824	1.4	0.1797	1.0	0.75	1065.2	10.3	1074.9	9.3	1094.6	18.4	1094.6	18.4	97.3
DEL082E-81	321	137574	1.1	13.5360	0.8	1.7730	1.0	0.1741	0.6	0.59	1034.4	5.7	1035.6	6.7	1038.1	16.8	1038.1	16.8	99.6
DEL082E-82	418	212016	3.5	12.7765	0.6	2.1255	1.9	0.1970	1.9	0.96	1158.9	19.7	1157.1	13.4	1153.7	11.2	1153.7	11.2	100.5
DEL082E-83	659	19710	4.6	12.8858	1.1	1.6324	7.6	0.1526	7.5	0.99	915.3	64.3	982.8	48.0	1136.8	22.4	1136.8	22.4	80.5
DEL082E-84	313	92281	2.2	13.5888	0.8	1.7788	1.3	0.1753	1.1	0.79	1041.3	10.1	1037.7	8.7	1030.2	16.6	1030.2	16.6	101.1
DEL082E-85	39	37484	0.8	12.7468	7.8	2.2161	8.2	0.2049	2.3	0.29	1201.5	25.7	1186.1	57.2	1158.3	155.5	1158.3	155.5	103.7
DEL082E-86	66	64212	2.5	12.2602	2.3	2.3797	3.9	0.2116	3.1	0.80	1237.4	35.1	1236.5	27.8	1235.1	45.6	1235.1	45.6	100.2
DEL082E-87	175	57036	2.1	12.7441	1.3	2.0769	1.5	0.1920	0.7	0.45	1132.0	6.8	1141.2	10.1	1158.7	26.0	1158.7	26.0	97.7
DEL082E-88	287	120679	1.4	11.1619	0.7	2.6944	3.5	0.2181	3.4	0.98	1271.9	39.2	1326.9	25.8	1416.8	14.3	1416.8	14.3	89.8
DEL082E-89	227	69867	2.4	12.8652	1.2	2.1102	3.8	0.1969	3.7	0.95	1158.6	39.0	1152.1	26.5	1139.9	22.9	1139.9	22.9	101.6
DEL082E-90	324	98542	2.3	12.1734	0.5	2.3846	1.4	0.2105	1.3	0.93	1231.7	15.0	1238.0	10.3	1249.0	10.3	1249.0	10.3	98.6
DEL082E-91	243	42181	10.1	14.4822	1.8	1.2961	3.0	0.1361	2.4	0.79	822.8	18.5	844.0	17.3	900.2	37.8	822.8	18.5	91.4
DEL082E-92	322	185997	1.3	10.1430	0.4	3.9980	2.6	0.2941	2.6	0.99	1662.0	37.6	1633.8	21.1	1597.6	7.1	1597.6	7.1	104.0
DEL082E-93	540	198717	3.2	12.8603	1.1	2.1035	2.0	0.1962	1.7	0.85	1154.9	18.2	1150.0	13.9	1140.7	21.0	1140.7	21.0	101.2
DEL082E-94	177	60271	2.2	12.5383	1.3	2.2463	2.0	0.2043	1.5	0.76	1198.2	16.9	1195.6	14.3	1190.9	26.2	1190.9	26.2	100.6
DEL082E-95	299	146908	2.4	12.7741	0.4	2.0600	2.3	0.1909	2.2	0.98	1126.0	23.2	1135.6	15.6	1154.1	8.7	1154.1	8.7	97.6
DEL082E-96	115	90161	2.2	12.3987	1.5	2.3051	1.7	0.2073	0.8	0.49	1214.3	9.0	1213.9	11.8	1213.0	28.7	1213.0	28.7	100.1
DEL082E-97	291	132059	3.9	12.6055	0.6	2.1805	1.2	0.1994	1.1	0.86	1171.8	11.4	1174.8	8.6	1180.4	12.5	1180.4	12.5	99.3
DEL082E-98	60	26423	1.7	12.4915	2.3	2.2618	2.4	0.2049	0.8	0.32	1201.6	8.4	1200.5	17.1	1198.3	45.3	1198.3	45.3	100.3
DEL082E-100	276	59044	1.6	11.6137	1.0	2.6446	1.8	0.2228	1.6	0.85	1296.4	18.4	1313.1	13.5	1340.5	18.4	1340.5	18.4	96.7

Appendix E: LA-ICP-MS U-Pb Zircon Geochronology (cont.)

DEL10-7a.1 (tonalite xenolith)				Isotope ratios							Apparent ages (Ma)								
Analysis	U (ppm)	206Pb 204Pb	U/Th	206Pb* 207Pb*	± (%)	207Pb* 235U*	± (%)	206Pb* 238U	± (%)	error corr.	206Pb* 238U*	± (Ma)	207Pb* 235U	± (Ma)	206Pb* 207Pb*	± (Ma)	'best age' (Ma)	± (Ma)	Conc (%)
DEL10-7a.1-1	368	71748	0.7	11.3470	0.9	2.7729	3.6	0.2282	3.4	0.97	1325.1	41.2	1348.3	26.6	1385.3	17.4	1385.3	17.4	95.7
DEL10-7a.1-2	265	132304	0.8	11.4270	1.4	2.8077	1.7	0.2327	1.1	0.63	1348.6	13.4	1357.6	13.1	1371.8	26.0	1371.8	26.0	98.3
DEL10-7a.1-3	432	61454	0.6	11.3658	0.9	2.8596	1.3	0.2357	0.9	0.70	1364.4	11.1	1371.3	9.7	1382.1	17.5	1382.1	17.5	98.7
DEL10-7a.1-4	779	141485	2.6	11.6578	0.8	2.7365	2.0	0.2314	1.8	0.92	1341.7	22.3	1338.4	14.9	1333.2	15.4	1333.2	15.4	100.6
DEL10-7a.1-5	616	149119	0.6	11.3197	1.0	2.8789	1.4	0.2364	0.9	0.65	1367.7	10.8	1376.4	10.2	1389.9	19.7	1389.9	19.7	98.4
DEL10-7a.1-7	338	58594	0.7	11.5492	1.0	2.6132	1.7	0.2189	1.4	0.81	1276.0	16.0	1304.3	12.5	1351.3	19.0	1351.3	19.0	94.4
DEL10-7a.1-8	488	83507	0.6	11.5955	1.0	2.6052	3.8	0.2191	3.6	0.96	1277.1	42.0	1302.1	27.5	1343.6	19.1	1343.6	19.1	95.1
DEL10-7a.1-10	456	72031	0.7	11.5208	1.3	2.6823	3.7	0.2241	3.5	0.94	1303.6	41.5	1323.6	27.7	1356.0	24.7	1356.0	24.7	96.1
DEL10-7a.1-11	303	50756	1.1	11.8162	1.2	2.2342	3.1	0.1915	2.9	0.92	1129.3	29.8	1191.8	22.0	1307.1	24.0	1307.1	24.0	86.4
DEL10-7a.1-12	410	101895	0.7	11.5752	1.3	2.7606	1.9	0.2318	1.3	0.71	1343.7	16.0	1344.9	13.9	1346.9	25.3	1346.9	25.3	99.8
DEL10-7a.1-13	426	107422	0.6	11.3736	0.7	2.8639	3.2	0.2362	3.2	0.97	1367.1	38.8	1372.5	24.4	1380.8	14.4	1380.8	14.4	99.0
DEL10-7a.1-14	400	100777	0.7	11.3902	0.6	2.7518	1.1	0.2273	0.9	0.82	1320.5	10.9	1342.6	8.3	1378.0	12.4	1378.0	12.4	95.8
DEL10-7a.1-15	796	168597	0.5	11.4981	0.5	2.6541	1.1	0.2213	1.0	0.88	1288.9	11.3	1315.8	8.1	1359.8	10.2	1359.8	10.2	94.8
DEL10-7a.1-16	441	88927	2.8	11.8908	1.0	2.5722	1.9	0.2218	1.7	0.85	1291.5	19.4	1292.8	14.3	1294.8	20.0	1294.8	20.0	99.7
DEL10-7a.1-17	467	167085	0.7	11.3877	1.1	2.8389	1.9	0.2345	1.6	0.82	1357.9	19.2	1365.9	14.3	1378.4	21.0	1378.4	21.0	98.5
DEL10-7a.1-18	329	90102	0.8	12.2671	2.3	2.3219	2.8	0.2066	1.5	0.56	1210.6	17.0	1219.0	19.7	1234.0	45.2	1234.0	45.2	98.1
DEL10-7a.1-19	439	76049	0.7	11.9010	0.6	2.4846	1.2	0.2145	1.1	0.88	1252.5	12.5	1267.6	9.0	1293.1	11.3	1293.1	11.3	96.9
DEL10-7a.1-20	922	247408	0.5	11.5399	0.5	2.6112	1.9	0.2185	1.8	0.97	1274.2	21.0	1303.8	13.8	1352.8	9.5	1352.8	9.5	94.2
DEL10-7a.1-21	541	49947	0.7	12.8129	1.6	2.0243	2.7	0.1881	2.1	0.79	1111.1	21.7	1123.7	18.2	1148.1	32.3	1148.1	32.3	96.8
DEL10-7a.1-22	509	84661	0.7	12.0178	0.6	2.4932	1.7	0.2173	1.6	0.93	1267.6	18.0	1270.1	12.3	1274.1	12.5	1274.1	12.5	99.5
DEL10-7a.1-23	569	112528	0.6	11.9928	1.3	2.4979	2.9	0.2173	2.6	0.90	1267.4	30.0	1271.4	21.1	1278.2	25.0	1278.2	25.0	99.2
DEL10-7a.1-24	631	112889	0.6	11.6831	0.8	2.6415	2.7	0.2238	2.6	0.96	1302.0	30.8	1312.3	20.1	1329.0	15.6	1329.0	15.6	98.0
DEL10-7a.1-25	282	58902	0.8	11.5496	0.7	2.7048	3.7	0.2266	3.6	0.98	1316.5	42.6	1329.8	27.1	1351.2	14.2	1351.2	14.2	97.4

Appendix E: LA-ICP-MS U-Pb Zircon Geochronology (cont.)

DEL10-7a.2 (tonalite xenolith)				Isotope ratios							Apparent ages (Ma)								
Analysis	U (ppm)	206Pb 204Pb	U/Th	206Pb* 207Pb*	± (%)	207Pb* 235U*	± (%)	206Pb* 238U	± (%)	error corr.	206Pb* 238U*	± (Ma)	207Pb* 235U	± (Ma)	206Pb* 207Pb*	± (Ma)	'best age' (Ma)	± (Ma)	Conc (%)
DEL10-7A.2-1	258	83292	0.7	11.6106	1.3	2.6272	1.6	0.2212	1.0	0.61	1288.4	11.7	1308.3	12.1	1341.0	25.3	1341.0	25.3	96.1
DEL10-7A.2-2	351	55558	0.7	12.0515	1.3	2.4238	2.2	0.2119	1.8	0.81	1238.7	20.4	1249.7	16.2	1268.7	26.0	1268.7	26.0	97.6
DEL10-7A.2-3	365	65439	2.6	13.9230	1.2	1.4036	3.1	0.1417	2.9	0.92	854.5	22.9	890.5	18.5	981.0	24.7	981.0	24.7	87.1
DEL10-7A.2-4	236	40229	2.0	11.6581	2.0	2.5353	8.5	0.2144	8.3	0.97	1252.0	94.1	1282.2	62.1	1333.2	39.0	1333.2	39.0	93.9
DEL10-7A.2-5	353	126555	0.7	11.8781	1.4	2.6749	5.0	0.2304	4.8	0.96	1336.8	58.1	1321.6	37.2	1296.9	28.0	1296.9	28.0	103.1
DEL10-7A.2-6	112	27359	1.3	12.4386	5.2	2.3149	5.4	0.2088	1.7	0.31	1222.6	19.1	1216.9	38.6	1206.7	101.8	1206.7	101.8	101.3
DEL10-7A.2-7	367	90673	0.8	12.2799	1.1	2.1412	1.5	0.1907	1.0	0.67	1125.2	10.1	1162.2	10.1	1231.9	21.2	1231.9	21.2	91.3
DEL10-7A.2-8	511	61471	0.7	12.2005	1.9	2.4931	3.4	0.2206	2.8	0.83	1285.1	32.8	1270.0	24.6	1244.6	37.0	1244.6	37.0	103.2
DEL10-7A.2-9	496	78054	0.6	11.9714	2.5	2.4763	3.5	0.2150	2.4	0.70	1255.4	27.5	1265.1	25.1	1281.7	48.4	1281.7	48.4	98.0
DEL10-7A.2-10	486	111086	0.7	11.5083	0.6	2.7147	1.1	0.2266	0.9	0.81	1316.6	10.4	1332.5	8.0	1358.1	12.2	1358.1	12.2	96.9
DEL10-7A.2-11	473	38275	0.7	12.1996	1.0	2.0731	1.7	0.1834	1.4	0.82	1085.7	13.8	1139.9	11.6	1244.8	18.9	1244.8	18.9	87.2
DEL10-7A.2-12	219	93218	1.4	11.7899	2.0	2.5605	2.7	0.2189	1.8	0.66	1276.3	20.3	1289.4	19.4	1311.4	38.8	1311.4	38.8	97.3
DEL10-7A.2-13	123	8268	1.0	12.3080	2.8	2.2743	4.0	0.2030	2.8	0.71	1191.5	30.8	1204.4	28.2	1227.4	55.3	1227.4	55.3	97.1
DEL10-7A.2-14	202	31788	0.8	11.6900	2.1	2.5898	2.6	0.2196	1.6	0.59	1279.6	18.0	1297.8	19.2	1327.9	40.9	1327.9	40.9	96.4
DEL10-7A.2-15	158	24639	0.8	11.9798	2.9	2.3543	3.2	0.2046	1.3	0.42	1199.7	14.6	1228.8	22.5	1280.3	55.7	1280.3	55.7	93.7
DEL10-7A.2-16	693	230558	0.4	11.7134	0.7	2.4452	1.5	0.2077	1.4	0.91	1216.7	15.3	1256.0	11.0	1324.0	12.6	1324.0	12.6	91.9

Appendix E: LA-ICP-MS U-Pb Zircon Geochronology (cont.)

DEL10-7d (amphibolite xenolith)				Isotope ratios							Apparent ages (Ma)								
Analysis	U (ppm)	206Pb 204Pb	U/Th	206Pb* 207Pb*	± (%)	207Pb* 235U*	± (%)	206Pb* 238U	± (%)	error corr.	206Pb* 238U*	± (Ma)	207Pb* 235U	± (Ma)	206Pb* 207Pb*	± (Ma)	'best age' (Ma)	± (Ma)	Conc (%)
DEL10-7D-1	114	13409	1.4	13.2220	5.7	1.4816	9.3	0.1421	7.4	0.79	856.4	59.5	922.9	56.7	1085.3	113.8	1085.3	113.8	78.9
DEL10-7D-2	655	143712	1.5	11.5735	0.6	2.7615	1.0	0.2318	0.8	0.80	1343.9	10.1	1345.2	7.8	1347.2	12.0	1347.2	12.0	99.8
DEL10-7D-3	106	20219	1.6	14.0141	5.4	1.5879	6.5	0.1614	3.6	0.55	964.5	32.2	965.5	40.6	967.7	110.9	967.7	110.9	99.7
DEL10-7D-4	810	177862	2.1	11.5381	0.5	2.6568	4.3	0.2223	4.3	0.99	1294.2	50.6	1316.5	32.1	1353.1	9.9	1353.1	9.9	95.6
DEL10-7D-5	227	31100	3.6	12.2120	3.6	2.3546	6.9	0.2085	5.9	0.86	1221.1	65.8	1228.9	49.3	1242.8	69.8	1242.8	69.8	98.3
DEL10-7D-6	310	58403	1.2	12.8243	1.7	2.0012	2.1	0.1861	1.2	0.59	1100.4	12.5	1115.9	14.3	1146.3	33.9	1146.3	33.9	96.0
DEL10-7D-7	171	22105	1.7	12.4461	2.3	2.1272	10.3	0.1920	10.0	0.97	1132.3	103.7	1157.7	71.0	1205.5	46.3	1205.5	46.3	93.9
DEL10-7D-9	725	59957	4.1	11.9935	1.3	2.1480	6.2	0.1868	6.0	0.98	1104.2	61.2	1164.4	42.8	1278.1	25.6	1278.1	25.6	86.4
DEL10-7D-10	749	164423	2.5	11.7146	0.8	2.5634	3.0	0.2178	2.9	0.97	1270.2	33.7	1290.3	22.1	1323.8	15.0	1323.8	15.0	96.0
DEL10-7D-11	831	128070	3.2	11.4824	0.6	2.9947	10.0	0.2494	10.0	1.00	1435.3	128.5	1406.3	76.3	1362.5	11.0	1362.5	11.0	105.3
DEL10-7D-12	200	42016	1.2	11.5444	2.0	2.7507	2.9	0.2303	2.1	0.73	1336.1	25.4	1342.3	21.4	1352.1	37.6	1352.1	37.6	98.8
DEL10-7D-13	1050	74512	2.3	12.4533	2.5	2.2967	6.2	0.2074	5.6	0.91	1215.2	62.4	1211.3	43.7	1204.3	49.7	1204.3	49.7	100.9
DEL10-7D-14	392	113379	1.4	12.0781	1.5	2.3838	3.5	0.2088	3.1	0.90	1222.5	34.8	1237.7	24.9	1264.4	29.7	1264.4	29.7	96.7
DEL10-7D-15	302	118517	1.9	11.7088	1.7	2.5913	4.2	0.2201	3.9	0.92	1282.2	45.3	1298.2	31.1	1324.8	32.3	1324.8	32.3	96.8
DEL10-7D-16	708	120137	2.6	11.5826	0.8	2.7840	3.6	0.2339	3.5	0.98	1354.8	42.4	1351.3	26.6	1345.7	15.2	1345.7	15.2	100.7

Appendix E: LA-ICP-MS U-Pb Zircon Geochronology (cont.)

DEL10-11 (hornblende gneiss)				Isotope ratios							Apparent ages (Ma)								
Analysis	U (ppm)	206Pb 204Pb	U/Th	206Pb* 207Pb*	± (%)	207Pb* 235U*	± (%)	206Pb* 238U	± (%)	error corr.	206Pb* 238U*	± (Ma)	207Pb* 235U	± (Ma)	206Pb* 207Pb*	± (Ma)	'best age' (Ma)	± (Ma)	Conc (%)
DEL10-11-1	1985	340282	5.6	12.6856	0.4	2.1683	5.0	0.1995	5.0	1.00	1172.6	53.4	1170.9	34.7	1167.8	7.0	1167.8	7.0	100.4
DEL10-11-3	1954	276529	6.4	12.9017	1.0	2.1819	2.9	0.2042	2.7	0.93	1197.6	29.1	1175.3	19.9	1134.3	20.6	1134.3	20.6	105.6
DEL10-11-4	1357	117343	2.1	13.0611	0.8	1.8443	6.5	0.1747	6.5	0.99	1038.0	62.1	1061.4	43.0	1109.8	15.6	1109.8	15.6	93.5
DEL10-11-5	969	50411	2.5	12.9292	1.3	2.1243	6.4	0.1992	6.2	0.98	1171.0	66.6	1156.7	43.9	1130.1	25.7	1130.1	25.7	103.6
DEL10-11-6	91	21310	0.6	13.6359	4.8	1.8168	5.5	0.1797	2.7	0.49	1065.2	26.4	1051.5	36.0	1023.2	97.1	1023.2	97.1	104.1
DEL10-11-7	1894	470782	5.7	12.7510	0.9	2.2378	6.5	0.2070	6.5	0.99	1212.6	71.4	1193.0	45.8	1157.6	18.3	1157.6	18.3	104.7
DEL10-11-8	2036	249891	4.9	12.9115	0.8	2.1099	7.0	0.1976	6.9	0.99	1162.3	73.8	1152.0	48.2	1132.8	16.4	1132.8	16.4	102.6
DEL10-11-9	352	94859	2.4	12.5458	0.9	2.4373	5.2	0.2218	5.1	0.98	1291.2	59.3	1253.7	37.1	1189.8	18.5	1189.8	18.5	108.5
DEL10-11-10	1897	274732	5.0	12.7666	0.6	2.2106	1.7	0.2047	1.6	0.94	1200.5	17.7	1184.4	12.1	1155.2	11.9	1155.2	11.9	103.9
DEL10-11-11	104	31092	0.5	13.4774	6.3	1.7595	6.6	0.1720	1.7	0.26	1023.0	16.4	1030.7	42.5	1046.9	127.6	1046.9	127.6	97.7
DEL10-11-12	1018	120134	1.6	12.6332	0.7	2.2035	6.9	0.2019	6.9	1.00	1185.5	74.7	1182.2	48.4	1176.1	13.1	1176.1	13.1	100.8
DEL10-11-13	1426	327701	5.1	12.6170	0.6	2.3330	3.2	0.2135	3.2	0.98	1247.4	35.8	1222.4	22.8	1178.6	11.0	1178.6	11.0	105.8
DEL10-11-14	53	8138	0.2	13.8493	7.4	1.7788	8.0	0.1787	2.9	0.37	1059.7	28.6	1037.7	52.0	991.7	151.4	991.7	151.4	106.9
DEL10-11-15	2244	262285	2.4	13.0183	0.5	1.9684	4.1	0.1859	4.0	0.99	1098.9	40.9	1104.8	27.5	1116.4	10.3	1116.4	10.3	98.4
DEL10-11-16	1651	255935	5.2	12.8580	0.6	2.0748	1.9	0.1935	1.8	0.95	1140.2	18.9	1140.5	13.1	1141.1	12.1	1141.1	12.1	99.9
DEL10-11-17	85	22080	1.3	12.6111	4.2	2.4335	7.2	0.2226	5.8	0.81	1295.5	68.2	1252.6	51.5	1179.5	82.7	1179.5	82.7	109.8
DEL10-11-18	77	11095	0.3	14.0871	5.1	1.6985	5.3	0.1735	1.2	0.23	1031.6	11.8	1008.0	33.7	957.0	105.0	957.0	105.0	107.8
DEL10-11-19	1315	105152	2.2	13.1560	2.4	2.1097	4.6	0.2013	3.9	0.86	1182.3	42.5	1152.0	31.7	1095.4	47.7	1095.4	47.7	107.9
DEL10-11-20	2123	429147	4.3	13.1048	0.6	2.0417	1.4	0.1940	1.3	0.91	1143.3	13.3	1129.5	9.4	1103.2	11.2	1103.2	11.2	103.6
DEL10-11-21	1783	122778	4.9	13.9388	0.4	1.6304	1.3	0.1648	1.3	0.96	983.5	11.5	982.0	8.3	978.6	7.8	978.6	7.8	100.5
DEL10-11-22	1446	208869	3.8	13.7333	0.5	1.7429	2.9	0.1736	2.9	0.98	1031.9	27.2	1024.5	18.7	1008.8	10.2	1008.8	10.2	102.3
DEL10-11-23	513	166726	1.4	12.3837	0.8	2.3859	6.2	0.2143	6.2	0.99	1251.6	70.0	1238.4	44.4	1215.4	16.5	1215.4	16.5	103.0

Appendix E: LA-ICP-MS U-Pb Zircon Geochronology (cont.)

DEL10-11 (hornblende gneiss cont.)				Isotope ratios							Apparent ages (Ma)							
Analysis	U (ppm)	206Pb 204Pb	U/Th	206Pb* 207Pb*	± (%)	207Pb* 235U*	± (%)	206Pb* 238U	± (%)	error corr.	206Pb* 238U*	± (Ma)	207Pb* 235U	± (Ma)	206Pb* 207Pb*	± (Ma)	'best age' (Ma)	± (Ma)	Conc (%)
DEL10-11-25	884	117878	2.6	12.8610	0.9	2.0350	2.8	0.1898	2.6	0.94	1120.4	26.8	1127.3	18.8	1140.6	18.2	1140.6	18.2	98.2
DEL10-11-26	94	19097	0.7	13.7527	7.9	1.8155	8.2	0.1811	2.0	0.24	1072.9	19.8	1051.1	53.6	1005.9	161.3	1005.9	161.3	106.7
DEL10-11-28	87	10612	0.3	14.2078	9.1	1.6459	9.4	0.1696	2.6	0.27	1009.9	24.2	988.0	59.6	939.6	186.1	939.6	186.1	107.5
DEL10-11-29	84	16172	0.5	13.5084	6.5	1.8261	8.0	0.1789	4.7	0.59	1061.0	45.9	1054.9	52.7	1042.2	131.5	1042.2	131.5	101.8

DEL10-29 (augen gneiss)				Isotope ratios							Apparent ages (Ma)							
Analysis	U (ppm)	206Pb 204Pb	U/Th	206Pb* 207Pb*	± (%)	207Pb* 235U*	± (%)	206Pb* 238U	± (%)	error corr.	206Pb* 238U*	± (Ma)	207Pb* 235U	± (Ma)	206Pb* 207Pb*	± (Ma)	'best age' (Ma)	± (Ma)	Conc (%)
DEL10-29-1	315	83564	1.7	12.7659	2.1	2.0926	2.6	0.1937	1.5	0.56	1141.6	15.2	1146.4	17.7	1155.3	42.2	1155.3	42.2	98.8
DEL10-29-2	734	148660	3.3	12.5977	0.5	2.1646	1.8	0.1978	1.7	0.96	1163.4	18.6	1169.8	12.7	1181.6	10.2	1181.6	10.2	98.5
DEL10-29-5	287	2484	1.4	13.2475	3.3	1.7420	10.5	0.1674	9.9	0.95	997.6	91.9	1024.2	67.7	1081.5	66.0	1081.5	66.0	92.2
DEL10-29-6	784	64232	1.1	12.5133	1.1	2.0164	3.1	0.1830	2.9	0.94	1083.3	29.2	1121.0	21.3	1194.9	21.9	1194.9	21.9	90.7
DEL10-29-7	812	55258	1.3	12.7048	1.5	2.0513	4.0	0.1890	3.6	0.92	1116.0	37.4	1132.7	27.0	1164.8	30.5	1164.8	30.5	95.8
DEL10-29-10	312	25065	1.4	12.6513	2.2	2.0643	2.5	0.1894	1.2	0.47	1118.2	12.0	1137.0	17.1	1173.2	43.8	1173.2	43.8	95.3
DEL10-29-13	1719	28114	20.1	13.6567	0.7	1.5981	1.6	0.1583	1.4	0.90	947.3	12.5	969.5	9.9	1020.1	14.0	1020.1	14.0	92.9
DEL10-29-14	908	42724	2.8	12.7317	0.7	2.0274	1.9	0.1872	1.8	0.94	1106.2	18.0	1124.7	12.9	1160.7	13.2	1160.7	13.2	95.3
DEL10-29-16	1049	14171	4.7	12.7989	1.4	1.8340	4.1	0.1702	3.8	0.94	1013.4	35.7	1057.7	26.7	1150.2	27.7	1150.2	27.7	88.1
DEL10-29-17	322	7344	1.2	12.4102	2.8	1.9986	5.4	0.1799	4.6	0.86	1066.4	45.7	1115.1	36.7	1211.2	55.1	1211.2	55.1	88.0
DEL10-29-18	176	25848	2.3	12.8760	2.7	2.0585	3.7	0.1922	2.6	0.68	1133.5	26.5	1135.1	25.5	1138.3	54.3	1138.3	54.3	99.6
DEL10-29-19	144	35304	3.5	12.3303	4.5	2.1124	6.3	0.1889	4.4	0.70	1115.4	45.0	1152.8	43.1	1223.9	87.5	1223.9	87.5	91.1

Appendix F: SHRIMP-II U-Pb Zircon Geochronology

DEL10-30 (augen gneiss)			Isotope ratios							Apparent ages (Ma)						
Spot Name	ppm U	ppm Th	204 /206	% err	207 /206	% err	208 /206	% err	206 /238	206Pb /238U	1s (Ma)	207Pb /206Pb	1s (Ma)	208Pb /232Th	1s (Ma)	% Discor-dance
1030-1.1	297	159	2.9E-5	50	0.0798	0.59	0.164	0.71	0.507	1164	17	1182	13	1146	20	+2
1030-1.2	478	343	4.8E-5	29	0.0781	0.45	0.222	0.47	0.563	1127	17	1133	10	1115	18	+1
1030-2.1	114	38	-3.8E-5	71	0.0781	0.97	0.102	1.46	0.493	1146	18	1164	21	1153	28	+2
1030-2.1…dup1	114	47	----	---	0.0792	1.48	0.127	2.32	0.490	1147	19	1178	29	1141	33	+3
1030-4.1	903	173	-1.1E-5	45	0.0788	0.33	0.056	0.66	0.536	1181	17	1171	7	1138	20	-1
1030-4.2	80	46	8.2E-5	58	0.0796	2.05	0.173	1.35	0.489	1175	24	1158	45	1132	32	-2
1030-6.1	166	46	---	---	0.0780	0.83	0.083	1.37	0.474	1118	17	1146	16	1082	24	+3
1030-7.1	62	40	9.5E-5	58	0.0777	1.27	0.192	1.39	0.522	1187	20	1103	33	1137	30	-8
1030-11.1	250	223	1.7E-5	71	0.0786	0.64	0.270	1.01	0.508	1111	20	1157	13	1084	24	+4
1030-12.1	121	74	5.4E-5	58	0.0790	0.95	0.182	1.08	0.501	1154	18	1152	22	1102	24	-0
1030-13.1	41	22	-1.8E-4	58	0.0777	1.74	0.166	2.06	0.444	1142	21	1202	49	1196	43	+6
1030-14.1	569	273	-2.5E-5	41	0.0786	0.45	0.146	0.57	0.490	1045	15	1170	10	1025	18	+12
1030-16.1	230	87	----	---	0.0795	0.64	0.114	0.91	0.551	1131	19	1186	13	1099	23	+5
1030-16.2	156	110	7.5E-5	45	0.0778	0.90	0.217	0.94	0.439	1109	17	1114	22	1088	24	+1
1030-16.3	393	180	1.9E-5	50	0.0783	0.48	0.135	0.63	0.575	1155	17	1149	10	1097	19	-1
1030-17.1	274	118	----	---	0.0780	0.67	0.134	0.87	0.452	1089	16	1146	13	1089	22	+5
1030-17.2	310	63	1.8E-4	24	0.0801	0.70	0.068	2.10	0.395	1017	15	1138	21	998	39	+11

Appendix F: SHRIMP-II U-Pb Zircon Geochronology (cont.)

DEL10-7b (hornblende gneiss)			Isotope ratios								Apparent ages (Ma)						
Spot Name	ppm U	ppm Th	204 /206	% err	207 /206	% err	208 /206	% err	206 /238	206Pb /238U	1s (Ma)	207Pb /206Pb	1s (Ma)	208Pb /232Th	1s (Ma)	% Discor-dance
107-7.1	477	327	----	---	0.0871	0.41	0.206	0.47	0.584	1371	20	1362	8	1344	22	-1
107-7.2	528	323	3.3E-6	100	0.0875	0.61	0.181	0.46	0.620	1335	19	1371	12	1293	21	+3
107-6.1	1194	539	1.4E-5	33	0.0861	0.27	0.138	3.19	0.597	1341	22	1337	5	1338	64	-0
107-10.1	414	171	4.7E-6	100	0.0859	0.51	0.125	1.10	0.549	1293	19	1335	10	1271	25	+3
107-7.1…dup1	214	126	3.3E-5	50	0.0854	0.61	0.179	2.18	0.595	1302	27	1315	13	1281	51	+1
107-12.1	285	150	---	---	0.0864	0.53	0.152	0.68	0.631	1291	22	1347	10	1219	24	+5
107-14.1	337	215	----	---	0.0825	0.90	0.190	0.62	0.505	1185	18	1258	18	1146	19	+6
107-14.2	376	87	5.2E-5	30	0.0859	0.78	0.066	0.90	0.608	1339	22	1320	16	1221	27	-2
107-18.1	312	229	-2.2E-5	50	0.0875	0.50	0.219	0.55	0.618	1342	20	1379	10	1316	23	+3
107-22.1	478	462	1.2E-5	58	0.0853	0.43	0.291	0.41	0.534	1252	18	1319	9	1223	20	+6
107-22.2	290	150	4.5E-5	35	0.0871	0.50	0.156	0.72	0.620	1318	23	1348	11	1282	26	+2
107-26.1	443	314	2.7E-5	38	0.0859	0.42	0.216	0.51	0.594	1306	19	1326	9	1288	21	+2
107-26.2	600	378	---	---	0.0868	0.37	0.188	1.22	0.529	1293	38	1356	7	1260	46	+5
107-27.1	437	210	-1.8E-5	50	0.0859	0.45	0.144	1.17	0.500	1339	22	1342	9	1309	28	+0
107-27.2	473	282	1.5E-5	50	0.0850	0.97	0.179	0.83	0.564	1334	19	1311	19	1300	23	-2
107-31.1	816	430	6.3E-6	58	0.0858	0.31	0.157	0.63	0.584	1306	21	1331	6	1269	23	+2
107-32.1	324	22	1.4E-4	20	0.0844	0.50	0.024	3.47	0.561	1266	21	1256	14	1157	76	-1
107-33.2	671	590	1.3E-5	50	0.0857	0.38	0.257	1.39	0.498	1387	21	1327	8	1328	28	-5
107-33.1	419	208	1.7E-5	58	0.0866	0.50	0.149	0.66	0.459	1324	29	1347	10	1291	32	+2
107-35.1	594	287	----	---	0.0782	0.89	0.145	1.05	0.431	1134	22	1151	18	1101	26	+2
107-34.1	40	94	2.6E-4	50	0.0775	1.80	0.721	1.14	0.401	1018	19	1037	64	995	24	+2
107-38.1	496	253	5.8E-6	100	0.0857	0.51	0.150	1.47	0.425	1388	20	1329	10	1341	30	-5

Appendix F: SHRIMP-II U-Pb Zircon Geochronology (cont.)

DEL10-7b (hornblende gneiss cont.)			Isotope ratios								Apparent ages (Ma)					
Spot Name	ppm U	ppm Th	204 /206	% err	207 /206	% err	208 /206	% err	206 /238	206Pb /238U	1s (Ma)	207Pb /206Pb	1s (Ma)	208Pb /232Th	1s (Ma)	% Discor-dance
107-39.1	502	323	2.6E-5	38	0.0854	0.41	0.190	0.48	0.571	1318	22	1316	9	1265	24	-0
107-43.1	713	350	3.1E-6	100	0.0878	0.77	0.146	0.50	0.498	1374	20	1378	15	1333	24	+0
107-45.1	305	116	3.9E-5	41	0.0829	0.90	0.115	0.80	0.516	1217	28	1254	19	1180	31	+3
107-48.1	728	1052	5.8E-5	20	0.0850	0.33	0.421	0.57	0.610	1248	19	1296	7	1176	21	+4
107-46.1	677	461	----	---	0.0831	0.78	0.205	0.90	0.533	1237	19	1272	15	1209	23	+3

CHAPTER VIII. REFERENCES

Aleinikoff, J.N., Zartman, R.E., Walter, M., Rankin, D.W., Lyttle, P.T., and Burton, W.C., 1995, U-Pb ages of metarhyolites of the Catoctin and Mount Rogers Formations, Central and Southern Appalachians: Evidence for two pulses of Iapetan rifting: American Journal of Science, v. 295, p. 428–454, doi:10.2475/ajs.295.4.428.

Aleinikoff, J.N., Burton, W.C., Lyttle, P.T., Nelson, A.E., and Southworth, C.S., 2000, U-Pb geochronology of zircon and monazite from Middle Proterozoic (1.15–1.05 Ga) granitic gneiss of the northern Blue Ridge, Virginia: Precambrian Research, v. 99, p. 113–146.

Aleinikoff, J.N., Horton, J.W., Drake, A.A., Jr., Wintsch, R.P., Fanning, C.M., and Yi, K., 2004, Deciphering multiple Mesoproterozoic and Paleozoic events recorded in zircon and titanite from the Baltimore Gneiss, Maryland: SEM imaging, SHRIMP U-Pb geochronology and EMP analysis, in Bartholomew, M.J., Corriveau, L., McLelland, J., and Tollo, R.P., eds., Proterozoic Evolution of the Grenville Orogen in North America: Geological Society of America Special Paper, Memoir 197.

Aleinikoff, J.N., Southworth, S., Merschat, A., 2012, Late Mesoproterozoic (ca. 1.0 Ga) deposition of protoliths of the Carvers Gap and Cloudland gneisses, Mars Hill terrane, NC-TN: New SHRIMP U-Pb ages of detrital zircon and monazite: Geological Society of America Abstracts with Programs, v. 44, no. 7, p. 171.

Anderson, A.D., 2011, Petrologic, geochemical, and geochronologic constraints on the tectonic evolution of the southern Appalachian orogen, Blue Ridge Province of western North Carolina [unpublished Ph.D. dissertation]: University of Kentucky, Lexington, Kentucky, 280 p.

Anderson, E.D., and Moecher, D.P., 2008, Geochronology and geochemistry of basement rocks, Dellwood area, eastern Great Smoky Mountains, NC: Geological Society of America Abstracts with Programs, v. 40, no. 4, p. 19.

Arndt, N.T., and Goldstein, S.L., 1987, Use and abuse of crust-formation ages; Geology, v. 15, p. 893-895, doi: 10.1130/0091-7613(1987)15<893:UAAOCA>2.0.CO;2.

Berquist, P.J., Fisher, C.M., Miller, C.F., Wooden, J.L., Fullagar, P.D., and Loewy, S.L., 2005, Geochemistry and U-Pb zicon geochronology of Blue Ridge basement, western North Carolina and eastern Tennessee: Implications for tectonic assembly, in Hatcher, R. D., Jr., and Merschat, A. J., eds., Blue Ridge Geology Geotraverse East of the Great Smoky Mountains National Park, Western North Carolina: North Carolina Geological Survey, Carolina Geological Society Annual Field Trip Guidebook, p. 33-44.

Bream, B.R., Hatcher, R.D, JR, Miller, C.F., and Fullagar, P.D., 2004, Detrital zircon ages and Nd isotopic data from the southern Appalachian crystalline core, Georgia, South Carolina, North Carolina, and Tennessee: new provenance constraints for part of the Laurentian margin, in Tollo, R.P., Corriveau, L., McLelland, J.M., and Bartholomew, M.J., eds., Proterozoic Tectonic Evolution of the Grenville Orogen in North America: Geological Society of America, Memoir 197, p. 459–475.

Cameron, K.L., and Ward, R.L., 1998, Xenoliths of Grenvillian granulite basement constrain models for the origin of voluminous Tertiary rhyolites, Davis Mountains, west Texas: Geology, v. 26, no. 12, p. 1087–1090.

Carrigan, C.W., Miller, C.F., Fullagar, P.D., Hatcher, R.D., Jr., Bream, B.R., and Coath, C.D., 2003, Ion microprobe age and geochemistry of southern Appalachian basement, with implications for Proterozoic and Paleozoic reconstructions: Precambrian Research, v. 120, p. 1–36.

Chakraborty, S., 2010, Provenance of the Neoproterozoic Ocoee Supergroup, eastern Great Smoky Mountains [unpublished Ph.D. dissertation]: University of Kentucky, Lexington, Kentucky, 307 p.

Chakraborty, S., Moecher, D.P., Samson, S.D., 2012, Provenance of the lower Ocoee Supergroup, eastern Great Smoky Mountains: Geological Society of America Bulletin, v. 124, p. 1278-1292.

Clemons, K.M., and Moecher, D.P., 2009, Reinterpretation of the Greenbrier fault, Great Smoky Mountains: New petrofabric constraints and implications for southern Appalachian tectonics: Geological Society of America Bulletin, v. 121, no. 7-8, p. 1108-1122, doi:10.1130/B26480.1

Corfu, F., Hanchar, J.M., Hoskin, P.W.O., and Kinny, P.D., 2003, Atlas of Zircon Textures: Reviews in Mineralogy and Geochemistry, v. 53, p. 469-500.

Daly, J., and McLelland, J., 1991, Juvenile Middle Proterozoic crust in the Adirondack Highlands, Grenville Province, northeastern North America: Geology, v. 19, p. 119–122, doi: 10.1130/0091-7613(1991)019<0119: JMPCIT>2.3.CO;2.

DePaolo, D.J., 1981, Neodymium isotopes in the Colorado Front Range and crust-mantle evolution in the Proterozoic: Nature, v. 291, p. 193–196.

DePaolo, D.J., and Wasserburg, G. J., 1976, Nd Isotopic Variations and Petrogenetic Models: Geophysical Research Letters, v. 3, No. 5, p. 249-252

DeWolf, C.P., and Mezger, K., 1994, Lead isotope analyses of leached feldspars: Constraints on the early crustal history of the Grenville Orogen: Geochimica et Cosmochimica Acta, v. 58, p. 5537-5550, doi: 10.1016/0016-7037(94)90248-8

Fetter, A.H., and Goldberg, S.A., 1995, Ages and geochemical characteristics of bimodal magmatism in the Neoproterozoic Grandfather Mountain rift basin: The Journal of Geology, v. 103, p. 313–326, doi:10.1086/629749.

Fisher, C.M., 2006, An exotic southern and central Appalachian basement: Pb and Nd isotopic evidence [unpublished M.S. thesis]: Vanderbilt University, Nashville, Tennessee, 54 p.

Fisher, C.M., Loewy, S.L., Miller, C.F., Berquist, P., Van Schmus, W.R., Hatcher, R.D., Jr., Wooden, J.L., and Fullagar, P.D., 2010, Whole-rock Pb and Sm-Nd isotopic constraints on the growth of southeastern Laurentia during Grenvillian orogenesis: Geological Society of America, v. 122, p. 1646-1659.

Fullagar, P.D., Goldberg, S.A., and Bulter, J.R., 1997, Nd and Sr isotopic characterization of crystalline rocks from the Southern Appalachian Piedmont and Blue Ridge, North and South Carolina, in Sinha, A.K., et al., eds., The Nature of Magmatism in the Appalachian Orogen: Boulder, Colorado, Geological Society of America Memoir 1991, p. 165–179.

Gehrels, G.E., Valencia, V.A., and Ruiz, J., 2008, Enhanced precision, accuracy, efficiency, and spatial resolution of U-Pb ages by laser ablation-multicollector-inductively coupled plasma-mass spectrometry: Geochemistry Geophysics Geosystems, v. 9, n. 3, 13 p., doi:10.1029/2007GC001805

Goldstein, S.L., O'Nions, R.K., and Hamilton, P.J., 1984, A Sm-Nd isotopic study of atmospheric dusts and particulates from major river systems: Earth and Planetary Science Letters, v. 70, p. 221-236.

Hadley, J.B., and Goldsmith, R., 1963, Geology of the eastern Great Smoky Mountains North Carolina and Tennessee: U.S. Geological Survey Professional Paper 349-B. 118p.

Johnson, D.M., Hooper, P.R., and Conrey, R.M., 1999, XRF analysis of rocks and minerals for major and trace elements on a single low dilution Li tetraborate fused bead: Advances in X-ray Analysis, v. 41, p. 843-867.

Hamilton, W., 1979, Tectonics of the Indonesian region: U.S. Geological Survey Professional Paper 1078, 345 p.

Hatcher, R.D., Jr., 1989, Tectonic synthesis of the U.S., Appalachians, Chapter 14, in Hatcher, R.D., Jr., et al., eds., The Appalachian-Ouachita orogen in the United States: Boulder, Colorado, Geological Society of America, The Geology of North America, v. F-2, p. 511–535.

Hatcher, R.D., Jr., and Butler, J.R., 1979, Guidebook for Southern Appalachian Field Trip in the Carolinas, Tennessee and Northeastern Georgia: Blacksburg, Virginia, International Geological Correlation Program, Caledonide Orogen Program Symposium, 117 p.

Hatcher, R.D., Jr., Bream, B.R., Miller, C.L., Eckert, J.O., Jr., Fullagar, P.D., and Carrigan, C.W., 2004, Paleozoic structure of Southern Appalachian Blue Ridge Grenvillian Internal Basement Massifs, in Bartholomew, M.J., Corriveau, L., McLelland, J., and Tollo, R.P., eds., Proterozoic Evolution of the Grenville Orogen in North America: Geological Society of America Special Paper, v. 197, p. 525-547.

Hamilton, P.J., O'Nions, R.K., Bridgwater, D. and Nutman, A., 1983, Sm-Nd studies of Archean metasediments and metavolcanics from West Greenland and their implications for the Earth's early history. Earth Planet. Sci. Lett., v. 62, p. 263-72

Hoffman, P.F., 1988, United Plates of America, the Birth of a Craton: Early Proterozoic Assembly and Growth of Laurentia: Annual Reviews Earth and Planetary Science, v. 16, p.543-603, doi: 0084-6597/88/0515-0543$02.00.

Jacobs, J., Pisarevsky, S., Thomas, R.J., Becker, T., 2008, The Kalahari Craton during the assembly and dispersal of Rodinia: Precambrian Research, v. 160, p. 142-158, doi:10.1016/j.precamres.2007.04.022.

King, P.B., 1964, Geology of central Great Smoky Mountains, Tennessee: U.S. Geological Survey Professional Paper 349-C. 148p. King, P.B., Hadley, J.B., Neuman, R.B., and Hamilton, W., 1958, Stratigraphy of Ocoee Series, Great Smoky Mountains, Tennessee and North Carolina: Geological Society of America Bulletin, v. 69, p. 947-966.

Kohn, M.J., and Malloy, M.A., 2004, Formation of monazite via prograde metamorphic reactions among common silicates: implications for age determinations: Geochimica et Cosmochimica Acta, v. 68, i. 1, p. 101-113.

Liew, T.C., and McCulloch, M.T., 1985, Genesis of granitoid batholiths of Peninsular Malaysia and implications for models of crustal evolution: Evidence from a Nd-Sr isotopic and U-Pb zircon study: Geochimica et Cosmochimica Acta, v. 49, p. 587-600.

Loewy, S.L., Connelly, J.N., Dalziel, I.W.D., and Gower, C., 2003, Eastern Laurentia in Rodinia: Constraints from whole-rock Pb and U/Pb geochronology: Tectonophysics, v. 375, p. 169-197.

Loewy, S.L., Connelly, J.N., and Dalziel, I.W.D., 2004, An orphaned basement block: The Arequipa-Antofalla basement of the central Andean margin of South America: Geological Society of America Bulletin, v. 116, p. 171-187.

Loughry, D.F., 2010a, Origin of Blue Ridge basement rocks, Dellwood Quad, Western NC: New evidence from U-Pb zircon geochronology and whole rock geochemistry [M.S. thesis]: University of Kentucky, 136p.

Loughry, D.F., Jr., Moecher, D.P., 2010b, Origin of Blue Ridge basement rocks, Dellwood quad, western NC: New evidence from U-Pb zircon geochronology and whole rock geochemistry: Geological Society of America Abstracts with Programs, v. 42, No. 1, p. 18.

Ludwig, K., 1980, Calculation of uncertainties of U-Pb isotope data: Earth and Planetary Science Letters, v. 46, p. 212-220.

Ludwig, K., 1999, Isoplot/Ex v. 2.10b.

Ludwig, K.R., 2009. SQUID 2 (rev. 2.50), A User's Manual, Berkeley Geochronology Ctr. Special Publication vol. 5. 104 p.

Massey, M.A., and Moecher, D.P., 2005, Deformation and metamorphic history of the Western Blue Ridge-Eastern Blue Ridge terrane boundary, southern Appalachian Orogen: Tectonics, v. 24, p. 1-18.

McLelland, J., Daly, S., and McLelland, J., 1996, The Grenville orogenic cycle: An Adirondack perspective: Tectonophysics, v. 265, p. 1–29, doi: 10.1016/S0040- 1951(96)00144-8.

Merschat, C.E., and Wiener, L.S. (1988), Geology of the Sandymush and Canton quadrangles, North Carolina. North Carolina Geological Survey, Bulletin 90, 66 p.

Michard, A., Guvriet, P., Soudant, M., and Albarede, F., 1985, Nd isotopes in French Phanerozoic shales: External vs. internal aspects of crustal evolution: Geochimica et Cosmochimica Acta, v. 49, p. 601-610.

Moecher, D.P., Massey, M.A. & Tracy, R.J., 2005. Timing and pattern of metamorphism in the western and central Blue Ridge, TN and NC: status and outstanding problems. Carolina Geological Society, Annual Field Trip, 57–66.

Moecher, D.P., Hietpas, J., Samson, S.D., and Chakraborty, S., 2011, Insights into Southern Appalachian tectonic history from ages of detrital monazite and zircon in modern alluvium and bedrock sources: Geosphere, v. 7, no. 2, p. 494–512, doi:10.1130/GES00615.1.

Montes C., 1997, The Greenbrier and Hayesville faults in central-western North Carolina [M.S. thesis]: Knoxville University of Tennessee, 145 p.

Montes C., Hatcher R.D., Jr., 1999, Documenting Late Proterozoic rifting in the Ocoee basin, western Blue Ridge, North Carolina: Southeastern Geology, v. 39, p. 37– 50.

Nelson, B.K., and DePaolo, D.J., 1984, 1700 Myr greenstone volcanic successions in southwestern North America and isotopic evolution of the Proterozoic mantle: Nature, v. 312, p. 143-146.

Nelson, B.K. and DePaolo, D.J., 1985, Rapid production of continental crust 1.7 to 1.9 b.y. ago: Nd isotopic evidence from the basement of the North American mid-continent. Geolo. Soc. Amer. Bull. 96, p. 746-754.

Ownby S.E., Miller C.F., Berquist P.J., Carrigan C.W., Wooden J.L., Fullagar P.D., 2004, U-Pb geochronology and geochemistry of a portion of the Mars Hill terrane, North Carolina–Tennessee; constraints on origin, history, and tectonic assembly, in Tollo R.P., Corriveau L., McLelland J., Bartholomew M.J., eds., Proterozoic Tectonic Evolution of the Grenville Orogen in North America: Geological Society of America Memoir 197, p. 609– 632.

Patchett, J., and Kouvo, O., 1986, Origin of continental crust of 1.9-1.7 Ga age: Nd isotopes and U-Pb zircon ages in the Svecokarelian terrain of South Finland: Contributions to Mineralogy and Petrology, v. 92, n. 1, p. 1-12, doi: 10.1007/BF00373959

Payolla, B.L., Bettencourt, J.S., Kozuch, M., Leite, W.B., Jr., Fetter, A.H., Van Schmus, W.R., 2002, Geological evolution of the basement rocks in the east-central part of the Rondonia Tin Province, SW Amazonian craton, Brazil: U-Pb and Sm-Nd isotopic constraints: Precambrian Research, v. 119, p. 141-169.

Rast, N., and Kohles, K.M., 1986, The origin of the Ocoee Supergroup: American Journal of Science, v. 286, p. 593-616.

Rehkamper, M., and Hofmann, A.W., 1997, Recycled ocean crust and sediment in Indian Ocean MORB: Earth and Planetary Science Letters, v. 147, p. 93-106

Rohs, R.C., and Van Schmus, R.V., 2007, Isotopic connections between rocks exposed in the St. Francois Mountains and the Arbuckle Mountains, southern mid-continent, North America: International Journal of Earth Sciences, v. 96, p. 599–611, doi: 10.1007/s00531-006-0123-5.

Roller, E.A., 2004, Petrogenesis of the Llano granites, central Texas: Formation mechanism and tectonic implication or radiogenic isotopes [M.S. thesis]: The University of Texas at Austin, 115 p.

Ruiz, J., Tosdal, R.M., Restrepo-Pace, P.A., and Murillo- Muñetón, G., 1999, Pb isotope evidence for Colombia- southern México connections in the Proterozoic, in Ramos, V.A., and Keppie, J.D., eds., Laurentia-Gondwana connections before Pangea: Boulder, Colorado, Geological Society of America, p. 183–199.

Ryan, J.G., Yurkovich, S., Peterson, V., Burr, J., and Kruse, S., 2005, Geology and petrogenesis of mafic and ultramafic rocks of the Willets-Addie area, central Blue Ridge, NC, in Hatcher, R.D., Jr., and Merschat, A.J., eds., Blue Ridge Geology Geotraverse East of the Great Smoky Mountain National Park, Western North Carolina: North Carolina Geological Survey, Carolina Geological Society Annual Field Trip Guidebook, p. 91-98.

Sinha, A.K., Hogan, J.P., and Parks, J., 1996, Lead isotope mapping of crustal reservoirs within the Grenville Superterrane: I. Central and southern Appalachians: American Geophysical Union Geophysical Monograph, v. 95, p. 293–305.

Sinha, A.K., and McLelland, J.M., 1999, Lead isotope mapping of crustal reservoirs within the Grenville superterrane: II. Adirondack massif, New York, in Sinha, A.K., ed., Basement Tectonics, v. 13, p. 97–312.

Smith, D.R., Barnes, C., Shannon, W., Roback, R., and James, E., 1997, Petrogenesis of Mid-Proterozoic granitic magmas: Examples from central and west Texas: Precambrian Research, v. 85, p. 53–79, doi: 10.1016/S0301-9268(97)00032-6.

Southworth, S., Schultz, A., and Denenny, D., 2005, Geologic Map of the Great Smoky Mountains National Park Region, Tennessee and North Carolina: U.S. Geological Survey Open-File Report 2005-1225, available only online at: http://pubs.usgs.gov/of/2005/1225/

Southworth, S., Aleinikoff, J.N., Kunk, M.J., Naeser, C.W., and Naeser, N.D., 2005, Geochronology of the Great Smoky Mountains National Park region, TN/NC, with correlation to the rocks and orogenic events of the Appalachian Blue Ridge, in Hatcher, R.D., Jr., and Merschat, A.J., eds., Blue Ridge Geology Geotraverse east of the Great Smoky Mountains National Park, western North Carolina: North Carolina Geological Survey, Carolina Geological Society Annual Field Trip Guidebook, p. 45-56.

Southworth, S., Schultsz, A., Kunk, M.J., Aleinikoff, J.N., Clemons, K.M., Naeser, N.D., Naeser, C.W., and Denenny, D., 2006, The polygenetic Greenbrier fault, Great Smoky Mountains, TN/NC: Geological Society of America *Abstracts with Programs*, v. 38, no. 3, p. 66.

Stacey, J.S., and Kramers, J.D., 1975, Approximation of terrestrial lead isotope evolution by a two-stage model: Earth and Planetary Science Letters, v. 26, p. 207-221.

Stern, R.A., 2001. A new isotopic and trace element standard for the ion microprobe: preliminary TIMS U–Pb and electron microprobe data, current research. Radiogenic Age and Isotopic Studies: Report 14. Geological Survey of Canada, Ottawa, Canada.

Streckeisen, A., 1975, To each plutonic rock its proper name: Earth-Science Reviews, v. 12, p. 1-33

Tohver, E., Bettencourt, J.S., Tosdal R., Mezger, K., Leite, W.B., and Payolla, B.L., 2004, Terrane transfer during the Grenville orogeny: tracing the Amazonian ancestry of southern Appalachian basement through Pb and Nd isotopes: Earth and Planetary Science Letters, 228, p. 161-176.

Tohver, E., van der Pluijm, B.A., Scandolara, J.E., and Essene , E.J., 2005, Late Mesoproterozoic deformation of SW Amazonia (Rondonia, Brazil): Geochronological and structural evidence for collision with southern Laurentia: The Journal of Geology, v. 113, p. 309–323, doi: 10.1086/428807.

Tollo, R.P., Aleinikoff, J.N., Borduas, E.A., Hackley, P.C., and Fanning, C.M., 2004, Petrologic and geochronologic evolution of the Grenville orogen, northern Blue Ridge Province, Virginia, in Bartholomew, M.J., Corriveau , L., McLelland, J., and Tollo, R.P., eds., Protero zoic Evolution of the Grenville Orogen in North America: Geological Society of America Special Paper, Memoir 197.

Tollo, R.P., Aleinikoff, J.N., Wooden, J.L., Mazdab, F.K., Southworth, S., Fanning, C.M., 2010, Thermomagmatic evolution of Mesoproterozoic crust in the Blue Ridge of SW Virginia and NW North Carolina: Evidence from U-Pb geochronology and zircon geothermometry: The Geological Society of America, v. 206, p. 859-896., doi: 10.1130/2010.1206(33).

Van Schmus, W.R., Bickford, M.E., and Turek, A., 1996, Proterozoic geology of the east-central Midcontinent basement, in van der Pluijm, B.A., and Catacosinos, P.A., eds., Basement and Basins of Eastern North America: Boulder, Colorado, Geological Society of America Special Paper 308, p. 7–32.

Van Schmus, W.R., Schneider, D.A., Holm, D.K., Dodson, S., and Nelson, B.K., 2007, New insights into the southern margin of the Archean–Proterozoic boundary in the north-central United States based on U-Pb, Sm-Nd, and Ar-Ar geochronology: Precambrian Research, v. 157, p. 80–105, doi: 10.1016/j.precamres.2007.02.011.

Wasserburg, G.J., Jacobsen, S.B., DePaolo, D.J., McCulloch, M.T., and Wen, T., 1981, Precise determination of Sm/Nd ratios, Sm and Nd isotopic abundances in standard solutions: Geochimica et Cosmochimica Acta, v. 45, p. 2311-2323, doi: 0016-7037.81.122311-13$02.00/0

Whitehouse, M.J., 1988, Granulite facies Nd-Isotopic homogenization in the Lewisian complex of northwest Scotland. Nature v. 331, p. 705-7

Whitmeyer, S.J., and Karlstrom, K.E., 2007, Tectonic model for the Proterozoic growth of North America: Geosphere, v. 3, p. 220–259, doi: 10.1130/GES00055.1.

VITA

RYAN JOEL QUINN

BIRTHDATE: August 16, 1986, Framingham Massachusetts

Department of Earth and Environmental Sciences, University of Kentucky, Lexington, Ky, 40506-0053

EDUCATION:

A.S., McHenry Community College, 2007
B.A., Geology, University of Illinois at Urbana-Champaign, 2009

PROFESSIONAL EMPLOYMENT:

8/10-5/12	Teaching Assistant: University of Kentucky
5/10-8/10	NAGT intern, United States Geological Survey, Columbia, SC
1/09-5/09	Undergraduate Research Assistant: University of Illinois-Urbana Champaign

PUBLICATIONS:

Quinn, R.J., Moecher, D.P., Samson, S.D., Tohver, E., 2012, *Nd-Pb Isotope Systematics and Zircon U-Pb Geochronology Support a Native Crustal Component Within Grenville Basement, Eastern Great Smoky Mountains*, Geological Society of America *Abstracts with Programs*, Vol. 44, No. 7, p. 281.

Quinn, R.J., Moecher, D.P., Samson, S.D., Tohver, E., 2012, *Further Evidence for an Old Crustal Component in Southeast Laurentia Basement from U-Pb Zircon Geochronology, Eastern Great Smoky Mtns.*, Geological Society of America *Abstracts with Programs*, Vol. 44, No. 4, p. 64.

Quinn, R.J., Moecher, D.P., Samson, S.D., Tohver, E., 2011, *The Nature and Extent of Exotic Crustal Components in Southern Laurentia: New Age and Nd-Pb Isotope*

Evidence from Grenville Basement Gneisses, Eastern Great Smoky Mtns, Geological Society of America *Abstracts with Programs,* Vol. 43, No. 5, p. 490.

Leib, S.E., Quinn, R.J., RiCharde, G.E., Moecher, D.P., 2011, *Geothermobarometry on mafic and politic gneisses from Winding Stair to Dellwood, NC: filling the gap in Taconian P-T data in the central Blue Ridge*, Geological Society of America *Abstracts with Programs,* Vol. 43, No. 2, P. 30.

GRANTS AND FELLOWSHIPS:

- Pirtle Fellowship (University of Kentucky, 2011)
- Brown-McFarland Fund (University of Kentucky)
- Ferm-Fumd (University of Kentucky)
- Graduate Support Funding (University of Kentucky)

PROFESSIONAL AFFILIATIONS:

- American Association of Petroleum Geologists
- Geochemical Society
- Geological Society of America
- Mineralogical Society of America